Theory and computation of time-resolved spectroscopies for molecular systems in complex environments

Dissertation zur Erlangung des Doktorgrades
des Fachbereiches Physik
der Universität Hamburg

vorgelegt von

Abid Hussain

aus

Chiniot
Pakistan

Hamburg

2017

Gutachter der Dissertation:	Prof. Dr. Nils Huse Prof. Dr. Oriol Vendrell
Gutachter der Disputation:	Prof. Dr. Michael Rübhausen Prof. Dr. Gabriel Bester Prof. Dr. Julia Rehbein
Datum der Disputation:	03.07.2017
Vorsitzender des Fach-Promotionsausscuhsses:	Prof. Dr. Michael Rübhausen
Leiter des Fachbereiches Physik:	Prof. Dr. Michael Potthoff
Dekan der Fakultät für Mathematik, Informatik und Naturwissenschaften:	Prof. Dr. Heinrich Graener

Zusammenfassung

Der Fokus der vorliegenden Arbeit liegt auf der Anwendung von *ab initio* quantenchemischen Berechnungen zur Untersuchung des Einflusses von Wasserstoffbrückenbindungen und der elektrostatischen Umgebung auf die elektronische und molekulare Struktur von kleinen Molekülen. Des Weiteren werden anspruchsvolle Modelle der elektronischen Struktur zur präzisen Modellierung von multiplen lichtinduzierten transienten Produkten von schwefelhaltigen Verbindungen in Lösung angewandt. Diese Methoden ermöglichen die Charakterisierung jedes einzelnen elektronischen Zustand, und somit die Zuordnung der dominanten Übergänge des Röntgenabsorptionsspektrums. Weiterhin erlauben diese Methoden die Identifizierung des elektronischen Charakters jeder finalen Anregung der Valenz-Elektronen, die bei resonanter inelastischer Röntgenstreuung (RIXS) bei einer spezifischen Photonenenergie angeregt wird. Die Methoden sind jedoch durch ihren hohen Rechenaufwand verglichen mit anderen Methoden, insbesondere der Dichtefunktionaltheorie, begrenzt.

Eine detaillierte theoretische Studie des Einflusses von Wasserstoffbrückenbindungen und dem elektrostatischen Einfluss eines elektrischen Dipols auf die elektronische Struktur von Wasserstoffcyanid (HCN) wurde mittels *ab initio* quantenchemischen Berechnungen durchgeführt. Hierbei wurde der relative Einfluss verschiedener Molekülorbitale (MO) mit höchster chemischer Spezifität aufgeklärt, um den Ursprung von Nitril-spezifischen Raman Spektrallinien in RIXS-Spektren zu bestimmen. Die anomale Frequenzänderung der Nitril-Linie aufgrund von elektrostatischen Wechselwirkungen und von Wasserstoffbrückenbindungen wurde untersucht, um ihren elektronischen Ursprung aufzuklären. Die Hauptunterschiede der elektronischen Struktur von HCN sind elektrostatischer Natur und rühren von Dipol-Dipol Wechselwirkungen her. Die durch diese Wechselwirkungen induzierte relative Veränderung der CN-Streckschwingung und die Wasserstoffbrückenbindung mit einem Wassermolekül stimmen gut mit den experimentell gewonnenen spektralen Daten überein. Die Berechnungen sind ein weiterer Schritt, um den Einfluss von Wasserstoffbrückenbindungen auf die elektronische Struktur von Stickstoffatomen in Nitrilgruppen in dem organischen Molekül Acetonitril und seinen Komplex mit Wasser mittels RIXS zu untersuchen.*Ab initio* quantenchemischen Berechnungen wurden zur Interpretation der experimentellen Signatur von Übergängen der kernnahen Niveaus bei Stickstoff verwendet. Diese theoretischen Resultate sind in sehr guter Übereinstimmung mit den experimentellen Spektren und betonen somit die Sensitivität von

RIXS auch für schwache intermolekulare Wechselwirkungen.

Komplexe chemische Reaktionen können auf ihre grundlegenden Reaktionsschritte, die zumeist eine funktionelle Gruppe mit einem oder mehreren Hetero-Atomen, z.B. Sauerstoff, Stickstoff oder Schwefel beinhaltet, zurückgeführt werden. *Ab initio* Methoden wurden zur Bestätigung und zum Verständnis neuer Übergänge bei zeitaufgelöster Spektroskopie mittels Schwefel-1s-Anregungen und zur Modellierung von lichtinduzierten, elektronisch angeregten Reaktionswegen von Schwefel-Modelsystemen eingesetzt. Für ein aromatisches Thiol erklären Simulationen erfolgreich die Entstehung von Radikalen und die Regioselektivität der Thion-Isomerisationsreaktion.Des Weiteren wurde mittels zeitaufgelöster Röntgenabsorptionsspektroskopie (TRXAS) an der Schwefel K-Kante das UV-induzierte Aufbrechen der Disulfid-Bindungen bei Dimethyldisulfid (DMDS) untersucht. Mithilfe von RASSCF Rechnungen wurden das Methylthiyl und Methylperthiyl erfolgreich als transiente Photoprodukte identifiziert. Mit Hilfe dieser Berechnungen können chemische Reaktionswege und transiente Produkte von schwefelhaltigen Molekülen aus experimentellen Schwefel-1s Spektroskopiedaten abgeleitet werden.

Abstract

The work of this thesis is focused on employment of *ab initio* quantum chemistry calculations to probe the influence of hydrogen bonding and electrostatic environments on electronic and molecular structure of small molecules. In addition, high-level electronic structure methods are used for the accurate modelling of multiple light-induced transient products of sulfur-containing molecules in solution. These methods give explicit access to each electronic state with the extracted information allowing to assign the dominant transitions in the X-ray absorption spectrum. Additionally, these methods help to unearth the electronic character of every final valence excitation resulting from resonant inelastic X-ray scattering (RIXS) at a specific incident photon energy. However, they are limited by their high computational cost compared to other methods, especially density functional theory.

A detailed theoretical study of the influence of hydrogen bonding and electrostatic environment of an electric dipole on the electronic structure of hydrogen cyanide (HCN) was investigated with the help of *ab initio* quantum chemistry calculations. In the current study, the relative involvement of different molecular orbitals (MO) has been elucidated with highest chemical specificity in order to determine the origin of nitrogen-specific Raman spectral features from RIXS. The anomalous frequency of the nitrile group shift due to electrostatic interactions and hydrogen bonding was investigated to unravel its electronic origin. The major changes on the electronic structure of HCN were electrostatic in nature and originate from dipole-dipole interactions. The relative shifts of the CN stretching frequency induced by these interactions as well as hydrogen bonding with a water molecule are in good agreement with experimentally observed spectral changes. These calculations are taken one step forward to probe the influence of the hydrogen bonding on the electronic structure of the nitrogen atoms in nitrile containing organic molecule acetonitrile and its complex with water using RIXS. *Ab initio* quantum chemistry calculations have been utilized to interpret experimental electronic footprints via nitrogen core-level transitions. Our theoretical results are in very good agreement with experimental spectra, highlighting the sensitivity of RIXS even for weak intermolecular interactions.

Complex chemical reactions can be broken down into basic reaction steps, most

of which involve a functional group containing one or more hetero-atoms, e.g. oxygen, nitrogen or sulfur at the active site. *Ab initio* methods are employed to validate and understand the character of new transitions in time-resolved sulfur-1s spectroscopy to model an electronically excited light induced chemical reaction pathways for sulfur model systems. For an aromatic thiol model system, simulations successfully explain radical generation and the regioselectivity of the thione isomerization reaction. By studying the dimethyl disulfide (DMDS) with time-resolved X-ray absorption spectroscopy (TRXAS), the UV-induced disulfide bond breaking at the sulfur K-edge has been investigated. The formations of methylthiyl and methylperthiyl radicals as transient photoproducts are identified using RASSCF calculations. With these calculations, chemical reaction pathways and transient products of sulfur-containing molecules can be established from experimental sulfur-1s spectroscopic data.

Contents

List of Figures

List of Abbreviations

SD	**S**later **D**eterminant
HF	**H**artree **F**ock
MO	**M**olecular **O**rbital
CI	**C**onfiguration **I**nteraction
SCF	**S**elf-**C**onsistent **F**ield
MCSCF	**M**ulti-**C**onfigurational **S**elf-**C**onsistent **F**ield
CSF	**C**onfiguration **S**tate **F**unction
CASSCF	**C**omplete **A**ctive **S**pace **S**elf-**C**onsistent **F**ield
RASSCF	**R**estricted **A**ctive **S**pace **S**elf-**C**onsistent **F**ield
MRCI	**M**ulti-**R**eference **C**onfiguration **I**nteraction
CASPT2	**S**econd-**O**rder **P**erturbation **T**heory
DFT	**D**ensity **F**unctional **T**heory
LDA	**L**ocal **D**ensity **A**pproximation
GGA	**G**eneralized **G**radient **A**pproximation
CIS	**C**onfiguration **I**nteraction **S**ingles
XAS	**X**-ray **A**bsorption **S**pectroscopy
XANES	**X**-ray **A**bsorption **N**ear **E**dge **S**tructure
EXAFS	**E**xtended **X**-ray **A**bsorption **F**ine **S**tructure
TEY	**T**otal **E**lectron **Y**ield
FY	**F**luorescence **Y**ield
XES	**X**-ray **E**mission **S**pectroscopy
RIXS	**R**esonant **I**nelastic **X**-ray **S**cattering
QM/MM	**Q**uantum **M**echanics/**M**olecular **M**echanics
MEP	**M**inimum **E**nergy **P**ath
DMDS	**D**imethyl **D**isulfide
4-MTP	4-**M**ethyl**T**hio**P**henol
HCN	**H**ydrogen **C**yanide
TRXAS	**T**ime-**R**esolved **X**-ray **A**bsorption **S**pectroscopy
DNA	**D**eoxyribose **N**ucleic **A**cid

LIST OF PUBLICATIONS

I. Light-Induced Radical Formation and Isomerization of an Aromatic Thiol in Solution Followed by Time-Resolved X-ray Absorption Spectroscopy at the Sulfur K-Edge.
Miguel Ochmann, Inga von Ahnen, Amy A. Cordones, Abid Hussain, Jae Hyuk Lee, Kiryong Hong, Katrin Adamczyk, Oriol Vendrell, Tae Kyu Kim, Robert W. Schoenlein, and Nils Huse.
J. Am. Chem. Soc., **2017**, 139 (13), pp 4797–4804.

II. Sensitivity of core-level spectroscopy to hydrogen bonding and electrostatic environments of nitrile groups: *An ab* initio study.
Abid Hussain, Nils Huse, Oriol Vendrell.
In review at Structural Dynamics.

III. Tracking the UV-induced disulfide bond breaking in dimethyl disulfide with TRXAS at the sulfur K-Edge.
Miguel Ochmann, Abid Hussain, Amy A. Cordones-Hahn, Inga von Ahnen, Jae Hyuk Lee, Kiryong Hong, Katrin Adamczyk, Rory Ma, Tae Kyu Kim, Robert W. Schoenlein, Oriol Vendrell, and Nils Huse.
In Manuscript.

IV. Resonant inelastic X-ray Scattering (RIXS) Studies of Hydrogen-Bonded Cyano-Groups at the Nitrogen Kedge.
Abid Hussain, Simon Schreck, Philippe Wernet, Alexander Föhlisch, Oriol Vendrell, and Nils Huse.
In Manuscript.

Comments on my contribution

The sulfur-1s absorption spectroscopy experiments presented in paper **I** & **III** were performed by Miguel Ochmann, Inga von Ahnen, Amy A. Cordones, Kiryong Hong, Jae Hyuk Lee, and Nils Huse. I performed and contributed all quantum chemical calculations and wrote the relevant sections in the manuscript. For paper **II**, I led the research and undertook the calculations and analysis and wrote the manuscript with inputs from Nils Huse and Oriol Vendrell. Experiments reported in paper **IV** were performed by Simon Schreck, Philippe Wernet and Nis Huse, who also conceived the idea. Simon Schreck performed the analysis of the experimental data. I was involved with running RIXS simulations and also wrote the manuscript for this paper.

Chapter 1

Introdution

1.1 Molecular interactions

Molecular interactions are the interactions among the constituents of molecules as well as its nearby particles (e.g., atoms or ions). Forces mediating interactions between molecules and other nearby particles are termed as intermolecular forces. It is necessary to mention that intermolecular interactions of electrostatic nature (ion-ion interactions) have strength comparable to covalent bonds. The electrostatic interactions between the ion pairs of anionic and cationic moieties have significant importance in the stability and functionality of proteins and nucleic acids [1, 2]. The combination of ion-ion interactions and hydrogen bonds linking the charged groups of amino acids side chains is known as a salt bridge (Fig. 1.1e).

Clairault [3] was the first to present a theory which envisioned two kinds of interparticle forces during his work based on exploring interactions between water and glass and those between the liquid particles themselves. The next step in this direction was taken by Laplace [4] in his investigations regarding "Capillary Action". Two decades later, Gauss [5] explained this by considering three forces including gravity along with Clairault's suggested forces. Maxwell in his series of papers investigated gas phenomena on the basis of intermolecular forces to establish molecular or dynamic theory of matter whose foundations had already been laid by earlier studies. Sutherland's work on specific laws of attraction between gaseous molecules represents the next phase in the history of intermolecular interactions [6]. Inspired by Clausius' treatise [7] which presents heat as a phenomenon of motion, Johannes van der Waals successfully derived the equation of state covering both the liquid and gas phase within a unified framework. In 1921, Keesom was able to develop a first explanation for the dipole-dipole interaction existing between dipolar molecules by taking the average of the Coulombic potential over all mutual orientations using a Maxwell-Boltzman distribution [8]. Considering the polarization effects on a molecule in the external electric field, Debye developed the concept of the dipole moment and introduced the dielectric constant which explained the displacements of charges within molecules in

response to an electric field, a universal cause of intermolecular forces [9]. Explanations regarding the van der Waals interactions between the species lacking permanent dipole moments was given by London [10]. London proposed that electronic motions constitute an instantaneous nuclear-electronic dipole which induces a dipole in a neighbouring molecule. As a reciprocal interaction the second molecule induces a similar dipole on the first molecule which results in a universal attractive interaction independent of any permanent molecular dipole moment. Developments in the field of quantum chemistry paved the way to unravel these interactions ranging from the simplest molecular to complex biological systems [11–21].

Intermolecular interactions play a crucial role in chemical and biological assembly processes. These are directed by elegant expressions of collective behaviour on the molecular scale [22–27]. In supramolecular chemistry, these interactions drive the assembly of rationally designed molecular subunits to nanoscopic aggregates with targeted functions. A clear understanding and accurate description of the full panoply of interactions between molecules is essential for the elucidation of the mechanisms of biological functions, the development of new synthetic applications in catalysis, materials science and medicine. Intermolecular interactions include a wide range of attractive and repulsive forces of different nature, magnitude and directionality. However, the classification of such interaction is sometimes indistinct or has blurred, or overlapping boundaries. Several types of these interactions are introduced in the following subsections (Fig. 1.1)with special emphasis on hydrogen bonding which has been studied in detail.

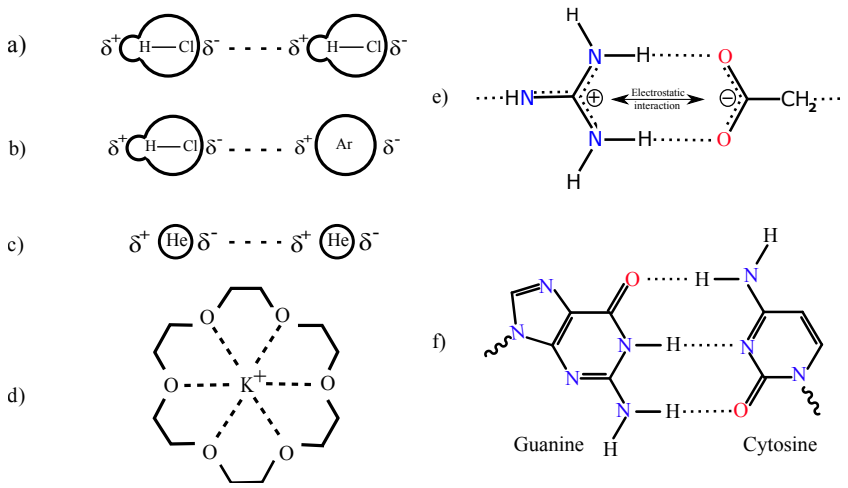

FIGURE 1.1: Illustration of different intermolecular interactions **a** : dipole-dipole interaction. **b** : dipole-induced dipole interaction. **c** : induced dipole-induced dipole interaction. **d** : ion-dipole interaction. **e** : Salt bridge consisting of hydrogen bonding and ion-ion interaction and **f** : hydrogen bonding.

1.1.1 Van der Waals interactions

The weak interactions between neutral molecules and atoms named after its discoverer Johannes Diderik Van der Waals play a subtle role in many fields including biochemistry, nanotechnology, supramolecular chemistry, surface science, condensed matter physics and polymer science [28–30]. These interactions include the following terms explained explicitly below.

The interaction between two dipolar molecules through space results in dipole-dipole interactions. It is an attractive interaction between the partially positive part of one polar molecule and the partial negative part of another molecule. This type of interaction plays a vital role in the functionality and dynamics of many biologically important species. These interactions are also referred to as Keesom interactions [8]. HCl is an example of a polar molecule in which the chlorine part is partially negative owing to the electronegativity of the chlorine atom and the hydrogen part is partially positive. So in a solution where there are thousands of such molecules with a slight charge on each side giving rise to the natural orientation of molecules in such a way that the positive part of one molecule will move until it is next to the negative part of a neighbouring molecule. These forces between molecules tend to make them 'stick' together.

The interaction between two molecules originates from the interaction between the permanent dipole moment of one of the molecules with the dipole moment it induces in the other one. The magnitude of the induced dipole moment depends on the magnitude of the permanent dipole moment, the spacing between the two molecules, and the polarizability of the molecule in which the dipole moment is induced.

These interactions are the weakest type of intermolecular interactions. As the electrons of all atoms and molecules are in constant motion, this produces transient oscillations in the electron density, leading to temporary fluctuating distortions in the charge clouds. These fleeting distortions in different molecules can interact with each other, resulting in an eventual synchronization of the oscillations and an attractive force between the molecules, e.g., an instantaneous dipole on helium atom induces a dipole on neighbouring atoms. For the first time these interactions were rationalized and described by London [10, 31], and hence are called London interactions. Long range London dispersions represent the important contribution to the van der Waals forces. These interactions explain the liquid behaviour of noble gases at low temperatures. The magnitude of dispersion interactions depend on the size of the electron cloud as it is easy to move or polarize an electron in response to an instantaneous dipole in larger molecules. As an example, the London interaction gains importance in nonpolar molecular complexes where it gives rise to the only binding force and also it is of paramount importance in large molecules with large polarizability.

It is an interaction between an ion and a neutral molecule with a permanent dipole. It is a fundamental attractive force akin to van der Waals and hydrogen bonding and of

importance for protein functionality [32] . A classic model of ion-dipole interaction is the solvation process of an ion, as for example, the Na+ cation in water. The complexes formed by crown ethers (the simplest of these compounds contains an 18-membered ring with 6 oxygen atom) and alkaline ions are other examples of ion-dipole interactions. This complex has a marked ionic character due to the interaction between a small polarising cation and the lone pairs of the oxygen atoms. Utilization of this motif is frequent in situations of high specificity, structural stability and fixed geometry is frequent [32].

1.1.2 Hydrogen bonding

The formation of a chemical bond is a result of the interaction between valence electrons residing on different atoms under certain conditions. In the simplest case a hydrogen bond is denoted by X-H ... A, where X-H is called the proton donor, and A is called the proton acceptor. In this notation the proton donor forms a covalent bond with the hydrogen atom. The hydrogen bond between the electron-deficient hydrogen and the electronegative acceptor is considerably weaker and shown in dots. The hydrogen bond consists of three interactions: electrostatic, induction and dispersion. Chemical variation of donor and acceptor moieties can alter the relative contributions of these interactions to the resulting hydrogen bond. As a result, hydrogen bonds exist with a continuum of strength.

Though, H-bonds are typically weaker than most covalent bonds, they are usually significantly stronger than Van der Waals interactions [33–36]. To give one scientist credit for the introduction of the hydrogen bond is difficult. However, Alfred Werner is credited for first suggesting a binding situation called *Nebenvalenz* (secondary valence) to explain the properties of ammonium salts [37] . Ten years later Moore and Winmill [38] used the concept introduced by Werner to explain their results on amines in aqueous solution. Finally, in 1920 Latimer, Rodebush and Huggins - three young scientists working in the laboratory of G. N. Lewis - defined the hydrogen bond concept as is accepted today based on the Lewis' dot formalism [39]. Pauling was most likely the one who introduced the term hydrogen bonding [40] to interpret the structure of the $[F:H:F]^-$. Intramolecular hydrogen bond formation in organic chemistry was first proposed by Pfeiffer [41]. Hydrogen bonding has unequivocal role in functionality, structure and dynamics of biomolecules. For example two secondary structure motifs found in proteins, the alpha-helix and the beta-sheet, rely on hydrogen-bonds between the amine (-NH_2 or -NH) and the carbonyl (C=O) groups of different amino acids. It was Pauling, Corey, and Branson who postulated the existence of the alpha-helix [42] whereas the beta-sheet was identified later by Blake and coworkers [43]. H-bonds also play an important role in protein folding and molecular recognition and have been implicated in many intermolecular interactions, including those

involving protein-protein, protein-ligand, and protein-nucleic acid complexes. Another elegant manifestation of hydrogen bonding in biology is the deoxyribose nucleic acid (DNA) which encodes genetic information. The helical double strands are held together by hydrogen bonds between the base pairs - a structure that has been predicted by Watson and Crick [44]. Hydrogen bonding is very directional and of short range. Elementary chemical reactions such as intra- and intermolecular proton and hydrogen transfer, are mediated by hydrogen bonds. The enormous effect of hydrogen bonds on proton transfer can be seen in the anomalous diffusion of protons in liquid water. Also, proton transfer is of great physiological importance in intra- and intercellular signalling pathways [45]. H-bonding along with π-stacking interactions is also responsible for the poor solubility of organic pigments or colorants [46]. An effort to understand the structure and dynamics of hydrogen-bonded systems at the molecular level using various experimental techniques advanced the knowledge of these complex systems considerably [47–52].

The nitrile group is sensitive to solvent polarity, local electric fields and hydrogen bonding. For that reason it is used as a vibrational probe to examine solvation and the electrophilicity of different solvents. The nitrile group provides the site for H-bond acceptance for proton donor groups like water due to a lone electron pair on the nitrogen atom, leading to an anomalous shift of the CN stretching vibration to higher frequency. This anomalous shift of the CN stretching vibration leading to bond stiffening is very unusual because almost all other stretching vibrations of HB acceptor groups with only few exception display a bond softening upon hydrogen bonding [53]. This shift by incorporation of nitrile-derivatized amino acids is of great use in the study of protein processes by using the nitrile group as spectroscopic label [54–57]. The native structure of proteins is only slightly perturbed by addition of such non-natural amino acids and these are very useful to constitute spectrally-isolated and well-distinguishable vibrational probes for electrostatic environments, charge transfer and migration, and structural dynamics of local protein environments. Accordingly, a number of studies have been reported on the use of nitrile groups to probe effects of the electric field on active sites in peptides and proteins, protein folding and unfolding dynamics, mechanisms of biological information transfer by nucleic acids, and many other biological processes [58–61]. It is therefore important to understand and gauge the electronic and structural response of the nitrile group to electrostatic and hydrogen bond interactions on the atomic level which is one of the aim of this work.

1.2 Heteroatoms in functional groups

A functional group is a group of atoms within organic molecules that govern the chemical properties of molecules. The carbonyl (-CO), hydroxyl (-OH), carboxyl (-COOH), nitrile (-CN), and amine (-NH_2 or -NH) groups are few examples. A heteroatom is any atom other than carbon and hydrogen in organic chemistry. The presence of one or more heteroatoms in an organic compound results in quite different physicochemical characteristics from analogues compounds lacking these atoms. Functional groups which contain nitrogen or sulfur at the reacting sites imply significance of their ubiquitous role in organic chemistry and are the main focus of this work.

1.2.1 Nitrogen-containing functional groups

Nitrogen containing compounds are very widely distributed in nature and are essential to life; they play a vital role in the metabolism of all living cells. Nitrogen can be found in variety of oxidation states ranging from +5 in the most oxidized compound (nitrate) to -3 in the most reduced form (ammonium), but it is almost exclusively present in the fully reduced state in biological compounds [62]. Its electronic versatility makes it an important element for many research fields ranging from organic synthesis, medicinal chemistry, and materials science. One example showing its significance in materials science are polymer emitting diodes (PLEDs). In PLEDs, nitrogen containing heterocycles such as pyridine and quinoxaline serve as efficient electron acceptors due to the presence of electron-deficient imine nitrogen C=N [63]. The combination of an electron-deficient acceptor with an electron-rich donor results in a conjugated polymer with a compressed band gap [64]. Aromatic nitrogen heterocycles represent an important class of ligands in coordination chemistry [65]. The essentiality of nitrogen is evidenced by its omnipresence in many biological compounds, including: amino acids, purines and pyrimidines which are the building blocks of proteins, nucleotides, and nucleic acids [66].

Organic compounds contain nitrogen in probably more combinations with oxygen, hydrogen, carbon, and itself than any other element. Its presence in several oxidation states enables it to form covalent bonds with these elements to produce a variety of nitrogen-containing functional groups. Amine, nitrile, amide, imine, pyridine and its derivatives are of main interest. Amines constitute an important class of organic compounds derived by replacing one or more hydrogen atoms of ammonia by alkyl/aryl group(s). Nucleophilic characteristic of amines confers them high reactivity which make them a key intermediate in chemical industry [67]. Amines are used in rapidly growing fields which produce polymers, agrochemicals, detergents, lubricants, food-additives, and also drugs [67, 68]. Amines are also used as a key monomers in the

synthesis of polyamides, polyureas, polyepoxydes, which are all of growing production in aerospace, automotive, or health applications [69,70]. In addition, amines are also found in many molecules essential to life, such as amino acids, hormones, neurotransmitters, and DNA.

The amide group displays a carbonyl group bonded to a nitrogen. The general formula is RCO-N$R'R''$ (with R',R''=H in case of simple amides and R',R''=alkyl, aryl in case of complex amides). Peptides and hence proteins consist of amino acids which are linked by amide bonds (peptide bonds). Existence of amide bonds is not limited to biological systems but also found in a huge array of molecules, including major marketed drugs [71]. Imines or Schiff bases are nitrogen analogues of an aldehyde or ketone in which the carbonyl group (C=O) has been replaced by an imine or azomethine group (C=N–). Schiff bases are condensation products of primary amines and carbonyl compounds and they were discovered by the German chemist Hugo Schiff in 1864 [72]. Imines constitute an important class of organic compounds with a broad spectrum of biological activities, including antibacterial, antifungal, antiprotozoal, antiviral and antibacterial properties [73,74]. Furthermore, imines are used as catalysts, dyes, pigments, polymer stabilizers and corrosion inhibitors [75,76]. In organic synthesis, imines are used as precursors to yield amines by reduction of the carbon-nitrogen double bond C=N using transition metal hydride complexes [77,78].

The nitrile group (−C≡N) is a key constituent of numerous natural products and has considerable importance as synthetic intermediate in dyes [79], agricultural chemicals, material sciences [80] and pharmaceuticals [81]. Nitriles also serve as chemical solvents and recrystallizing agents. Nitrile are utilized as an important synthon for preparation of carboxylic acids, aldehydes, amides, amines and ketones [81,82]. Additionally, the nitrile group is sensitive to hydrogen bonding, solvent polarity and local electric fields [83–88]. Therefore it has received attention regarding its use as vibrational probe of the local protein environment [88–98]. Incorporation of nitrile-derivatized amino acids into proteins therefore enable the study of electrostatic local environments, charge transfer processes and structural dynamics of local protein environments [58–61].

1.2.2 Sulfur-containing functional groups

Sulfur is an important element as it is the tenth most abundant element in the earth's crust [99,100]. Sulfur can be found in a variety of oxidation states, ranging from -2 to +6 due to which it can be found in multiple structural motifs with different properties [100,101]. Sulfur is an essential constituent of many chemical compounds, ranging from polymers, nanoparticles to many biomolecules due to its versatility and its prevalence in the primordial environment [102–104]. Also, sulfur has attracted much attention as thiophene-containing π-conjugated systems for use in the field of organic field-effect transistors (OFETs), organic light-emitting diodes (OLEDs), and organic

photovoltaics (OPVs) [105]. The importance of sulfur in biochemistry is evident as it is found in amino acids, such as methionine (a thioether) or cysteine (a thiol) [106] and in proteins as part of the tertiary structure due to covalent disulfide bonds between cysteine residues. Sulfur is not only an essential constituent of amino acids but also found as sulfide in the center of enzymes containing a metal-sulfide center [107].

Thiols are a class of organic compounds that contain a sulfhydryl group (-SH), also known as a thiol group, that is composed of a sulfur atom and a hydrogen atom attached to a carbon atom. Being the sulfur analogue of an alcohol group (-OH), this functional group is also referred to a sulfhydryl group. Thiol group plays a central role in biologically important reactions such as the formation of disulfide bridges in proteins and cyclic peptides. Formation of disulfide bridges, in fact, increase the biological activity and the stability of the molecules, inducing their natural folding and structural stabilization [108–112]. Furthermore, hydrogen donations to carbon-centered radicals by thiols are commonly invoked as the chemical repair reaction in biological systems with formation of the more stable S-centered thiyl radical as an intermediate [113,114]. Due to the ability of the thiol group to form a covalent bond with gold and to transport charge onto the gold surface it is used as an anchoring group for molecular wires and molecular junctions [115, 116].

A disulfide bond refers to the functional group with the structure R-S-S-R'. The linkage is also called an SS-bond, disulfide bridge, or crosslink. In proteins, disulfide bonds are formed as a result of oxidation reactions of the two thiols, thus linking the two cysteines and their respective main peptide chains by the covalent disulfide bond. Disulfide bonds are common structural motifs for the stability, folding, and functionality of many bioactive peptides and proteins including hormones, neurotransmitters, growth factors, enzyme inhibitors, and antimicrobial peptides [112, 117–119]. In addition, stability provided by disulfide bonds protects proteins from damage and increase their lifetime [120]which is useful in protein-based therapeutics. Likewise, increased stability of industrial enzymes can dramatically improve their yield and expand their operational range [121].

1.2.3 Radical chemistry

Radicals, a class of subvalent chemical species characterized by one or more unpaired electrons, are generally regarded as highly reactive, unstable transient species. Free radicals of low molecular weight are extremely reactive and short-lived with lifetimes ranging from nanoseconds to milliseconds [122]. Radicals are either electrophilic or nucleophilic. So this sentence is only half true. As you point out in the following sentence the radical acts either as oxidant or reductant(e.g., DNA, RNA, proteins and amino acids) and carbon-carbon double bond (e.g., polyunsaturated fatty acids and phospholipids). They behave as oxidant or reductant by either donating electron to or accepting an electron from other molecules, respectively [123]. Historically, there

were predictions about the existence of free radicals in the beginning of nineteenth century, but Fenton's free radical reaction was presumably the first reported [124]. In 1900, Gomberg was able to report convincing evidence for triphenylmethyl radical as the first organic free radical [125] by homolysis of triphenylmethyl chloride with a metal like silver or zinc in benzene or diethyl ether. The existence of this was also confirmed by Wilhem Schlenk and co-workers a decade later [126]. In 1929, Paneth and Hofeditz were able to identify simple alkyl radicals [127]. Wieland and co-workers conducted a series of experiments for detection and trapping of nitrogen centered radicals [128, 129]. The world of free radicals in biological systems was, in 1956, explored by D. Harman who proposed the concept of free radicals playing a role in the ageing process [130]. In 1977, Mittal and Murad provided evidence that the hydroxyl radical $OH^{\bullet}$ stimulates activation of guanylate cyclase [131]. Since then, a large body of evidence has accumulated that living systems have not only adapted to a coexistence with free radicals but have developed various mechanisms for the advantageous use of free radicals in various physiological functions. In addition, free radical reactions are widely used in the formation of carbon-heteroatom bonds, including carbon-sulfur bond formation [132, 133]. The reaction mechanism underlying these processes is fundamental to understand in order to advance the synthetic utility of free radicals. Fortunately, a large number of mechanistic studies on radical reactions are now available. Factors that control radical reactivity, (stereo)chemical selectivity and the reaction rate constant are being examined which will help to predict the reaction outcome [134,135].

A free radical is formed when a two-electron bond is broken symmetrically, by a process known as homolysis in which a single electron stays with each fragment. Sulfur-centered radicals or those influenced by the presence of a sulfur atom are crucial in many biochemical reactions. The most important classes of sulfur-containing radicals are thiyl and sulfonyl radicals for preparative organic chemistry. Thiyl radicals are of concern to this thesis. It has been shown that a disulfide bond can be broken by one electron reduction [136, 137] or via homolytic cleavage of the sulfur-sulfur bond using photolysis [138, 139]. The generation of $RS^{\bullet}$ radicals (with R=alkyl, aryl) by splitting of the sulfur-sulfur bond appears to be the major route of radical-induced disulfide destruction. Carbon-sulfur bond rupture may also occur, particularly when the disulfide bridge is attached with tertiary carbon substituents [138]. The dissociation pathway of the carbon-sulfur bond cleavage results in perthiyl radical formation, $RSS^{\bullet}$, a sulfur analogue of the chemically well-characterized and well-known peroxyl radical, $ROO^{\bullet}$ [140]. In biochemistry, a large wealth of information on the reactivity of oxygen-centered radical species exists in scientific literature. Surprisingly, not much attention has been paid to the biochemical aspects of sulfur-centered radicals. However, the discovery of $RS^{\bullet}$ radicals and development of related versatile chemistry in biological materials has imparted new directions to radical chemistry. The efficient addition of thiyl radicals to a wide range of unsaturated systems such as alkenes,

alkynes, isonitriles, and thiocarbonyl groups is very well known in synthetic applications [141]. Thiyl radicals display hydrogen abstraction and displacement reactions on sulfur atoms. Thiyl radicals react rapidly with molecular oxygen to form thiylperoxyl radicals ($RSOO^{\bullet}$). It has been found biochemically that $RS^{\bullet}$ initiates lipid peroxidation. However, the chemistry and biochemistry of perthiyl radical has received less attention despite its conceivable relevance in disulfide chemistry. The formation of the perthiyl radical resulting from photodisociation of dimethy disulfide is also featured in this thesis.

1.2.4 Reaction dynamics

The study of elementary physical and chemical processes occurring at the molecular level is termed as chemical reaction dynamics. It seeks to understand what actually happens during the course of physical or chemical transformations. In other words, chemical reaction dynamics is the research field which studies chemical events during the journey of reactants to products. In general, chemical reaction occurs on a large range of timescales. A large number of chemical transformations are involved in rearrangements of biomolecular structures, such as DNA multiplication or protein synthesis in ribosomes with a time span on the order of seconds to hours. The timescale of bimolecular reaction dynamics is of the order of nanoseconds. The dynamical event of a single-bond rearrangement, called elementary step in chemistry, appears to take place on femtosecond to picosecond timescales [142]. Bond fission, cis-trans isomerization, electron transfer, hydrogen and proton transfer are exemplified as ultrafast chemical reactions [143]. The dynamical events occurring during these elementary steps and means of probing, understanding, and controlling them is one of major goals of molecular reaction dynamics.

Transformations of matter that are being studied encompass a wide range of physical, chemical and biological systems in all phases of matter. Molecular reaction dynamics is not limited only to neutral reacting species but also applicable to charged species (cations and anions), either in their solvated or bare state. It explains the role of different interactions on the functionality and design of systems under considerations, e.g., electrostatic effects are central to biochemical reactions. For rational drug design it is important to consider the interactions between drug and receptor and how both are modified as a result of their interaction. The relevance of molecular reaction dynamics beyond the traditional boundaries of chemistry is increasing day by day due to today's scientific and technological challenges. It is very important to understand the structural and dynamical transformations on molecular and atomic levels. The reason for this lies in its importance for the understanding of chemical reactions in many fields of natural sciences ranging from ranging from biochemistry to material sciences. Molecular reaction dynamics has been used to develop new synthetic routes

and optimize existing ones on a lab or industrial scale due to its ability to unravel the time history of a chemical event and to describe the change on molecular scale.

It has long been a dream of scientists to understand the nature of inter- and intramolecular dynamics in detail, to visualize the making and breaking of bonds and to follow energy and charge flow in real time within molecular systems, to 'see' the geometrical rearrangements and chemical reaction after energy depositions. This dream came true after the developments in the field of short-pulsed laser systems that gave an opportunity to study ultrafast aforementioned changes using time-resolved electronic spectroscopy. For example, photodissociation, a process whereby a molecular system is broken into fragments of different ratios as a consequence of one or multi photon absorption has been studied with various ultrafast spectroscopies. The intensity of the laser beam can even alter the chemical reaction pathways. This has been observed for the photodissociation of acetophenone [144,145].

The essence of chemical reactions and indeed life is the making and breaking of molecular bonds. Elementary steps in bond transformation occur on the order of femtoseconds. Therefore in order to probe and disentangle these processes femtosecond time resolution is required. Additional high spatial resolution enables molecular structural changes to be followed in real-time. The developments of ultrafast technologies, especially of ultrabright free-electron lasers (FELs) providing unprecedented brilliance of photon flux has enabled several pioneering time-resolved structural studies [146–149] which has opened a new regime of studying dynamics of molecular structures, variation of valance-charge distribution and photochemical pathways during a chemical reaction. The application of spectroscopic techniques with the element specificity, chemical sensitivity, and temporal resolution has technically made it possible to probe molecular dynamics which has extended the capability of measurements to time and length scales on the order or shorter than periods of molecular vibrations.

Time-resolved X-ray spectroscopies have been used to study energy transfer and charge separation in photosynthetic systems [150], proton-transfer reactions in solution [151] the evolution of the valence charge distribution of transition-metal complexes [152], chemical reaction dynamics [153] and photochemical reaction pathways [154,155]. In order to track photochemical reaction pathways in model sulfur systems, time-resolved sulfur-1s absorption spectroscopy has been used in this work.

Chapter 2

Theoretical framework

This chapter includes a brief description of quantum chemical methods that are used to model the electronic spectra. The computational methods that have been used for the investigation of the electronic structure of molecular systems comprising this thesis are nowadays well established and in wide use for various applications in quantum chemistry. The following presentations of the computational methods focus on the general idea of each method, its strengths and weaknesses, and the benefits of using a particular method for computation of different spectral and electronic features. Since the underlying theory is too lengthy and technical to be presented in a concise manner, the interested reader is referred to the original literature or available compendia on electronic-structure methods [156–158]for a detail overview.

2.1 Quantum chemical methods

All quantum chemical methods ultimately stem from the solution of the Schrödinger equation. It treats molecules as a collection of charged particles: electrons and nuclei, without any reference to chemical bonds. All information about the molecular structure of the system is obtained from the solution of the Schrödinger equation, with the Coulomb interaction as a fundamental consitutent determining its chemistry. However, an analytic solution to the Schrödinger equation is only possible for one-electron systems (the hydrogen atom and He^+), and approximations have to be made for numerical solution of many-electron system. The nature of these approximations classifies the quantum chemical methods, which in terms of their reliability, capability and computational cost span over a wide range.

2.1.1 Born-Oppenheimer approximation

Any theory, describing stationary quantum states of a system is based on the Schrödinger equation. It is the basic tool that the quantum chemist work with. The time-independent Schrödinger equation has the form

$$\hat{\mathbf{H}}\Psi(\vec{r},\vec{R}) = E\Psi(\vec{r},\vec{R}) \tag{2.1}$$

where $\Psi(\vec{r},\vec{R})$ is the total molecular wave function, $\vec{r}$ and $\vec{R}$, the coordinates of all electrons and nuclei respectively, E is the energy and $\hat{\mathbf{H}}$ is the Hamiltonian of the system defined as

$$\hat{\mathbf{H}} = \hat{T}_{nuc} + \hat{T}_{el} + \hat{V}_{nuc,nuc} + \hat{V}_{el,el} + \hat{V}_{el,nuc} \tag{2.2}$$

This Hamiltonian describes the kinetic energy terms (T) for the nuclei and electrons, as well as the Coulombic electron-electron, nuclei-nuclei, and electron-nuclei interaction terms (V). Since it is not possible to separate internal degrees of freedom for chemical systems with more than two interacting particles (systems larger than the hydrogen atom and He^+), it is necessary to invoke a number of approximations to make practical use of the quantum mechanical formulation. The most important is the Born and Oppenheimer approximation used for quantum mechanical descriptions of large molecules [159]. Since the electrons are about three orders of magnitude lighter than the electrons and can respond much more quickly as compared to the the motions of the nuclei. The Born-Oppenheimer approximation simplifies the solution by separating nuclear and electronic motions. The physical picture of Born-Oppenheimer approximation is one where the fast-moving electrons are able to re-adapt instantaneously to new nuclear geometry, as a result of the light electron mass with respect to the nuclear one. The molecular wave function can be factorised into electronic and nuclear wave functions with this assumption

$$\Psi(\vec{r},\vec{R}) = \psi_{el}(\vec{r};\vec{R})\chi_{nuc}(\vec{R}) \tag{2.3}$$

$\psi_{el}(\vec{r};\vec{R})$ is the electronic wave function and $\chi_{nuc}(\vec{R})$ denotes the nuclear wave function. The electronic wave function is a function of the electronic coordinates, $\vec{r}$ along with the nuclear coordinates $\vec{R}$ parametrically, i.e. for different positions of nuclei $\vec{R}$, the electronic wave function is a different funcion of electronic coordinates $\vec{r}$. The Hamiltonian can be now written by considering only the electronic wave function

$$\hat{H}\psi_{el}(\vec{r};\vec{R}) = E(\vec{R})\psi_{el}(\vec{r};\vec{R}) \tag{2.4}$$

The solution of the electronic Schrödinger equation for different nuclear positions, constitute a potential energy surface (PES) on which the nuclei move.

2.1.2 Variational principle and Hartree-Fock theory

It can be shown that the expectation value of the energy for any wave function is always higher than the lowest energy E_0 of the exact solution of the Schrödinger equation Ψ

$$\frac{\langle\psi_{el}|\hat{H}|\psi_{el}\rangle}{\langle\psi_{el}|\psi_{el}\rangle} > E_0 \tag{2.5}$$

Also, the closer the wave function is to the exact ground state wave function, the lower is the energy expectation value. The variational principle states that the "best" wave function can be found by varying it until the energy is at a minimum. The separation of the potential energy operator corresponding to the Coulomb repulsion between the electrons in the electronic Hamiltonian is not possible. The complex dynamics of a many-electron system is decoupled to single particle with the independent particle approximation in which it is assumed that an individual electron moves in the potential created by the nuclei plus the average potential of the other electrons. The corresponding part of the Hamiltonian can hence be replaced by the interaction of the electrons with the average field in which they move. In the independent particle model, a many-electron problem can be described with a set of coupled single electron wave functions. Each of these one-electron Hamiltonian contains the kinetic energy of the electron and the potential energy created by the nuclei plus the mean field of other electrons.
A spatial function ϕ (an orbital) with a corresponding energy eigenvalue (solution of the Schrödinger equation with this Hamiltonian) is associated with each of these electrons. A complete description of an electron requires its spin along with the spatial wave function ϕ. Because electrons are fermions, the total wave function of all electrons cannot simply be expressed as a product of spatial and spin functions (spin orbitals) χ; it must be antisymmetric under the exchange of any two electrons (i.e. the Pauli exclusion principle).
In the Hartree-Fock method [160, 161], Slater determinants (SD) [162] are used to construct the approximate *N*-electron wave function with the *N* occupied spin orbitals χ's

$$\psi_{el} = (N!)^{-\frac{1}{2}} \begin{vmatrix} \chi_1(1) & \chi_2(1) & \cdots & \chi_N(1) \\ \chi_1(2) & \chi_2(2) & \cdots & \chi_N(2) \\ \vdots & \vdots & \ddots & \vdots \\ \chi_1(N) & \chi_2(N) & \cdots & \chi_N(N) \end{vmatrix} \tag{2.6}$$

where $(N!)^{-\frac{1}{2}}$ is a normalization factor. Note that the columns and the rows of *N*-electron Slater determinant are labelled by spin orbitals and electrons respectively.

Application of the minimization procedure leads to the general Hartree-Fock (HF)

equations for the spin-orbitals which transform to the canonical Hartree-Fock equations after a unitary transformation

$$\hat{F}\chi_j = \epsilon_j \chi_j \tag{2.7}$$

where $\hat{F}$ is the one-electron Fock operator defined as

$$\hat{F} = \hat{h} + V_{HF} = \hat{h} + \sum_i (J_i - Ki) \tag{2.8}$$

where $\hat{h}$ is one electron operator which describes the motion of a single electron in the field of the nuclei, while the Hartree-Fock potential (V_{HF}); two-electron operator, describes the interaction of each electron with the average field generated by the total electron density. The Hartree-Fock potential consists of the Coulomb operators (J_i), describing the electrostatic repulsion between the electrons and the exchange operator (K_i), a direct consequence of the antisymmetry of the many-electron wave function.

In modern computational chemistry, the molecular orbitals (MO) are described by the linear combination of atomic orbitals (LCAO) in a many-electron system. The molecular orbitals spanned by a finite set of basis functions ϕ_p is the second approximation in electronic structure theory. For *M* basis functions,

$$\chi_j = \sum_p^M C_{pj}\phi_j \tag{2.9}$$

where C_{pj} are the expansion coefficients of basis functions ϕ_p. By expanding the unknown MOs χ_j with known basis functions ϕ_p and substituting in Eq. 2.7 results in *M* linear equations that are called the Roothaan-Hall equations [163, 164]

$$\mathbf{FC} = \mathbf{SC}\epsilon \tag{2.10}$$

where $\mathbf{S}$ is the overlap matrix with elements $S_{ij} = \langle\phi_i|\phi_j\rangle$ and $\mathbf{F}$ is the matrix representation of the Fock operator with elements $F_{ij} = \langle\phi_i|\hat{F}|\phi_j\rangle$, $\mathbf{C}$ is a coefficients matrix and ϵ is the diagonal matrix of molecular orbital energies ϵ_i. The Eq. 2.10 is a matrix equation and can be solved by numerical iterative methods for coefficients and orbital energies. The Hartree-Fock method is widely used as an approximation for many-electron problems. Accordingly, every electron moves in the potential created by the nuclei plus the average potential of the other electrons. This leads to what is known as the independent particle model which essentially reduces the many-electron problem to the solving a set of coupled single electron equations. In the independent particle model, a molecule can be described with a set of one-electron wave functions. The one-electron Hamiltonian contains the kinetic energy of the electron and the potential energy of the electron in the field of the nuclei. A spatial function ϕ –an orbital and a

corresponding energy eigenvalue, obtained by solving the Schrödinger equation with this Hamiltonian are associated with each electron. Not only the spatial function, but also the spin, describes the electron. However, an *N*-electron wave function cannot simply be expressed as a product one-electron space and spin functions (spin orbitals) χ – it also has to be antisymmetric in order to obey the Pauli exclusion principle.

2.2 Electron correlation

As already mentioned, the Hartree-Fock method produces energy higher than the true energy. There are two major assumptions used in the Hartree-Fock namely (i) each electron moves in the field of the nuclei and average field of other electrons discarding the instantaneous interaction between electrons and (ii) the wave function can be written as a single Slater determinant which introduces an error in the wave function and the total energy. In addition, this theory lacks electron correlation effects and its incorporation is by no means trivial. The correlation energy E_{corr}, also referred to as electron correlation, is the difference between the exact non-relativistic energy E_{exact}, and the non-relativistic Hartree-Fock energy E_{HF}

$$E_{corr} = E_{exact} - E_{HF} \tag{2.11}$$

The electron correlation can be separated into two categories: dynamic and static. The dynamic correlation is short range and related to the movements of individual electrons. It corresponds to the decreased probability of finding electrons near each other due to Coulomb and Pauli repulsion. The assumption to approximate the electron's Coulomb interaction with other electrons via average charge density neglects the correlated motions of electrons with opposite spins. Static correlation (long range) becomes important for systems where molecular wave functions are degenerate or nearly degenerate or when the electronic wave function of a molecule is not accurately described by a single Slater determinant, i.e. when the actual wave function is described by the mixing of electronic configurations rather than single electron configuration.

2.3 Møller-Plesset perturbation theory

The use of perturbation theory to obtain electron correlation-corrected descriptions of the electronic structure of atoms and molecules has been started from the early days of quantum chemistry. In 1934, Møller-Plesset proposed the HF wave function and the corresponding HF energy can be used as zeroth order approximation to the exact wave function and energy, respectively. Møller-Plesset perturbation theory, abbreviated as MP$_n$, where *n* stands for order of the perturbation included in the calculations.

MP_n differs from second order perturbation theory by the choice of the perturbation operator. Møller and Plesset [165] suggested to use the Hartree Fock calculation as a starting point with zeroth order Hamiltonian as a sum of Fock operators

$$\hat{H}_0 = \sum_p \hat{f}_p \tag{2.12}$$

and the remaining term of the exact Hamiltonian as the perturbation

$$\hat{H}_1 = \sum_{p \geq q} \frac{1}{r_{pq}} - \sum_{p,i} [\hat{j}_i(p) - \hat{K}_i(p)] \tag{2.13}$$

where $\hat{j}_i(p)$ and $\hat{K}_i(p)$ are the Coulomb and exchange operators of electron p. Eq. 2.13 is also called either the correlation or the fluctuational potential. The zeroth-order wave function, the HF wave function ($\Psi_{(0)} = \Phi_{(HF)}$) is an eigenfunction of the zeroth-order Hamiltonian. The corresponding eigenvalue is given by the summation of occupied orbital energies:

$$E^{(0)} = E^{orb} = \sum_i^{occ} \epsilon_i \tag{2.14}$$

Applying the perturbation operator, the sum of zeroth-order and first-order perturbation energy results in a HF energy which was first computed by Møller and Plesset [165]. In order to introduce the correlation energy, one needs to apply second or higher order in the perturbation. Systematic studies using MP2 and higher order perturbations revealed that the method does not necessarily converge due to oscillating potential terms. The detailed studies on orderwise convergence rate, as well as the existence of convergence and its dependence on the precise chemical system have been presented by Leininger *et al*. [166]. Second order Møller-Plesset (MP2) [165] is nowadays the most used level of MP calculations and provides the best accuracy with respect to computational cost. It is important to remember that the MOs obtained from HF are not re-optimized at the MP2 level due to which all deficiencies of these orbitals are carried over to MP2. Spin contamination and symmetry breaking may be resulted as a consequence of unrestricted MP2 theory level.

2.4 Density functional theory

The methods described so far use the wave function as a central quantity and attempt to reach the exact energy by using the exact Hamiltonian and improving the wave function. However, it is clear that the wave function contains more information than needed. The idea of using the electron density as the main variable dates back to the advent of quantum mechanics. The electron density being a function of only three

space dimensions in contrast to a wave function (which has 3 dimensions per electrons) describes the complicated physics behind the many-electron interactions constituting a system. This is the principle of density functional theory (DFT).

The idea was rationalized by Hohenberg and Kohn [167] who proved that the density uniquely defines the Hamiltonian, which in turn implies that all necessary information is contained in density and that the energy could be written as a universal functional of ground state density. Electron-nuclei and electron-electron Coulombic interactions are a known functional of density, but the main problem is to determine the functional for kinetic energy and exchange-correlation terms. Several attempts have been made to derive such functionals based on analytical models, but with limited success. The main problem with those models is the kinetic energy, as it is of the same magnitude as the total energy (from the Virial Theorem). Therefore, a small error in its description results in catastrophic consequences. Kohn and Sham [168] suggested to reintroduce the wave function as a system of non-interacting electrons. Therefore, they constructed a fictitious system of non-interacting electrons with a density which is equivalent to density of a real system. The exact wave function of this non-interacting electron system is a single Slater determinant. This approximation represented a great leap forward for DFT as the kinetic energy of real system is far better approximated with the kinetic energy of this fictitious system than previously existing functionals. Currently, the Kohn-Sham framework is used in almost all DFT calculations. However, it is worth noting that efforts to develop orbital-free DFT are ongoing, due to a significant increase in the computational cost of DFT with orbital introduction. After the Kohn-Sham solution to the kinetic energy functional, DFT still needed the exchange-correlation as a functional of density. The local density approximation (LDA) functionals based on analytic formulas and accurate calculations on the uniform electron gas was the first step towards the solution of this problem. The main problem with LDA is that it treats all the system as uniform which limits this approximation especially for systems with highly non-local exchange term. In order to move forward, gradient information of density may be included into exchange-correlation functionals, giving the so-called generalised gradient approximation (GGA). These semi-local functionals can lead to significant improvements with accuracy, approaching the already established wave function methods, but for a cost similar or less than HF. Developments in DFT functionals then went into different directions. Some kept on improving GGA or meta-GGA functionals (the latter depending also on the second derivative of the density), while others continued in Kohn-Sham's steps by introducing more and more wave function terms with first the hybrid [169] and range-separated hybrid [170] functionals containing some HF exchange and then the double-hybrid [171] containing some wave function correlation.

2.5 Multi-configurational methods

The HF wave function is based on the mean field approximation. The wave function ansatz implies that the electrons are moving in the field of the nuclei and the average field of the other electrons. The instantaneous reaction to the motion of the other electrons is neglected, which is often called the neglect of electron correlation. Depending on the system, this may be a serious approximation, leading even to qualitatively incorrect results. In this section, different methods to include effects of electron correlation starting from the HF wave function are discussed.

2.5.1 Configuration interaction

The HF wave function ψ, is approximated by a single Slater determinant, but in configuration interaction (CI) a linear combination of all possible determinants formed from complete set of spin-orbitals χ's as a better approximation of N-electrons wave function. Slater determinants are built by taking into account all possible ways of arranging electrons in complete basis set

$$\Psi = c_0\phi_0 + \sum_{ia} c_i^a \phi_i^a + \sum_{\substack{i<j \\ a<b}} c_{ij}^{ab} \phi_{ij}^{ab} + \cdots \tag{2.15}$$

where c's are expansion coefficients (weights), ϕ_0 is the ground state HF wave function, complemented by a series of excited determinants. The singly excited determinants ϕ_i^a are equal to the HF reference, but with an electron excited from occupied molecular spin-orbital χ_i to unoccupied, virtual, spin-orbital χ_a. Virtual spin-orbitals are the one that form, together with the occupied spin-orbitals, a complete orthonormal set. ϕ_{ij}^{ab} is a doubly excited configuration state function involving excitations from spin-orbitals χ_i to χ_a and χ_j to χ_b. The wave function with all possible (up to N-fold) excitations together with the HF wave function constitutes a complete set. The procedure given by Eq. 2.15 in which all N-electrons are promoted from occupied to virtual spin-orbitals is referred to as the full CI. Full CI is computationally very expensive; therefore a truncation scheme is often applied up to a specified excitation level.

2.5.2 Multi-configurational self-consistent field methods

The static correlation based on multi-determinantal spin-orbitals is captured with the help of multi-configurational self-consistent field (MCSCF) method. In MCSCF, not only the coefficients C_{pj} Eq. 2.9 of spin-orbitals χ's but also the expansion coefficients c's for determinants of Eq. 2.15 are optimised, which makes the calculation computationally more demanding. As a result of optimising both sets of coefficients, more accurate results can be achieved with a smaller number of configuration state functions (CSFs). The selection of the necessary configurational space for the property of interest

is the major problem with MCSCF methods. Contrary to full CI in which the complete molecular spin-orbital space within a given basis is used; in MCSCF, a CI calculation within a selected subset of molecular spin-orbitals is performed. The MCSCF results obtained by performing full CI calculations for a subset of the molecular spin-orbitals is called the complete active space self-consistent field (CASSCF) method [172].

The CASSCF method constructs the wave function from two sets of molecular orbitals namely, active and inactive orbitals. The inactive orbitals are constrained to be doubly occupied or empty throughout the calculation and in active orbitals all permutations consistent with spin multiplicity and system symmetry are allowed. The CASSCF wave function method therefore, constitutes a full CI within the active orbitals (active space) as shown in Fig. 2.1a. In this way, an active space defines the realm in which the electrons can form all configurations giving all the excited states in addition to the ground state. The sound knowledge of the molecular system and its chemical properties under considerations is mandatory to select an active space so that all electronic excitations of interest are covered. Usually, selection of the active space is based on the inclusion of full π electronic system with chemically important lone pairs [173]. However, this recommendation becomes rather impractical for larger molecules due to restriction imposed by computational cost on size of active space. It is important to remember that the energy optimization of several states in the CASSCF calculations should be treated in a state-averaged manner to ensure the orthogonality of the different wave functions [174]. A common notation for the active space of CASSCF is [n, m] indicating n electrons distributed in m orbitals.

It is possible to restrict the rapid growth of CSF with the increase of MOs in the active space by splitting the active space into three subspaces as explained in Fig. 2.1b. The first subspace RAS1 includes orbitals which are mostly doubly occupied, but have the flexibility of a maximum number of holes. The second subspace RAS2 is equivalent to the active space in CAS type wave functions, i.e. all occupations are allowed. The third subspace RAS3 includes mostly unoccupied orbitals, but may have a maximum number of electrons. This way of subdividing the active space is referred to as the restricted active space SCF (RASSCF) method [175]. The RASSCF method is very versatile, since the wave function expansion can be equivalent to that of previously mentioned methods by choosing the active space in specific ways.

The RASSCF method is very useful for calculations with specific cases of ionized-excited or core-excited states. When all the valence orbitals (occupied and unoccupied) in the active space are placed in the RAS2 subspace, the core orbitals may be chosen to belong to the RAS1 or RAS3 subspace. In general, the best choice is to put the N_c core orbitals in the RAS3 subspace and allow one hole ($2N_c$-1 electrons) in this subspace which will ensure that the lowest states are those states which have a single core-hole as shown in Fig. 2.1c. Furthermore, the wave function collapse during the

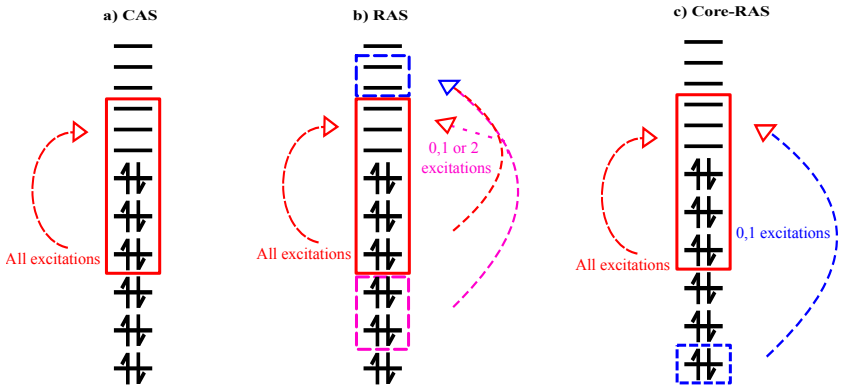

FIGURE 2.1: Illustration of the **a**) **CAS** : the active space is divided into the active and the inactive orbitals. A full CI is constructed in active orbitals. **b**) **RAS** : active space is divided into three subspaces. Doubly occupied orbitals are placed in RAS1 with flexibility of a maximum number of holes. All orbitals without occupational constraints are kept in the CAS equivalent subspace RAS2 and RAS3 subspace consisting of unoccupied orbitals where maximum number of electrons can be controlled. **c**) **Core** − **RAS** : RAS2, a CAS equivalent subspace without occupational constraints and RAS3, consisting of core-electrons with control over number of holes, generally, at most one electron is allowed to be excited.

RASSCF calculations and the presence of irrelevant low-energy configurations during the calculation of core excitations are avoided by grouping the active space in this way. This method is referred to core-RAS method [176] with a drawback that the CI expansion includes all (up to $2N_c$-fold) excitations from the core orbitals and, even though their contribution to the wave function is negligible, the number of determinants may become too large. If that is the case, placement of the core orbitals in the RAS1 subspace with up to one hole would be a better choice. The disadvantage of the core orbitals in RAS1 subspace is that the lowest states are states without a core-hole, which complicates the calculations. All computed results involving core-hole states in this thesis are obtained by using core-RAS method.

2.5.3 Multi-configurational perturbation theory

The use of the CASSCF wave function method accounts for quasi-degenerate correlation effects, often referred to as static or non-dynamic correlation. It describes the correlation between two largely separated electrons, e.g., a full valence CASSCF wave function will always dissociate a molecule correctly. However, the CASSCF wave function lacks the dynamic electron-correlation: only a small portion of the correlation energy of the electrons is captured by the CASSCF method. The dynamic electron-correlation energy needs to be included either by multi-reference CI (MRCI) treatment or second-order perturbation theory [177, 178]. In this work, the second order perturbation theory is used in which N-electron Hamiltonian is splitted into

reference and perturbed Hamiltonian (a two-electron operator). In perturbation theory, the correction to energy is computed by taking into account all combinations where two electrons in the reference wave function are excited to virtual orbitals. The CASSCF/RASSCF wave function is used as a reference wave function for second order perturbation theory CASPT2/RASPT2. The extensive use of the CASPT2 method in describing the electronic spectra of a wide range of molecular systems over the years revealed several shortcomings that arise from the use of a multiconfigurational wave function and a truncated active space. Examples of artifacts are the appearance of so-called intruder states and the strong mixing of valence-Rydberg states [179]. However, the problem of intruder states often arises in the use of the CASPT2 method. The reason for this problem is a substantial lowering of the energy of an electronic state resulting from perturbational correction that is not captured by the CASSCF reference wave function. The solution for this problem is the use of an imaginary shift, by adding a constant to the zeroth-order Hamiltonian. In addition to this limitation, the use of CASPT2 method has led to problems in calculating the potential energy surfaces at avoided crossings [180]. The CASPT2 method can be either used with a single reference state or with a two or more state-average states given by a multiconfiguration CASSCF type wave function giving rise to single state CASPT2 (SS-CASPT2) [181,182] and multi-state CASPT2 (MS-CASPT2) [183] respectively. In the latter method, the single-state CASPT2 is allowed to mix via an effective Hamiltonian. The studies presented in this thesis use both SS-CASPT2 and MS-CASPT2 methods.

2.6 Computing excited states

The ground state solution of the Schrödinger equation provides many chemically relevant properties of system. Different spectroscopic methods are in experimental use to analyse the structure and properties of matter. Specifically, theoretical methods for obtaining the excited state wave functions to obtain energies and other molecular properties (such as dipole moments) of a system have become a major tool to analyse experimentally observed spectral features.

Excited states are a direct consequence of computing full CI as higher order eigenvectors and eigenvalues of the Hamiltonian. Since all MCSCF methods, with or without perturbative corrections, also involve some form of CI expansion, they are also able to compute an arbitrary number of eigenvalues and eigenvectors. CASSCF coupled with CASPT2 is among one of the most accurate multi-configurational methods for computing excited states. Besides the high computational costs of CASSCF methods, the choice of active and configuration space is another disadvantage affecting their accuracy because photochemical excitations and static correlation highly depends upon this choice. For core-level spectroscopy, the core-RAS formalism is a convenient way to compute excited states within the state-averaged (SA-RASSCF)

method with a single set of molecular orbitals but with unique CI expansion coefficients for each state. In SA-RASSCF method, many states can be computed simultaneously without optimising each of them in a state specific fashion and also orthogonality of the different computed states is ensured. Dynamic correlation to each SA-RASSCF state is added by MS-CASPT2 method with the only limitation that this approach creates singularity points for states close in energy.

For single-reference calculations, a class of methods employing the ground state scheme to both the excited state and the ground state to compute energy difference is referred to as the ΔSCF method. In the ΔSCF scheme, the orbital occupation has to be fixed by symmetry or by spatial constraints in order to avoid variational collapse in the excited state. In the ΔSCF method, the excitation energies are found by means of single-reference SCF calculations for different electronic configurations. This method can be difficult to converge and is not strictly rigorous for DFT as the theory is normally valid only for the ground state [184]. A commonly used zeroth-order method to compute excited states of variety of molecular systems is CI singles (CIS). In CIS approach, the wavefunction is obtained by linear combination of all single excitations in HF wavefunction. CIS approach is very useful to get insight into charge transfer states and can be used to compute many excited states. Another very common way to deal with excited states is to add the electromagnetic field of the light in the Hamiltonian and to solve the resulting time-dependent Schrödinger equation, usually by (perturbative) linear response methods. One thus obtains the so-called time-dependent HF (TD-HF), also known as random phase approximation (RPA), which is very similar to the CI singles (CIS). When this approach is used for DFT, the resulting equations are the time-dependent DFT (TD-DFT) [185], which are now the popular methods to compute excited states. On top of the intrinsic approximations of methods (HF or DFT), these methods also have errors arising from the linear response approximation. In particular, TD-DFT is unable to describe charge-transfer excitations, spin-orbit coupling for heavy open shell systems and can only describe single excitations within the adiabatic approximation [186, 187].

2.7 State interaction

Many properties of interest are related to matrix elements of one-electron operators between the ground state and some excited states. These include transition dipole moments to calculate the intensity of electronic transitions in spectroscopic studies. To find the required matrix elements, independent states are computed with the CASSCF wave function methods which are further utilized to find interactions between these states by using the state interaction procedure. Let us assume that two states functions

(i.e., $|\Psi_1\rangle$ and $|\Psi_2\rangle$) are expressed on different, mutually non-orthogonal orbital basis

$$|\Psi_1\rangle = \sum_{\mu} C_{\mu}^{A} \Phi_{\mu}^{A} \tag{2.16}$$

$$|\Psi_2\rangle = \sum_{\mu} C_{\mu}^{B} \Phi_{\mu}^{B} \tag{2.17}$$

where the index μ is a list (p...q) of the occupied orbitals. Φ_{μ}^{A} is the CSF on the basis of SD constructed by some specific spin-coupling scheme with a set of orbitals χ_{p}^{A} and likewise for index B. The transition matrix element for a one-electron operator can be written as expression:

$$\langle \Psi_1 | \hat{f} | \Psi_2 \rangle = \sum_{\mu,\nu} \sum_{p,q} C_{\mu}^{A} C_{\nu}^{B} A_{pq}^{\mu\nu} \langle \chi_{p}^{A} | \hat{f} | \chi_{q}^{B} \rangle = \sum_{p,q} \Gamma_{pq}^{AB} f_{pq} \tag{2.18}$$

where $\Gamma_{p,q}^{AB}$ contains the dipole matrix element which can be computed from two sets of CI expansion coefficients and one-electron operators coefficients

$$\Gamma_{p,q}^{AB} = \sum_{\mu,\nu} C_{\mu}^{A} C_{\nu}^{B} A_{pq}^{\mu\nu} \tag{2.19}$$

and $f_{pq} = \langle \chi_{p}^{A} | \hat{f} | \chi_{q}^{B} \rangle$ is the matrix element of the operator $\hat{f}$ over a basis of orthonormal one-particle orbitals.

RASSCF wave functions describing two electronic states are used to calculate the transition dipole moment between them using the method of Restricted Active Space State Interaction (RASSI) module implemented in MOLCAS package. The RASSI method calculates the electronic dipole transitions based on either RASSCF wave function, or CASSCF-type wave function using Eq. 2.18. It is noteworthy to mention that the RASSI method computes the interaction among CASSCF states expanding the same set of configurations i.e., having the same active space size and number of electrons.

The RASSI method can use spin-free states as a basis to compute spin-orbit interactions matrix elements and the spin-orbit eigenstates are then obtained by diagonalising the spin-orbit interaction matrix. Apart from computing dipole transition elements, the RASSI method can be used to compute overlaps and Hamiltonian matrix elements which are further used to compute electron transfer rates.

2.8 Core-level spectroscopy

The electronic structure of molecules can be divided into the inner shell (core) orbitals and outer shell (valence) orbitals. The formation of chemical bonds results from the

electrons in valence orbitals with binding energies in the range of visible or ultraviolet light. The nature of a chemical bond can thus be understood by analysing the valence electronic structure. The core-electrons, on the other hand, are localized around the atomic centres (nuclei) with well-separated binding energies, usually in the X-ray region of the electromagnetic spectrum. They do not take part in the formation of a chemical bond and can be considered 'inert' to the chemical state of an atom or a molecule. The core-level of a specific element has its characteristic spectrum at which it absorb energy, therefore, spectral features originating from a specific element are easily identified. This ability to probe the local and geometric structure around a specific element in a molecule by examining X-ray spectra result in considerable interest in using core-level spectroscopy as a tool.

The spectroscopic calculations used in this thesis are mainly in the soft X-ray regime in which the wavelength of the radiation is longer than the atomic dimension (~ 1). Therefore, the transition probability of dipole-allowed transitions dominate over electronic quadrupole or magnetic dipole transitions which are significantly weaker. This assumption is called the dipole approximation. In this thesis, spectral features on the nitrogen K-edge and the sulfur K-edge in dipole approximation regime are explained using multi-configurational quantum chemical methods.

2.8.1 X-ray absorption spectroscopy

X-ray absorption spectroscopy (XAS) is an element specific technique which measures the absorption as a function of incident X-ray energy E_{in}. XAS of any material, be it atomic or molecular, is characterised by absorption edges. For a particular edge, an electron is initially excited to empty or partially filled orbitals yielding information about the unoccupied density of states. The absorption edge is defined by the energetic position of a specific shell (K, L, M...) of an element making X-ray spectroscopy an element specific probe of the electronic structure. The K-edge absorption corresponds to an excitation of a 1s core electron into the empty 2p level and an L-edge absorption to the excitation from a 2s or 2p level to an unfilled d orbitals as shown in Fig. 2.2.

The oxidation and spin state of the absorbing atom can be characterised by the energy of the absorption edge. The cross-section of electronic transitions between two states can be described by the Fermi's Golden Rule, which treats light field within first order perturbation theory for the light field and the light-matter interaction is treated in the semi-classical approximation. The absorption cross-section is expected to be linearly proportional to the transition probability from an initial state to a final state. The X-ray absorption cross section is written within the one-electron transition model

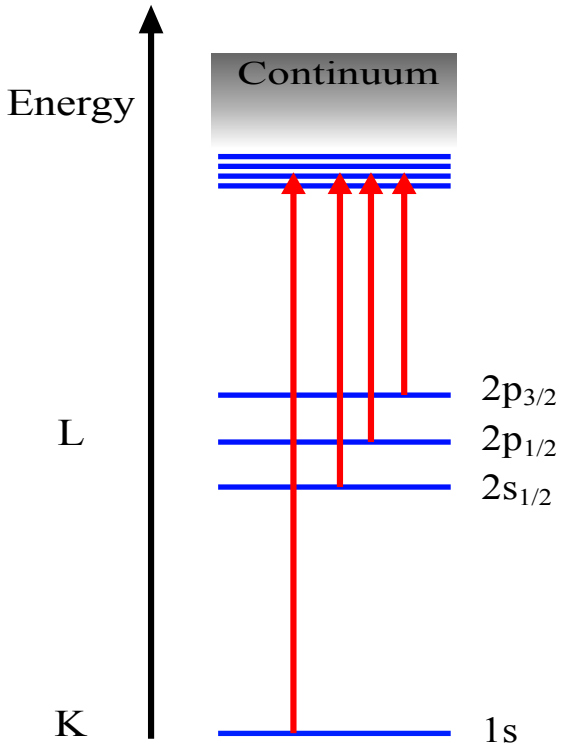

FIGURE 2.2: Schematic depiction of the relationship between X-ray absorption edges and the corresponding excitations of core electrons is shown. The excitation corresponding to the K and L X-ray absorption edges are shown. The threshold energy difference is displayed by arrows. Any transitions higher in energy to the continuum are also allowed.

in terms of a dipole matrix element from initial state $|g\rangle$ to $|f\rangle$

$$\sigma\left(\omega'\right) = \frac{4\pi^2 e^2}{3\hbar c}\hbar\omega' \sum_f |\langle f|\hat{T}|g\rangle|^2 \times \frac{\Gamma_f/2\pi}{(\hbar\omega_f - \hbar\omega_g - \hbar\omega')^2 + \Gamma_f^2/4} \tag{2.20}$$

where $\hbar\omega'$ is the incident photon energy; $\hbar\omega_g, \hbar\omega_f$ are energies of ground and intermediate states and the parameter Γ_f is the core-hole lifetime broadening, e is the elementary charge and c is the speed of light. The matrix elements of the transition operator $\hat{T}$ between two states $|f\rangle$ and $|g\rangle$ are given by Eq. 2.18. An electric dipole transition will only take place if the transition dipole matrix element for the corresponding transition is non-zero. If the cross-section for an electric dipole transition operator is zero, the transition is forbidden. The chemical information that is contained in each transition is governed by the nature of the atomic and valence orbitals of the surrounding atom. Due to the atomic nature of X-ray absorption spectroscopy, the transitions corresponding to each edge follow the standard selection rule of atomic spectroscopy

($\Delta\ell$=$\pm$1). Dipole-allowed transition from 1s to 2p levels are probed in K-edge spectroscopy whereas electronic transitions from 2p to 3d energy states are dominant in L-edge spectroscopy.

The region around the absorption edge up to 20-50 eV corresponds to the X-ray Absorption Near Edge Structure (XANES). In this region, photoelectrons with low energies undergo multiple scattering events which enables XANES to provide information about the three dimensional structure around the absorbing atom (bond distances and bond angles) in many biological systems [188], surfaces [189], solids and solutions [190]. Extended X-Ray Absorption Fine Structure (EXAFS) is obtained by excitations from a core level to the continuum states, far from the threshold (>50 eV). Due to higher energies, single scattering events of the photoelectrons usually dominate as scattering cross-section decrease with increasing energy. The information about coordination number and bond distances of first coordination shell around the absorbing atom can be obtained in EXAFS region.

XAS spectra can be obtained by fluorescence yield (FY) and total electron yield (TEY). The FY method is based on the detection of emitted photon due to relaxation of electrons from the excited state. If no energy discrimination of the out coming photons is employed in the detection method and a spectrum is obtained by a summation over all emitted photons, then the term total fluorescence yield (TFY) is used to describe the technique. Measured TFY spectra suffer distortions due to self-absorption and saturation effects [191, 192]. Monitoring a particular fluorescence transition or a set of transitions using an energy dispersive detector is called partial fluorescence yield (PFY). The contributions from undesired electronic transitions are avoided by selecting emitted photons with high energy precision [193]. The total electron yield (TEY) measurements detect the number of electrons that are ejected from a sample as a function of excitation energy. This quantity is proportional to the number of photons absorbed by the sample at a given energy. Electrons from the ground flow into the sample due to the removal of an electron from the sample resulting in a current [194] which can be measured.

Time-resolved absorption spectroscopy

Time-resolved spectroscopy encompasses a valuable set of techniques that allow for probing and characterizing electronic and structural dynamics in isolated and solvated molecules. A complete photophysical profile of the ensemble under investigation is obtained by utilizing the flexible and tunable light sources with wide range of spectral and temporal resolution. In time-resolved X-ray absorption spectroscopy, a sample is promoted to electronically excited state by means of an excitation (pump) pulse. The simplest and most common method of measuring transient spectrum is schematically shown in Fig. 2.3. To avoid multiphoton/multistep processes, a weak probe pulse is sent through sample with a time delay Δt with respect to the pump

pulse. In general, one is interested in the change in absorbance ΔA(λ,Δt) induced by the pump pulse defined as the difference between the absorbance of the pumped (A$_p$(λ,Δt)) and the unpumped sample (A$_u$(λ)).

$$\Delta A(\lambda, \Delta t) = A_p(\lambda, \Delta t) - A_u(\lambda) \tag{2.21}$$

The change in absorbance ΔA(λ,Δt) contains the information required to explain the dynamical processes such as excited state energy migration, chemical reaction pathways, isomerization, electron and/or photon transfer processes and intersystem crossings occurring in the photosynthetic system under study [154, 195].

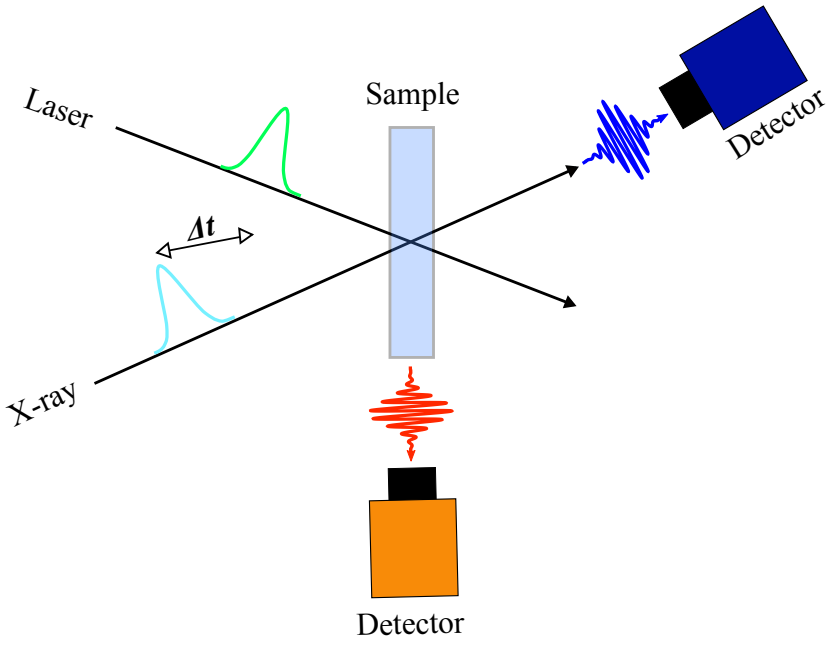

FIGURE 2.3: Schematic depiction of a typical time-resolved XAS setup for the study of liquid samples. The continuously-refreshed sample can be a flow-cell, high speed liquid jet or a flow capillary. Δt is the time delay between laser pump and X-ray probe.

Time-resolved X-ray absorption spectroscopy (TRXAS) is a tool, capable to follow reaction dynamics with element specificity. It is possible to track the structural dynamics of the relevant atomic species in a ultrafast chemical reaction by combining the high chemical specificity of spectroscopic techniques with time resolved methods. TRXAS has an advantage over valence spectroscopic techniques to follow the electronic and molecular structure during photochemical reaction as it exploits the fact that atomic species with different spin and oxidation states have distinct spectral features. X-ray absorption spectrum is sensitive to bond order, symmetry and valance charge distributions which helps to identify different intermediates and photoproducts, especially when multiple reaction pathways are available.

2.8.2 X-ray emission spectroscopy

The complementary technique to X-ray absorption is X-ray emission (XES) as it probes the occupied states contrary to absorption measurements which provide an energy resolved picture of unoccupied states in the material. Like XAS experiments, the XES measurements are element-selective, site-selective, and obeying dipole selection rules that determine the symmetry of the electron orbitals that can participate in the transition. The first step in the emission process is to create an excited state through the interaction of a photon with a core electron as in XAS and in the second step, the probability for the relaxation to the final state (the emission process) is explained. XES can be described by a two-step model in which absorption and emission are considered as two decoupled processes. Soft X-ray emission techniques can be divided into two

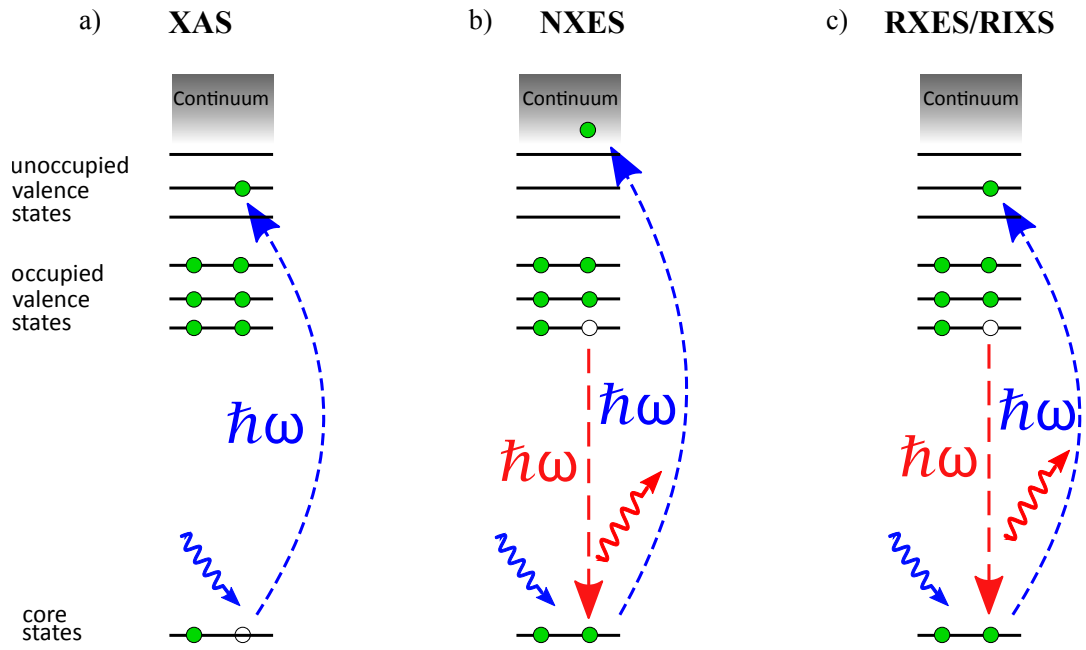

FIGURE 2.4: Schematic representation of **a**) **XAS** : resonant absorption of X-ray photon, promoting a core electron to an unoccupied orbital under the condition of dipole symmetry selection rules. **b**) **NXES** : The molecule is core ionized by an X-ray photon. A valence electron from an occupied orbital of same symmetry, refills the core-hole with emission of a photon. **c**) **RXES/RIXS** : a core electron is promoted to an unoccupied orbital by resonant absorption. The core-hole is filled by a valence electron under selection rules with emission of a photon.

general categories based on the choice of excitation energy as shown schematically in Fig. 2.4. The simplest case is non-resonant X-ray emission spectroscopy. The absorption of a photon above the ionization potential leads to the core ionization of the molecule. This results in fluorescence as an electron from an occupied state relaxes down to fill the core hole. A valuable information about the electronic structure of

the material is obtained by this emitted photon. The spectral weights for this case are largely independent of incident photon energy and $\Gamma_n + \Gamma_f$ corresponds to the lifetime broadening of the spectrum.The other case involves resonant excitation, in which the excitation energy corresponds to an absorption resonance, and so the electron is promoted to a bound state. Resonant excitation is used in resonant inelastic X-ray scattering (RIXS) measurements discussed in the proceeding section.

2.8.3 Resonant inelastic X-ray spectroscopy (RIXS)

In RIXS, the incident photon energy is tuned to the energy of an unoccupied orbital below the ionization potential as shown in Fig. 2.4c. On absorption of an incident photon, several intermediate states are accessible, each with a specific symmetry setting and certain constraints for the decay considering the symmetry and polarization of the emission. The intermediate core-excited states can decay into many final states via emission of a photon. Therefore, coherently coupled absorption and emission processes in RIXS can be considered as a single-step scattering event. Coherently correlated absorption and emission processes are treated by the Kramers-Heisenberg formula [196–198] containing the sum over all possible intermediate and final states. The interference effects between different states close in energy are taken into account by summation over all these states in square modulus of the scattering amplitude

$$F(\omega,\omega') = \sum_f \left| \sum_n \frac{\langle f\,|T_1|\,n\rangle\,\langle n\,|T_2|\,g\rangle}{\hbar\omega_g - \hbar\omega_n - \hbar\omega + i\frac{\Gamma_n}{2}} \right|^2 \times \frac{\frac{\Gamma_f}{2\pi}}{(\hbar\omega_g - \hbar\omega_f - \hbar\omega + \hbar\omega')^2 + \frac{\Gamma_f^2}{4}} \tag{2.22}$$

where $\hbar\omega$ and $\hbar\omega'$ are the energies of the incident and emitted photon; $\hbar\omega_{g,n,f}$ are energies of electronic configurations involved and T_1 and T_2 are transition dipole operators. The energies of all intermediate and final states are related to same reference state by defining $\hbar\omega - \hbar\omega'$, the energy transfer. The matrix elements of dipole operators between two states are given by Eq. 2.18 as implemented in the RASSI program. RIXS being a second-order process can be described by coherently coupled absorption and emission processes. Due to this coupling, interference effects of intermediate states decaying to the same final state are characteristic for this type of spectroscopy [196, 199]. The spectra are broadened by Γ_n along incident energy and by Γ_f along energy transfer $(\hbar\omega - \hbar\omega')$, where Γ_n and Γ_f are the lifetime broadening of intermediate and final states respectively.

Among the many salient features, RIXS helps to understand the chemical sensitivity of the different types of atoms in a simple way due to its ability to be an element and an orbital specific by tuning the incident photon energy. Such transitions are

called absorption edges. With distinguishable absorption edges, RIXS can individuate different valencies, the inequivalent chemical bondings sites or inequivalent crystallographic positions of same the chemical element [196, 197]. In addition, by tuning to electronic excitations at different X-ray edges of the same chemical element (K-edge and L-edge); a variety of information can be collected. Compared to the available spectroscopic methods, RIXS uniquely combines the advantages of bulk sensitivity, momentum and energy resolution, while at the same time requiring only small sample volumes. The inelastic transitions are further categorised as d-d transitions and charge transfer transition. Transitions in the range of 0-5 eV are termed as d-d transitions while charge transfer transitions often occur in the range of 4-15 eV. RIXS offers a much higher spectral resolution when compared to XES. The reason for sharper spectral line width lies in longer lifetime of the final state contrary to XES in which the intermediate state limits the spectral resolution. Final states do not contain a core hole, which results in a comparatively longer lifetime and therefore narrower peak width of the final state. The limitation of RIXS lies in its complex instrumentation. It requires an intense and tunable photon beam to collect a reasonable amount of scattered photons. However this requirement for high photon flux can be fulfilled by a synchrotron source.

Chapter 3

The influence of hydrogen bonding and electrostatic interactions on nitrile groups

Understanding the influence of hydrogen bonding on the molecular level is a fundamentally important challenge. *Ab initio* quantum chemistry calculations give explicit access to each electronic state and help to unearth the electronic character of every final valence excitation. In addition, these calculations are of great use to determine the origin of nitrogen-specific Raman spectral features from resonant inelastic X-ray scattering (RIXS). Furthermore, the effects of hydrogen bonding on valence charge density, the interplay between the valence orbitals and the associated molecular structural changes were investigated with nitrogen-1s RIXS spectroscopy. RIXS spectroscopy is a uniquely suited method to provide quantitative information on electronic structure details such as covalency, charge delocalization, and spin/oxidation states.

A detailed theoretical study to probe the influence of hydrogen bonding and electrostatic environment of an electric dipole on the electronic structure of hydrogen cyanide (HCN) was employed. The relative involvement of different molecular orbitals (MO) was elucidated with highest chemical specificity to determine the origin of nitrogen-specific Raman spectral features from RIXS. For the calculations of the nitrogen-1s RIXS spectrum, the first principles multi-reference RASSCF method with active space comprising mainly of the orbitals having π, σ and π^* characters was used with no symmetry imposed. On comparison of isolated HCN and HCN-water, the spectral shifts of transitions originating from the lone pair orbital on the nitrogen atom were an indication of its stability. The predominant electrostatic nature in this weak hydrogen bonding was demonstrated and linked to the anomalous frequency shift of the nitrile stretching vibration by replacing water molecules with an electric dipole. The placement of dipole charge distributions on a distance equal to the hydrogen bond distance along the nitrile group leads to a CN bond strengthening by lowering of lone pair orbital energy. In addition, computed vibrational modes and blue shift of the Raman UV line at 10.5 eV was also in good agreement with the literature. The dominant

transitions based analysis is used to understand altered charge distributions caused by electrostatic dipole field. The weakening of the CN bond, reshuffling of σ and π originated dominant transitions and the splitting of π orbitals relaxations due to molecular symmetry breakage were significant changes on the placement of dipole perpendicular to the nitrile group. In addition, the induced effects with dominant contributions from electrostatic interactions were not linked to any particular ligand around the nitrile group. The results based on this study show that *ab initio* quantum chemistry calculations are helpful in combining electronic and structural probes for comprehensive understanding of a nitrile model system subjected to hydrogen bonding and electric dipoles. Understanding the effects of electrostatic interactions of electric dipole is useful to unearth the nitrile response to such interactions on an atomic level in a systematic way and may act as a probe of electrostatic environments in solvated systems and small peptides.

This approach was taken one step forward: computational findings are further elaborated by an experimental study using acetonitrile as a model system and employing XAS and RIXS to specifically study the influence of hydrogen bonding on the electronic structure of this molecule. The choice of acetonitrile for experimental study is due to toxic effects and considerable dissociation of HCN in water. Acetonitrile is an important solvent and cosolvent for many hydrophobic and hydrophilic materials and has been studied using RIXS at the nitrogen K-edge to investigate different aspects of nitrile groups [84,88]. Also, it is reported that acetonitrile provides two sites for hydrogen bonding namely the lone pair electrons centered on the nitrogen atom and the other on the C≡N triple bond. The former is termed as σ bonding which was only possible energy minima in HCN case and the later, the perpendicular arrangement with triple bond is referred to as π bonding which was not the energetic minimum in case of HCN. Among aprotic solvents, acetonitrile is one that has miscibility with water at any ratio. Therefore, acetonitrile is a good starting point to establish a connection of the nitrile group interactions with its environment already reported for HCN.

The effects of the influence of hydrogen bonding on the electronic structure of acetonitrile and acetonitrile-water complex were investigated using XAS, RIXS and electronic structure calculations. These calculations give explicit access to each electronic state with the extracted information allowing assignment of the dominant transitions in the X-ray absorption spectrum, and unearthing the electronic character of every final valence excitation resulting from RIXS at a specific incident photon energy. Our theoretical results are in very good agreement with experimental spectra, highlighting the sensitivity of RIXS even for weak interactions. In comparison to computed spectrum of the HCN-water complex, similar spectral shifts indicative of stabilization of the lone pair orbital on the nitrogen atom of the acetonitrile-water complex are

observed. Also, the relative shifts of the CN stretching frequency induced by dipole-dipole interactions with a water molecule are in good agreement with computed spectral changes.

Sensitivity of core-level spectroscopy to hydrogen bonding and electrostatic environments of nitrile groups: An ab initio study

Abid Hussain,[1] Nils Huse,[1,2] and Oriol Vendrell[3,4]
[1)] *Max Planck Institute for the Structure and Dynamics of Matter, Center for Free Electron Laser Science, 22761 Hamburg, Germany.*
[2)] *Department of Physics, University of Hamburg, 22761 Hamburg, Germany.*
[3)] *Center for Free-Electron Laser Science, DESY and The Hamburg Centre for Ultrafast Imaging, 22761 Hamburg, Germany.*
[4)] *Department of Physics and Astronomy, Aarhus University, Ny Munkegade 120, DK-8000 Aarhus C, Denmark.*

Ab initio quantum chemistry calculations have been performed to probe the influence of hydrogen bonding on the electronic structure of hydrogen cyanide (HCN). Our calculations determine the origin of nitrogen-specific Raman spectral features from resonant inelastic X-ray scattering (RIXS) occurring in the presence of a water molecule and an electric dipole field. The similarity of the two interactions in altering the electronic structure of the nitrogen atom differs only in the covalent contributions from the water molecule. The CN stretching mode as a structural probe was also investigated to study the electronic origin of the anomalous frequency shift of the nitrile group when subjected to hydrogen bonding and an electrostatic dipole field. The major changes on the electronic structure of HCN are electrostatic in nature and originate from dipole-dipole interactions. The relative shifts of the CN stretching frequency are in good agreement with those experimentally observed.

I. INTRODUCTION

Noncovalent interactions are important for the functionality of biomolecules and play a major role in the structure and dynamics of a wide class of molecular systems.[1–13] Understanding the influence of noncovalent interactions, namely electrostatic, hydrogen bond (HB), and van der Waals interactions, on the electronic structure poses a considerable challenge and has been the topic of extensive studies in protein structure and dynamics.[14,15] A large number of studies on hydrogen bonding at the molecular level have shed light on spectroscopic changes taking place in these complex systems.[16–21] Among the noncovalent interactions, hydrogen bonding is very directional, of short range, stronger than van der Walls interactions, and crucial for proton transfer.

Of the many accepting groups in hydrogen bonds, we have a particular interest in the nitrile group for reasons that we detail below. There are several studies on donor-acceptor interactions of nitrile groups with different solvents to determine electrophilicity and solvation properties. The nitrile group is a weak HB acceptor which is sensitive to hydrogen bonding, solvent polarity, and surrounding electric fields.[9,15,22–32] The presence of a lone electron pair on the nitrogen atom of the nitrile group provides the site for hydrogen bond acceptance of the proton donor group such as water, leading to an anomalous shift of the CN stretching vibration to higher energy. This bond stiffening is unusual because almost all other stretching vibrations of HB acceptor groups (with the exception of diazo and azide groups for instance) display bond softening upon hydrogen bonding.[33] Studies of protein processes have made use of this shift by incorporation of nitrile-derivatized amino acids.[14,15,34,35] Such non-natural amino acids cause only small perturbations in the native structure of proteins and constitute spectrally isolated and well distinguishable vibrational probes for electrostatic environments, charge transfer and migration, and structural dynamics of local protein environments. Accordingly, a number of reports have been published on the use of nitriles as a probe of protein folding and unfolding dynamics, electric field effects on active sites in peptides and proteins, mechanisms of biological information transfer by nucleic acids, and other biological processes.[36–39] It is therefore important to understand and gauge the electronic and structural response of nitriles to electrostatic and hydrogen bond interactions on the atomic level.

The HCN molecule is the simplest molecule containing a nitrile group and represents a good starting point for establishing basic principles of interaction of the nitrile group with its environment. Several prior studies on hydrogen cyanide (HCN)[40–45] exist. However, a combined systematic study of X-ray methods as element-specific probes of electronic and molecular structure is missing. Such an approach would generally highlight the interplay of electronic and structural degrees of freedom. Over the last decade developments in the fields of synchrotron radiation research and sample delivery opened up new scientific avenues for more advanced core-electron spectroscopic methods, allowing for investigation of complex chemical reactions and local effects in heterogeneous environments due to surrounding solvent molecules, interfaces, or electrostatic fields from charge distributions generated by, for instance, protein side chains. *Ab initio* methods help to establish a connection between physical observables and electronic structure to guide the interpretation of spectral features observed experimentally. In particular, solvent-solute interactions can be energetically decomposed into their contributing parts using *ab initio* methods.[17,18,20,21,46]

The nitrogen K-edge provides an element-specific resonance with an initial state having a highly localized 1s-

electron that allows studying the nitrile group in the presence of protic solvents like water and surrounding electrostatic environments directly at the interaction site. As structural and electronic changes generally manifest sensibly in the infrared and the ultraviolet spectral range, respectively, it is of particular interest to understand and link complementary local structural and electronic probes. Such insight could shed light on the origins of the anomalous frequency shift of the stretching vibration of the nitrile group (also found in the corresponding vibrations of the diazo, and azide groups) which has not been satisfactorily explained on the level of atomic charge distributions. This work investigates the response of HCN to model electrostatic environments and relates this response to electronic and structural changes detectable in nitrogen-1s resonance Raman spectra in the ultraviolet (more commonly known as resonant inelastic X-ray scattering or RIXS) and frequency shifts of the CN stretching vibration in the infrared. We compare computed nitrogen-1s RIXS spectra of HCN to the response of the HCN-water complex and similar calculations for dipoles of varying strength in axial and equatorial configuration in order to separate and classify the observed spectral features arising from covalent and purely electrostatic interactions of HCN and water.

RIXS is an element-specific form of resonance Raman

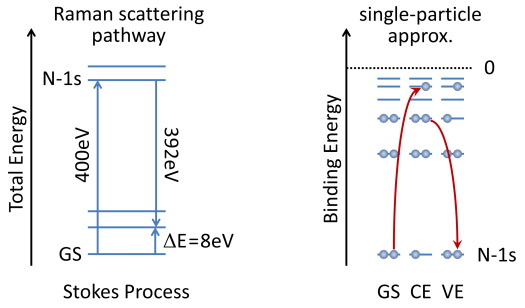

FIG. 1. Schematic representation of Raman processes exploiting a nitrogen-1s core-level excitation. The Stokes process will promote the system into an excited state. Within the single particle picture, the RIXS process that starts from the electronic grounds state (GS) can be subdivided into a core-level excitation (CE), lasting a few femtoseconds, and a subsequent relaxation into a valence-excited (VE) state. A similar excited state could be reached with direct (dipole) excitation but with different quantum mechanical selection rules.

scattering, in which a core-excitation of a particular element is exploited to achieve chemical specificity while obtaining Raman spectra of molecular excitations. The Raman process is not limited to vibrational excitations but can be employed to measure element-specific electronic spectra in the visible and ultraviolet as Fig. 1 illustrates. An X-ray-initiated Stokes process can result in an electronic excitation in the ultraviolet while an anti-stokes process in the multi-eV range cannot be effected thermally under standard temperature and pressure conditions. However, anti-Stokes scattering pathways have been exploited using short light pulses (promoting the molecular system into an electronically excited state).[47] As customary in Raman spectroscopy, the energy difference between incoming and inelastically scattered photon (the energy loss) is plotted which provides the studied system's vibrational and valence electronic excitations.

A. Computational Details

The equilibrium geometries of HCN and the HCN-water complex were optimized at second order Møller-Plesset theory(MP2) level with the Dunning correlation consistent basis set aug-cc-pvtz.[48] The results of the vibrational frequency analysis reveal that the computed structures are those of true energy minima. Geometries were optimized using the Gaussian 09 suite[49] of programs.

RIXS spectra were calculated with the first-principles multi-configuration restricted active space self-consistent field (RASSCF) approach[50] using the Dunning correlation consistent basis[48] set aug-cc-pvtz for all atoms. No symmetry is imposed for the RIXS calculations. The active space of HCN comprises 8 electrons distributed in 8 orbitals having characters of π, σ and π^*. For the HCN-water complex, the active space comprises 12 electrons distributed in 11 orbitals with 8 of them having same character as those of the isolated HCN molecule. These two orbital sets are shown in Fig. 2.

For the calculation of valence states, state averaging with 13 states is performed, whereas for the calculation of core-hole states the energies of three states are averaged in the self-consistent calculation. All orbitals without occupational constraints are kept in the active subspace RAS2 while core electrons are placed in the active subspace RAS3, where at most one electron is excited (thus suppressing configurations with a doubly filled or excited nitrogen core orbital). Grouping the excitations in such a way avoids the presence of

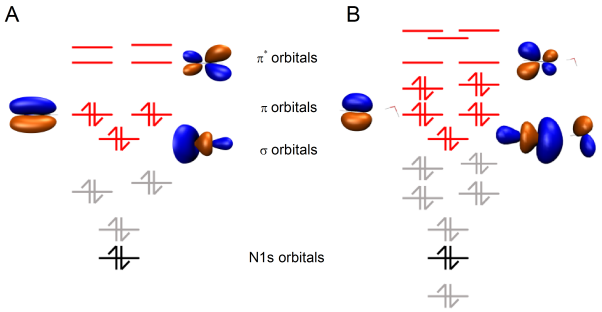

FIG. 2. Energy level diagram of HCN (**A**) and the HCN-water complex (**B**). Molecular orbitals (MOs) marked in red and black are included in the active spaces for RIXS computations. These orbitals are partitioned into the two subspaces RAS2 (red occupied and virtual orbitals) and RAS3 (black nitrogen-1s core-level). For orbitals involved in dominant transitions isodensity surfaces are plotted.

irrelevant low-energy configurations during the calculation of core excitations and prevents the variational collapse of the wave function during the RASSCF calculations. Dynamic correlations are included by multistate second-order perturbation theory (MS-RASPT2)[51–53] using 0.25 Hartree for the ionization potential electron affinity (IPEA) shift and an imaginary shift of 0.3 Hartree to avoid intruder states. The dipole transition moment between any two RASSCF wave functions is obtained by restricted active space state-interaction (RASSI)[54,55] calculations. RASSCF/RASSI calculations were performed using the MOLCAS 7.8 suite.[56]

RIXS intensities are computed within the static approximation (without propagation of the system while in the core-excited state) by the Kramers-Heisenberg relation using matrix elements obtained by the state interaction framework over RASSCF wave functions.[50] We have chosen a scattering geometry that is customary for solution-phase RIXS experiments, with photons incident on the sample having a k-vector $\vec{k}_{in} \parallel \vec{u}_x$ and a polarization $\vec{\epsilon}_{in} \parallel \vec{u}_y$. Scattered photons are detected if $\vec{k}_{scat} \parallel \vec{u}_y$ and $\vec{\epsilon}_{scat} \parallel \vec{u}_z$. A liquid jet would have a flow velocity $\vec{v}_{jet} \parallel -\vec{u}_z$. The unit vectors $\vec{u}_i$ define an orthogonal coordinate system with $\vec{u}_z$ pointing upward. This perpendicular arrangement suppresses the elastic peak to acceptable levels allowing for the largest signals to arise from inelastically scattered photons. The scattering cross-section (in atomic units), averaged over all orientations of the molecule and integrated over all directions and polarizations, is[57,58]

$$\sigma^{i\to f} = \frac{8\pi\omega_S^3\omega_I'}{9c^4}\sum_{\rho\lambda}\left|\left(\alpha_{fi}\right)_{\rho\lambda}\right|^2 \qquad (1)$$

where $\left(\alpha_{fi}\right)_{\rho\lambda}$ is the polarizability tensor element describing inelastic scattering according to

$$\left(\alpha_{fi}\right)_{\rho\lambda} = \sum_n \frac{\langle f|T_\rho|n\rangle\langle n|T_\lambda|i\rangle}{E_n - E_g - \hbar\omega_I - i\Gamma_n}. \qquad (2)$$

The integral RIXS cross-section coincides with the scattering cross-section at the so-called "magic" angle (54.74°) between the polarization of incident and scattered photons.[58] In the above equations, ω_I and ω_S are the angular frequencies of the incident and scattered photons. $E_{i,n,f}$ correspond to the energies of the initial, intermediate, and final states, respectively. The subscripts ρ and λ denote x-, y- and z-components of the electric dipole transition operator T. The lifetime broadening of the intermediate states is denoted by Γ and c is the speed of light ($\sim$137 in atomic units). Equation 2 describes a resonant process while non-resonant terms are irrelevant in this case and have been omitted. Interference effects of intermediate states decaying to the same final state are characteristic for this type of spectroscopy.[58,59]

Orbital energies were used to rationalize the variation in electronic eigenstate energies as a function of dipole strength. Orbital energies correspond to Hartree-Fock ground electronic state calculations, and for the multiconfigurational electronic wavefunctions it was in all cases possible to identify a leading configuration and a well defined excitation character in terms of those single-particle functions. In order to correlate structural and electronic degrees of freedom, the potential energy surface (PES) of CN bond stretching in HCN in the presence of dipoles of varying strengths is computed by changing the CN bond length within the small (i.e. harmonic) variation limit. The CN bond length is varied in such a way that the center of the CN bond and the length of the CH bond are fixed. From the computed curvature of the PES for each dipole configuration and strength, the frequency of the CN stretching vibration is calculated according to $\nu_{CN} = (2\pi)^{-1}\sqrt{k/\mu}$, with k as the molecular force constant derived from the PES curvature by finite differences and μ as the reduced mass of the C and N atoms. For the strongest dipole we constructed a two-dimensional section of the PES along the CH and CN stretching coordinates and diagonalized the corresponding Hessian matrix to obtain the vibrational frequencies and normal modes. Owing to the small coupling between the two stretching vibrations, treating the CN stretching mode as an isolated vibration does not alter the results.

II. RESULTS AND DISCUSSIONS

A. Isolated HCN

Spectroscopic studies on isolated HCN and its clusters have reported the electronic and molecular structure.[40–42,60] This work focuses on exploring the sensitivity of nitrogen-1s RIXS as a probe of weak to intermediate solvent-solute interactions by identifying particular spectral features of an altered valence charge distribution with atomic detail and correlating them with structural probes. The calculated RIXS spectra of HCN at the nitrogen K-edge are obtained at 400 eV incident photon energy where the maximum absorption is predicted. The corresponding loss spectra are presented in Fig. 3 (black line) along with the lowest unoccupied molecular orbitals (LUMOs) involved in the dominant core-level transitions. Our theoretical assignment attributes the elastic peak at zero loss energy to the relaxation of the core-level excitation from a π^* LUMO subsequent to N-1s excitation. The first inelastic peak is observed at a loss energy of 8.5 eV. It is due to a relaxation originating from two occupied MOs of π character. The next higher RIXS feature manifests at a loss energy of 10.22 eV. It stems from valence-to-core transitions originating from molecular orbitals of mainly σ character. The spectral feature observed at about 12.6 eV corresponds to a Rydberg state of very mixed character with major contributions from π orbitals. A similar theoretical feature in acetonitrile is characteristic of an isolated molecule which vanishes in solution.[21,61]

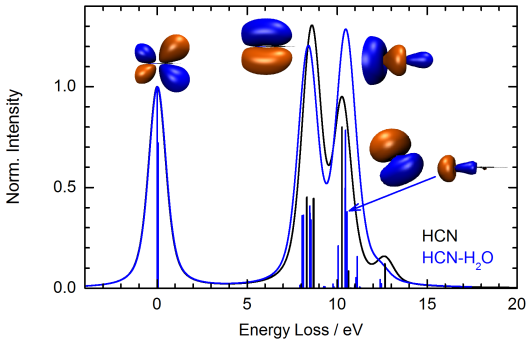

FIG. 3. Loss spectra of HCN (black) and hydrogen bonded HCN (blue). Lineshapes are the same for both calculations. The isosurfaces represent the orbitals from which the core-hole is predominantly filled, the LUMO π^*, the HOMO π, and the lone-pair σ orbital. The HCN-water complex features additional transitions between 10 eV and 11 eV from hybridized HCN-water orbitals as indicated by the blue arrow.

B. HCN-water complex

Next, we investigate the N-1s RIXS spectra of HCN interacting with one water molecule. The loss spectrum of hydrogen-bonded HCN (blue line) is also plotted in Fig. 3. Clearly, all the major spectral features for isolated HCN are preserved in the relatively weakly interacting complex. The elastic peak originates from the two π^* orbitals populated upon core-level excitation and core-hole relaxation without photon energy loss. The relaxation from initially occupied π orbitals is now shifted to slightly lower energy loss of 8.3 eV. The largest change occurs at the peak originating from the relaxation of the lone pair electrons in the σ orbital, resulting in a loss energy transition of 10.44 eV. Owing to hydrogen bond formation, the resonant enhancement occurs at a lower emission energy, i.e. larger loss energy—a clear indication of orbital stabilization. In the same range of the loss spectrum additional transitions appear upon hydrogen bonding (cf. blue arrow in Fig. 3) which enhance the peak at 10.5 eV. These transitions originate from orbitals of mixed HCN-water character, pointing to orbital covalency between the two molecule. We conclude that even weak hydrogen bonds with lengths as large as $d_{NO} = 3.05$ Å are not entirely electrostatic in nature.

The increased binding energy of the lone-pair electrons can be correlated with a stiffened CN bond as frequency calculations on the ground electronic state PES show: The CN stretching frequency is predicted to shift from 2200 cm^{-1} for isolated HCN to 2206.5 cm^{-1} for the HCN-water complex, in agreement with results reported by Purcell, and are also found theoretically as well as experimentally in other systems containing nitrile groups.[62,63]

C. HCN-dipole interaction

One aim of this study is to explore the response of the nitrile group to charge distributions. Moreover, the separation of electrostatic from covalent interactions in the observed spectral shifts can be attempted by placing a dipole of varying strength along the symmetry axis of an isolated HCN molecule. The positive charge of the dipole is thereby facing the nitrogen lone-pair at a distance of 2Å, which is equal to the distance R(N$\cdots$H) in the HCN$\cdots H_2O$ complex (the corresponding hydrogen bond length is the donor acceptor distance of 3Å). The effects of such a dipole on the loss spectrum of HCN are presented in Fig. 4. All spectral features have the same assignments as those of isolated and hydrogen-bonded HCN. It is clear from these spectra that the peaks resulting from the elastic scattering transition and those of the occupied π orbitals to the core-level do not show significant changes as a function of dipole strength. The major change is observed in the transitions involving the occupied σ orbital. These transitions exhibit a pronounced shift to higher energy with increasing dipole strength, correlating with the stabilization of the σ orbital as already discussed for the HCN-water complex. This is a clear indication of the largely (but not entirely) electrostatic nature of weak hydrogen bonds formed with weak hydrogen bond acceptor groups such as the nitrile group interacting with a water molecule. Importantly, this result indicates that such a shift is universal rather than linked to the particular hydrogen bond donor that we chose to investigate. We conclude that such shifts can be used as quantitative probes of an electrostatic environment in more complex systems.

Further insight into the altered charge distribution

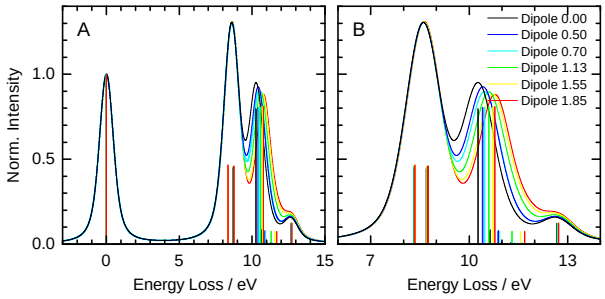

FIG. 4. Simulated N-1s loss spectra of HCN in the presence of an axial dipole of increasing strength as indicated in the legend. **A**. Computed energy loss range. **B**. Energy loss region with largest spectral changes. Vertical lines indicate transitions without broadening.

of the nitrile group subjected to an axial dipole can be gained from analysis of the dominant transitions and the Hartree-Fock-based orbital energies of the relevant highest occupied molecular orbitals (HOMOs). Both quantities are plotted in Fig. 5A and Fig. 5B, respectively. The orbital energies of the π HOMOs show only small changes

while the energy of the σ HOMO orbital exhibits a linear dependence on the dipole strength. This increasing stabilization with a stronger dipole results in lower emission energy of the transition from the core-excited (CE) to a valence-excited (VE) state (cf. Fig. 1) and therefore larger energy loss (i.e. increased binding energy) in the computed spectra of Fig. 4.

It is informative to examine the dependence of the CN stretching frequency on the dipole strength. The results, computed by variation of the CN bond distance, are plotted in Fig. 5C. The CN stretching vibration shifts to higher energy with increasing dipole strength, signaling a stiffened CN bond. This behavior and the increasing σ orbital stabilization (directly manifesting in the loss spectra) can be related to the charge density difference between the isolated and the field-subjected HCN molecule. Differential isosurfaces for four dipole strengths are presented in Fig. 5D. The charge density difference shows the expected shift of charge from the nitrogen atom towards the applied dipole. But the response of the nitrile charge distribution to a dipole or a hydrogen bond donor group is remarkable because it not only results in a shift of the lone-pair electrons of the nitrogen atom toward the dipole/HB donor (thereby inducing a dipole) but it actually creates an additional charge density modulation between the nitrogen and the carbon atom that polarizes the HCN molecule. This density modulation is shown in Fig. 5E. Its shape resembles the nitrogen σ-orbital that participates in the triple CN bond (Fig.3). It appears that the induced lone-pair dipole acts as a transducer, polarizing the nitrogen σ-orbital along its nodal lines. This effect, we conclude, holds responsible for the computationally observed bond shortening by a fraction of a picometer which also shifts the CN stretching frequency higher by 3-4 cm$^{-1}/D$. We also find the same charge density modulation in the HCN-water complex. This finding provides an atomically-resolved explanation of the well-known anomalous blue-shift of the nitrile stretching frequency as observed, for instance, in acetonitrile.[22] We expect this mechanism to be of more general validity, not just dictating the response of nitrile groups to an electrostatic dipole but also acting in a similar fashion in diazo and azide groups.

D. HCN-dipole interaction in perpendicular arrangement

Lastly, we present simulated results on the HCN molecule in the presence of a dipole that is arranged perpendicularly to the CN bond. The loss spectrum is calculated by placing the dipole 2Å away from the midpoint of the CN bond. This dipole arrangement can be envisioned for structurally fairly well-defined environments such as proteins while in solutions, solvent molecules with an intrinsic dipole would orient antiparallel to the nitrile group. In aqueous solution, HCN is not stable and dissociates. Nonetheless, for the purpose of establishing an understanding of electrostatic sensing on a fundamental

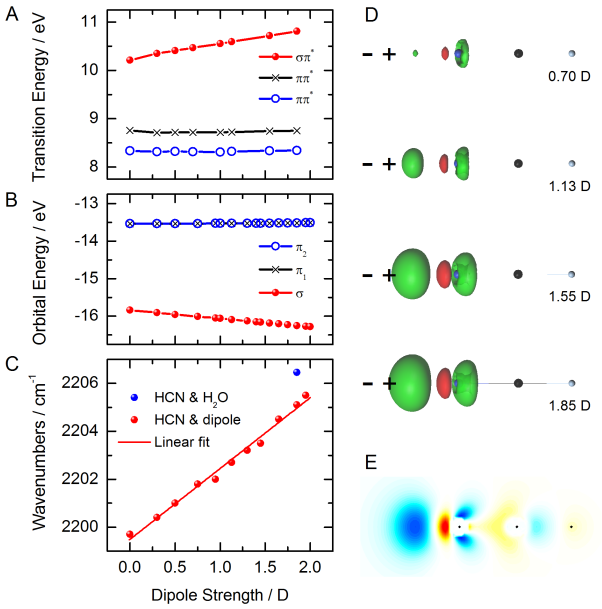

FIG. 5. **A**. Energies of valence excitation as a function of dipole strength. **B**. Hartree-Fock orbital energies of the HOMO-π and HOMO-σ orbitals as a function of applied dipole strength**C**. Computed CN stretching frequency of HCN in harmonic approximation as a function of dipole strength. **D**. Isodensity surfaces (at 0.005 value) of differential charge density between isolated HCN and HCN in the presence of an axial dipole. Green regions denote positive (increased) and red regions denote negative (decreased) charge density.**E**. Cross-section of the differential charge density for the 1.85 D dipole. Blue and yellow to red areas represent increased and decreased charge density, respectively.

level and relating structural degrees of freedom to valence charge distributions, HCN is a good starting point.

The dipole in a perpendicular arrangement is breaking the molecular symmetry, thereby re-hybridizing the nitrile's π and σ orbitals. The computed loss spectra are shown in Fig. 6. A very small negligible shift of the elas-

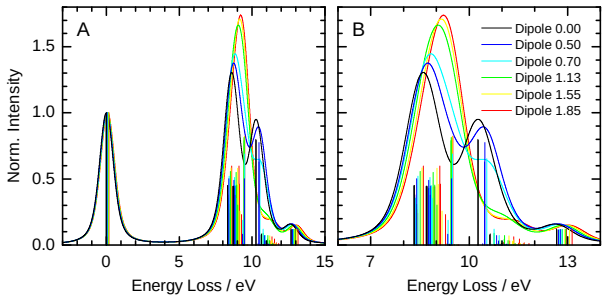

FIG. 6. Simulated N-1s loss spectra of HCN in the presence of an equatorial dipole of increasing strength as indicated in the legend. **A**. Computed energy loss range. **B**. Energy loss region with largest spectral changes. Vertical lines indicate transitions without broadening.

tic line can be observed with respect to the dipole-free case. The behavior of the σ and π orbitals leads to an increasingly complex loss spectrum as a consequence of the symmetry loss. The transitions originating from π orbitals split as is evident from comparison of the transitions in panel Fig. 4B with those in Fig. 6B at 8-9 eV energy loss. The decrease in symmetry affects the π_1 orbital facing the dipole in an manner opposite to that of the π_2 and σ orbitals resulting in the following trends in the loss spectra: (i) the loss transitions associated with the two $\pi \rightarrow \pi^*$ transition at 8.3 and 8.7 eV shift to higher energy monotonically by about 0.1 eV/D. (ii) The $\sigma \rightarrow \pi^*$ transition at 10.3 eV migrates to higher energy and rapidly diminishes with increasing dipole strength while also changing its character to a $\pi_1 \rightarrow$ LUMO+2 transition. (iii) A $\pi_1 \rightarrow$ LUMO+2 transition of negligible oscillator strength grows in with increasing dipole strength at 9.3 eV which conversely changes its character to a $\sigma \rightarrow \pi^*$ transition to become the dominant transition of the loss spectrum. We note that it is indeed a very abrupt change in transition character and not a gradual spectral migration

In order to understand this behavior, valence excitation energies between the ground electronic state and the low-lying excited states with intensity in the loss spectra are displayed in Fig. 7A, and Hartree-Fock orbital energies as a function of the dipole strength are presented in Fig. 7B. The symmetry change lifts the degeneracy of the π orbitals and engenders an energetic approach of the σ and π_1. Structurally, the CN bond softens considerably as Fig. 7C reveals. The bond softening can be traced to the dipole-induced delocalization in charge density. We visualize this change in charge density again as isosurfaces of the total charge density difference between no dipole and a dipole of varying strength in Fig. 7D. Thus, a very characteristic spectral reshaping of the loss spectrum characterizes a perpendicular arrangement that can act as a proxy for this kind of electrostatic environment in more complex systems. Lastly, we note that the somewhat artificial case of a water molecule place in perpendicular arrangement to the HCN molecule is predicted to induce very similar changes to the electronic structure of HCN.

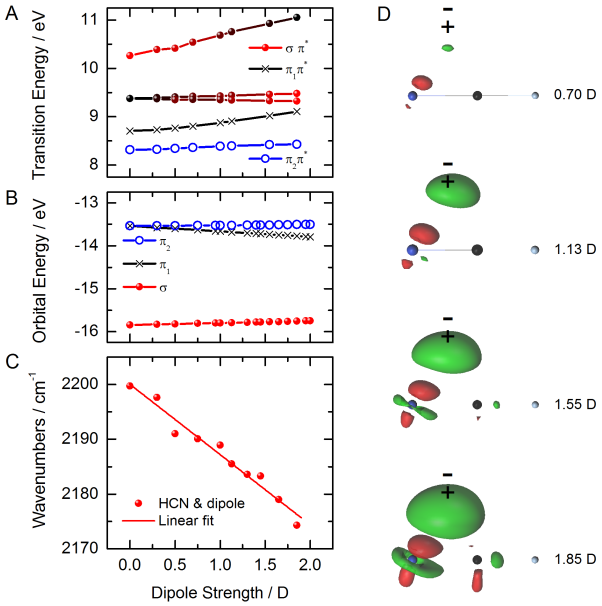

FIG. 7. **A**. Energies of valence excitation as a function of dipole strength. **B** Hartree-Fock orbital energies of the HOMO-π and HOMO-σ orbitals as a function of applied dipole strength **C**. Computed CN stretching frequency of HCN in harmonic approximation as a function of dipole strength. **D**. Isodensity surfaces (at 0.005 value) of differential charge density between isolated HCN and HCN in presence of a perpendicular dipole. Green regions denote positive (increased) and red regions denote negative (decreased) charge density.

III. CONCLUSIONS

The interaction of a nitrile group with one water molecule and an electric dipole have been investigated by utilizing *ab initio* RASSCF theory to calculate RIXS and spectra and vibrational frequencies. In comparison to isolated HCN, we find spectral shifts indicative of lone pair orbital stabilization on the nitrogen atom of the HCN-water complex. The spectral features due to hydrogen bonding are further investigated by replacing water with an electric dipole. The shift of the CN stretching mode to higher frequency is found for both, a dipole and a hydrogen bond, in agreement with reported results.[22,63,64]

We conclude from these results that the effects of hydrogen bonding are mostly of electrostatic nature. These effects are therefore universal and not linked to particular ligands around the nitrile group. A dipole charge distribution aligned with the nitrile group lowers the energy of the σ orbital and leads to a strengthening of the CN bond via polarization of the σ-symmetry orbitals. This can be distinctly seen in the corresponding vibrational frequency, but also very clearly as a marked shift in the Raman UV line at 10.5 eV. The effect is the opposite when the dipole is placed perpendicular to the nitrile group, leading to a weakening of the CN bond. The dominant σ and π transitions are reshuffled and the transitions corresponding to relaxations from the π orbitals split because the molecular symmetry is broken by the electrostatic environment.

Our analysis approach links UV excitations of the electronic system to the molecular structure which is important for understanding the interplay of electronic and nuclear degrees of freedom. This work also indicates that RIXS spectroscopy of nitrile groups may act as a sensitive and complimentary tool of hydrogen bonding and electrostatic environments in solvated systems or small model peptides. The electronic structure information can facilitate the interpretation and deepen the understanding of local dynamics where such vibrational reporters are

employed. Further investigations of different nitrogen-containing functional groups and more complex electrostatic environments will follow.

[1] H.-S. Shieh, H. M. Berman, M. Dabrow, and S. Neidle, "The structure of drug-deoxydinucleoside phosphate complex; generalized conformational behavior of intercalation complexes with RNA and DNA fragments," Nucl. Acids Res. **8**, 85–98 (1980).

[2] S. Burley and G. Petsko, "Aromatic-aromatic interaction: a mechanism of protein structure stabilization," Science **229**, 23–28 (1985).

[3] W. Saenger, *Principles of Nucleic Acid Structure*, Springer Advanced Texts in Chemistry (Springer, New York, USA, 1984).

[4] J.-M. Lehn, "Supramolecular chemistry–scope and perspectives molecules, supermolecules, and molecular devices," Angew. Chem. Int. Ed. **27**, 89–112 (1988).

[5] A. Warshel and J. Aqvist, "Electrostatic energy and macromolecular function," Annu. Rev. Biophys. Biophys. Chem. **20**, 267–298 (1991).

[6] M. Elstner, P. Hobza, T. Frauenheim, S. Suhai, and E. Kaxiras, "Hydrogen bonding and stacking interactions of nucleic acid base pairs: A density-functional-theory based treatment," J. Chem. Phys. **114**, 5149–5155 (2001).

[7] E. A. Meyer, R. K. Castellano, and F. Diederich, "Interactions with aromatic rings in chemical and biological recognition," Angew. Chem. Int. Ed. **42**, 1210–1250 (2003).

[8] K. Heyne, N. Huse, E. T. J. Nibbering, and T. Elsaesser, "Coherent vibrational dynamics of intermolecular hydrogen bonds in acetic acid dimers studied by ultrafast mid-infrared spectroscopy," J. Phys.: Condens. Matter **15**, S129 (2003).

[9] A. Warshel, P. K. Sharma, M. Kato, Y. Xiang, H. Liu, and M. H. M. Olsson, "Electrostatic basis for enzyme catalysis," Chem. Rev. **106**, 3210–3235 (2006).

[10] T. Elsaesser, N. Huse, J. Dreyer, J. R. Dwyer, K. Heyne, and E. T. Nibbering, "Ultrafast vibrational dynamics and anharmonic couplings of hydrogen-bonded dimers in solution," Chem. Phys. **341**, 175–188 (2007).

[11] H. Wen, N. Huse, R. W. Schoenlein, and A. M. Lindenberg, "Ultrafast conversions between hydrogen bonded structures in liquid water observed by femtosecond x-ray spectroscopy," J. Chem. Phys. **131**, 234505 (2009).

[12] S. D. Fried and S. G. Boxer, "Measuring electric fields and noncovalent interactions using the vibrational stark effect," Acc. Chem. Res. **48**, 998–1006 (2015).

[13] D. J. Bakker, A. Peters, V. Yatsyna, V. Zhaunerchyk, and A. M. Rijs, "Far-infrared signatures of hydrogen bonding in phenol derivatives," J. Phys. Chem. Lett. **7**, 1238–1243 (2016).

[14] M. M. Gromiha, K. Saraboji, S. Ahmad, M. Ponnuswamy, and M. Suwa, "Role of non-covalent interactions for determining the folding rate of two-state proteins," Biophys. Chem. **107**, 263–272 (2004).

[15] P. Deb, T. Haldar, S. M. Kashid, S. Banerjee, S. Chakrabarty, and S. Bagchi, "Correlating nitrile IR frequencies to local electrostatics quantifies noncovalent interactions of peptides and proteins," J. Phys. Chem. B **120**, 4034–4046 (2016).

[16] T. Elsaesser and H. J. Bakker, eds., *Ultrafast Hydrogen Bonding Dynamics and Proton Transfer Prosesses in the Condensed Phase*, Vol. 23 (Kluwer Academic Publishers, 2002).

[17] S. Myneni, Y. Luo, L. Å. Näslund, M. Cavalleri, L. Ojamäe, H. Ogasawara, A. Pelmenschikov, P. Wernet, P. Väterlein, C. Heske, Z. Hussain, L. G. M. Pettersson, and A. Nilsson, "Spectroscopic probing of local hydrogen-bonding structures in liquid water," J. Phys.: Condens. Matter **14**, L213 (2002).

[18] J.-H. Guo, Y. Luo, A. Augustsson, J.-E. Rubensson, C. Såthe, H. Ågren, H. Siegbahn, and J. Nordgren, "X-ray emission spectroscopy of hydrogen bonding and electronic structure of liquid water," Phys. Rev. Lett. **89**, 137402 (2002).

[19] N. Huse, K. Heyne, J. Dreyer, E. T. J. Nibbering, and T. Elsaesser, "Vibrational multilevel quantum coherence due to anharmonic couplings in intermolecular hydrogen bonds," Phys. Rev. Lett. **91**, 197401 (2003).

[20] P. Wernet, D. Nordlund, U. Bergmann, M. Cavalleri, M. Odelius, H. Ogasawara, L. Å. Näslund, T. K. Hirsch, L. Ojamäe, P. Glatzel, L. G. M. Pettersson, and A. Nilsson, "The structure of the first coordination shell in liquid water," Science **304**, 995–999 (2004).

[21] L. Weinhardt, E. Ertan, M. Iannuzzi, M. Weigand, O. Fuchs, M. Bar, M. Blum, J. D. Denlinger, W. Yang, E. Umbach, M. Odelius, and C. Heske, "Probing hydrogen bonding orbitals: resonant inelastic soft x-ray scattering of aqueous NH_3," Phys. Chem. Chem. Phys. **17**, 27145–27153 (2015).

[22] G. Eaton, A. S. Pena-Nunez, and M. C. R. Symons, "Solvation of cyanoalkanes [CH_3CN and $(CH_3)_3CCN$]. an infrared and nuclear magnetic resonance study," J. Chem. Soc., Faraday Trans. 1 **84**, 2181–2193 (1988).

[23] R. A. Nyquist, "Solvent-induced nitrile frequency shifts: Acetonitrile and benzonitrile," Appl. Spectrosc. **44**, 1405–1407 (1990).

[24] D. Jamroz, J. Stangret, and J. Lindgren, "An infrared spectroscopic study of the preferential solvation in water-acetonitrile mixtures," J. Am. Chem. Soc. **115**, 6165–6168 (1993).

[25] W. R. Fawcett, G. Liu, and T. E. Kessler, "Solvent-induced frequency shifts in the infrared spectrum of acetonitrile in organic solvents," J. Phys. Chem. **97**, 9293–9298 (1993).

[26] J. E. Bertie and Z. Lan, "Liquid water-acetonitrile mixtures at 25°C: The hydrogen-bonded structure studied through infrared absolute integrated absorption intensities," J. Phys. Chem. B **101**, 4111–4119 (1997).

[27] J. R. Reimers and L. E. Hall, "The solvation of acetonitrile," J. Am. Chem. Soc. **121**, 3730–3744 (1999).

[28] E. S. Kryachko and M. T. Nguyen, "Hydrogen bonding between phenol and acetonitrile," J. Phys. Chem. A **106**, 4267–4271 (2002).

[29] S. H. Brewer and S. Franzen, "A quantitative theory and computational approach for the vibrational stark effect," J. Chem. Phys. **119**, 851–858 (2003).

[30] K. A. S. Sergio D. Dalosto, Jane M. Vanderkooi, "Vibrational stark effects on carbonyl, nitrile, and nitrosyl compounds including heme ligands, CO, CN, and NO, studied with density functional theory," J. Phys. Chem. B **108**, 6450–6457 (2004).

[31] M. G. Maienschein-Cline and C. H. Londergan, "The CN stretching band of aliphatic thiocyanate is sensitive to solvent dynamics and specific solvation," J. Phys. Chem. A **111**, 10020–10025 (2007).

[32] C. T. Liu, J. P. Layfield, R. J. Stewart, J. B. French, P. Hanoian, J. B. Asbury, S. Hammes-Schiffer, and S. J. Benkovic, "Probing the electrostatics of active site microenvironments along the catalytic cycle for escherichia coli dihydrofolate reductase," J. Am. Chem. Soc. **136**, 10349–10360 (2014).

[33] G. M. Chaban, "Anharmonic vibrational spectroscopy of nitriles and their complexes with water," J. Phys. Chem. A **108**, 4551–4556 (2004).

[34] Z. Getahun, C.-Y. Huang, T. Wang, B. De Léon, W. F. DeGrado, and F. Gai, "Using nitrile-derivatized amino acids as infrared probes of local environment," J. Am. Chem. Soc. **125**, 405–411 (2003).

[35] S. Bagchi, S. G. Boxer, and M. D. Fayer, "Ribonuclease S dynamics measured using a nitrile label with 2D IR vibrational echo spectroscopy," J. Phys. Chem. B **116**, 4034–4042 (2012).

[36] G. A. Jeffrey and W. Saenger, *Hydrogen bonding in biological structures* (Springer Science & Business Media, 2012).

[37] E. G. Robertson and J. P. Simons, "Getting into shape: Conformational and supramolecular landscapes in small biomolecules and their hydrated clusters," Phys. Chem. Chem. Phys. **3**, 1–18 (2001).

[38] M. S. de Vries and P. Hobza, "Gas-phase spectroscopy of biomolecular building blocks," Annu. Rev. Phys. Chem. **58**, 585–612 (2007).

[39] E. Garand, M. Z. Kamrath, P. A. Jordan, A. B. Wolk, C. M. Leavitt, A. B. McCoy, S. J. Miller, and M. A. Johnson, "Deter-

mination of noncovalent docking by infrared spectroscopy of cold gas-phase complexes," Science **335**, 694–698 (2012).
[40]B. F. King and F. Weinhold, "Structure and spectroscopy of $(HCN)_n$ clusters: Cooperative and electronic delocalization effects in C–H$\cdots$N hydrogen bonding," J. Chem. Phys. **103**, 333–347 (1995).
[41]R. Z. Martínez, K. K. Lehmann, and S. Carter, "Spectroscopy of highly excited vibrational states of HCN in its ground electronic state," J. Chem. Phys. **120**, 691–703 (2004).
[42]D. H. Rank, G. Skorinko, D. P. Eastman, and T. A. Wiggins, "Vibration-rotation spectra of HCN," J. Opt. Soc. Am. **50**, 421–432 (1960).
[43]S. P. Platt, I. K. Attah, M. S. El-Shall, R. Hilal, S. A. Elroby, and S. G. Aziz, "Unconventional $CH^{\delta+}\cdots N$ hydrogen bonding interactions in the stepwise solvation of the naphthalene radical cation by hydrogen cyanide and acetonitrile molecules," Phys. Chem. Chem. Phys. **18**, 2580–2590 (2016).
[44]A. C. Legon, D. J. Millen, and S. C. Rogers, "Spectroscopic investigations of hydrogen bonding interactions in the gas phase. i. the determination of the geometry, dissociation energy, potential constants and electric dipole moment of the hydrogen-bonded heterodimer HCN$\cdots$HF from its microwave rotational spectrum," Proc. Roy. Soc. A **370**, 213–237 (1980).
[45]J. E. Del Bene, "Hydrogen bonding: Methodology and applications to complexes of HF and HCl with HCN and CH_3CN," Int. J. Quantum Chem. **44**, 527–541 (1992).
[46]I. Josefsson, K. Kunnus, S. Schreck, A. Föhlisch, F. de Groot, P. Wernet, and M. Odelius, "Ab initio calculations of x-ray spectra: Atomic multiplet and molecular orbital effects in a multiconfigurational scf approach to the L-edge spectra of transition metal complexes," J. Phys. Chem. Lett. **3**, 3565–3570 (2012).
[47]P. Wernet, K. Kunnus, I. Josefsson, I. Rajkovic, W. Quevedo, M. Beye, S. Schreck, S. Grübel, M. Scholz, D. Nordlund, W. Zhang, R. W. Hartsock, W. F. Schlotter, J. J. Turner, B. Kennedy, F. Hennies, F. M. F. de Groot, K. J. Gaffney, S. Techert, M. Odelius, and A. Föhlisch, "Orbital-specific mapping of the ligand exchange dynamics of $Fe(CO)_5$ in solution," Nature **520**, 78–81 (2015).
[48]T. H. Dunning, "Gaussian basis sets for use in correlated molecular calculations. I. The atoms boron through neon and hydrogen," J. Chem. Phys. **90**, 1007–1023 (1989).
[49]M. J. Frisch, G. W. Trucks, H. B. Schlegel, G. E. Scuseria, M. A. Robb, J. R. Cheeseman, G. Scalmani, V. Barone, B. Mennucci, G. A. Petersson, H. Nakatsuji, M. Caricato, X. Li, H. P. Hratchian, A. F. Izmaylov, J. Bloino, G. Zheng, J. L. Sonnenberg, M. Hada, M. Ehara, K. Toyota, R. Fukuda, J. Hasegawa, M. Ishida, T. Nakajima, Y. Honda, O. Kitao, H. Nakai, T. Vreven, J. A. Montgomery, Jr., J. E. Peralta, F. Ogliaro, M. Bearpark, J. J. Heyd, E. Brothers, K. N. Kudin, V. N. Staroverov, R. Kobayashi, J. Normand, K. Raghavachari, A. Rendell, J. C. Burant, S. S. Iyengar, J. Tomasi, M. Cossi, N. Rega, J. M. Millam, M. Klene, J. E. Knox, J. B. Cross, V. Bakken, C. Adamo, J. Jaramillo, R. Gomperts, R. E. Stratmann, O. Yazyev, A. J. Austin, R. Cammi, C. Pomelli, J. W. Ochterski, R. L. Martin, K. Morokuma, V. G. Zakrzewski, G. A. Voth, P. Salvador, J. J. Dannenberg, S. Dapprich, A. D. Daniels, Ö. Farkas, J. B. Foresman, J. V. Ortiz, J. Cioslowski, and D. J. Fox, "Gaussian 09, Revision E.01," (2009), Gaussian Inc., Wallingford, CT.
[50]P. Å. Malmqvist, A. Rendell, and B. O. Roos, "The restricted active space self-consistent-field method, implemented with a split graph unitary group approach," J. Phys. Chem. **94**, 5477–5482 (1990).
[51]K. Andersson, P. Å. Malmqvist, B. O. Roos, A. J. Sadlej, and K. Wolinski, "Second-order perturbation theory with a CASSCF reference function," J. Phys. Chem. **94**, 5483–5488 (1990).
[52]K. Andersson, P. Å. Malmqvist, and B. O. Roos, "Second-order perturbation theory with a complete active space self-consistent field reference function," J. Chem. Phys. **96**, 1218–1226 (1992).
[53]P. Å. Malmqvist, K. Pierloot, A. R. M. Shahi, C. J. Cramer, and L. Gagliardi, "The restricted active space followed by second-order perturbation theory method: Theory and application to the study of CuO_2 and Cu_2O_2 systems," J. Chem. Phys. **128**, 204109 (2008).
[54]P. Å. Malmqvist and B. O. Roos, "The CASSCF state interaction method," Chem. Phys. Lett. **155**, 189–194 (1989).
[55]P. Å. Malmqvist, B. O. Roos, and B. Schimmelpfennig, "The restricted active space (RAS) state interaction approach with spin-orbit coupling," Chem. Phys. Lett. **357**, 230–240 (2002).
[56]F. Aquilante, L. De Vico, N. Ferré, G. Ghigo, P. Å. Malmqvist, P. Neogrády, T. B. Pedersen, M. Pitoňák, M. Reiher, B. O. Roos, L. Serrano-Andrés, M. Urban, V. Veryazov, and R. Lindh, "MOLCAS 7: The next generation," J. Comput. Chem. **31**, 224–247 (2010).
[57]H. A. Kramers and W. Heisenberg, "Über die Streuung von Strahlung durch Atome," Zeitschrift für Physik **31**, 681–708 (1925).
[58]F. Gel'mukhanov and H. Ågren, "Resonant X-ray Raman scattering," Phys. Rep. **312**, 87–330 (1999).
[59]A. Kotani and S. Shin, "Resonant inelastic x-ray scattering spectra for electrons in solids," Rev. Mod. Phys. **73**, 203–246 (2001).
[60]A. Hitchcock and C. Brion, "K-shell excitation of HCN by electron energy loss spectroscopy," J. Electron Spectrosc. Relat. Phenom. **15**, 201–206 (1979).
[61]J. Niskanen, K. Kooser, J. Koskelo, T. Kaambre, K. Kunnus, A. Pietzsch, W. Quevedo, M. Hakala, A. Fohlisch, S. Huotari, and E. Kukk, "Density functional simulation of resonant inelastic X-ray scattering experiments in liquids: acetonitrile," Phys. Chem. Chem. Phys. **18**, 26026–26032 (2016).
[62]K. F. Purcell and R. S. Drago, "Studies of the bonding in acetonitrile adducts," J. Am. Chem. Soc. **88**, 919–924 (1966).
[63]F. Muniz-Miranda, M. Pagliai, G. Cardini, and R. Righini, "Hydrogen bond effects in the vibrational spectra of 1,3-propanediol in acetonitrile: Ab initio and experimental study," J. Chem. Phys. **137**, 244501 (2012).
[64]W. R. Fawcett, *Liquids, solutions, and interfaces: from classical macroscopic descriptions to modern microscopic details* (Oxford University Press, 2004).

Cite this: DOI: 10.1039/xxxxxxxxxx

Resonant inelastic X-ray Scattering (RIXS) Studies of Hydrogen-Bonded Cyano-Groups at the Nitrogen K-edge

Abid Hussain,[a] Simon Schreck,[e] Philippe Wernet,[e] Alexander Föhlisch,[e] Oriol Vendrell*[c,d] and Nils Huse,*[a,b]

Received Date
Accepted Date

DOI: 10.1039/xxxxxxxxxx

www.rsc.org/journalname

The influence of hydrogen bonding on the electronic structure of the nitrogen atoms in cyano-groups has been explored for acetonitrile and acetonitrile-water mixtures using X-ray absorption spectroscopy and resonant inelastic X-ray scattering (RIXS) along with electronic structure calculations. We employed first principles restricted active space self-consistent field (RASSCF) calculations in order to interpret experimental electronic structure probes via nitrogen core-level transitions. In the current study, we elucidate with highest chemical specificity the relative involvement of different molecular orbitals (MO). These calculations give explicit access to each electronic state with the extracted information allowing to assign the dominant transitions in the X-ray absorption spectrum, and unearthing the electronic character of every final valence excitation resulting from RIXS at a specific incident photon energy. Our theoretical results are in very good agreement with experimental spectra, highlighting the sensitivity of RIXS even for weak interactions.

1 Introduction

Hydrogen bonding is an essential intra- and intermolecular interaction which has remarkable properties, i.e. this interaction is substantially weaker than covalent bonds[1,2] but often highly directional in comparison to diffusive interactions such as van der Waals forces.[3] Hydrogen bonds allow for well-defined long-lived structures and functional flexibility[4–7] but hydrogen-bonded systems span remarkably large ranges of dynamics, most prominently observed in neat water.[8–11] Proton-transfer reactions are greatly facilitated by hydrogen bonding, providing clear routes for protonation/deprotonation pathways and concerted proton motion over larger distances due to electronic/electrostatic correlations.[12–14] Vibrational spectroscopy is a prominent probe of hydrogen bonding for more than a century[8,15] due to the strong depence of vibrational modes to interactions with Hydrogen bond accepting groups (RX-H...YR'), expecially X-H streching vibrations, due to a strong dependence in anharmonicity of the underlying potential energy surfaces. Vibrational spectroscopy exploites local modes which are largely confined to two atoms or three atoms, a complimentary spectral probe of electronic stucture using core-level transitions in the X-ray regime is highly desireable for several reasons: (i) Core-level transitiosn provide elemental specificity such that for a small set of atomic species such as nitrogen atoms transitions originating from specific atoms, (ii) electronic probes provide additional information to understand the interplay of nuclear and electronic degrees of freedom, (iii) X-ray probes could in principle reach attosecond time-resolution in dynamic spectroscopy experiments to follow changes in charge distribution on the relevant timescales.

The acetonitrile (ACN) is one of the simple aprotic solvents due to its miscibility with water at any ratio. Furthermore, the interactions of ACN molecules are weak among themselves, while a hydrogen bond network is formed with water molecules. X-ray diffraction studies on pure acetonitrile molecules revealed that the ACN molecules are associated via weak dipole-dipole interactions[16]. In addition, ACN molecule can form hydrogen bonding either with lone pair electron on nitrogen atom (σ bonding) or with C≡N triple bond (π bonding). Several prior experimental studies on hydrogen bonded ACN-water mixtures using different spectroscopic methods[17–24] has been reported. Also, ACN-water complex has been topic of many theoretical studies using ab initio methods[25,26] and molecular dynamics simulations[27–29]. How-

[a] Max Planck Institute for the Structure and Dynamics of Matter, Center for Free Electron Laser Science, 22761 Hamburg, Germany.
[b] Department of Physics, University of Hamburg, 22761 Hamburg, Germany. Tel: +49 40 8998 6266; E-mail: nils.huse@uni-hamburg.de
[c] Center for Free-Electron Laser Science, DESY and The Hamburg Centre for Ultrafast Imaging, 22761 Hamburg, Germany.
[d] Department of Physics and Astronomy, Aarhus University, Ny Munkegade 120, DK-8000 Aarhus C, Denmark. Tel: +45 8 7155639; E-mail: oriol.vendrell@phys.au.dk
[e] Institute for Methods and Instrumentation in Synchrotron Radiation Research, Helmholtz-Zentrum Berlin,Albert-Einstein-Straße 15, 12489 Berlin.

ever, a systematic study on the origin of different observed spectral features using X-ray methods as element-specific probes of electronic structure is missing although core-level spectroscopic techniques are superb probes of element-specific electronic structure. In this paper we investigate the sensitivity of core-level transitions to weakly hydrogen-bonded systems to elucidate if very weak hydrogen bond interactions can be probed with X-ray spectroscopy.

2 Experimental Details

Experiments were performed at beamline U41-PGM at the synchrotron radiation source BESSY II of the Helmholtz-Zentrum Berlin. We measured RIXS spectra from liquid microjet in vacuum using the setup described by Kunnus et al.[30]. The setup uses a Grace XES 350 x-ray emission spectrometer, which is mounted under 90° with respect to the incident x-ray beam. We used linearly polarized x-rays with the polarization vector in the scattering plane. A 20μm diameter liquid jet and flow rates between 0.3 and 0.5 ml/min were used. For energy calibration of the incident x-ray beam we used the incident energy and corresponding signal at a particular channel. The slope of line obtained by the channel number to corresponding incident energy approximates elastic resonance. We calibrated the emission energy scale using the elastically scattered light from spectra measured at different excitation energies. Acetonitrile with a purity of 99.8% was purchased from Sigma-Aldrich and used as received. Deionized water was used for the aqueous mixtures. During measurements the sample reservoir was constantly flushed with nitrogen gas to prevent dilution of acetonitrile due to its high hygroscopic character.

3 Theory

3.1 Electronic Structure Calculations

Multi-configurational *ab initio* methods were employed for modeling and understanding the resonant inelastic X-ray scattering (RIXS) and X-ray absorption spectra (XAS) obtained experimentally for acetonitrile (ACN) and acetonitrile-water. The equilibrium singlet ground state geometries for acetonitrile and acetonitrile-water were obtained by using the ANO-L-VTZP basis set[31]. We used the multi-configurational restricted active space self-consistent field (RASSCF) method to calculate valence and core excited states. Dynamic correlation was included by second order perturbation theory RASPT2[32–34] on RASSCF wave functions with an imaginary level shift of 0.2 hartree. The multi-configurational computational study was carried out by using the MOLCAS 7.8 program suite[35]. GAUSSIAN09[36] was used for ground state geometry optimizations at the MP2 level of theory to perform normal mode vibrational analysis.

In the RASSCF calculations we set RAS3 subspace (where the number of electrons is restricted) as the Nitrogen 1s orbital, while all other active orbitals were placed in RAS2 subspace (where all configurations are permitted). The sorting of electrons into active spaces in this way is known as the core-RAS method and very useful in suppressing configurations with a doubly filled or excited nitrogen core orbital. In addition, such grouping of the RASSCF calculations prevents the variational collapse of the wave function as well as the presence of irrelevant low-energy configurations in the core excittations is avoided. The restricted active space state interaction (RASSI) routine[37] is used to obtain transition dipole moments between computed states.The active space for present studies of the Nitrogen K-edge XAS and RIXS is shown in Fig. 1. The ground state configuration of acetonitrile having symmetry C_{3v}[38–40] is $(core)^6(4a_1)^2(5a_1)^2(6a_1)^2(1e)^4(7a_1)^2(2e)^4$. The lowest unoccupied molecular orbitals are two 3e(antibonding $\pi^*C\equiv N$) and $8a_1$(antibonding σ^*C-C)orbitals. We computed the Nitrogen K-edge XAS and RIXS spectra of acetonitrile by employing the active space that consisted of twelve electrons distributed over eleven orbitals as shown in panel (a) of Fig. 1. These orbitals have mainly bonding $(\pi,\sigma)$and antibonding (π^*,σ^*) character. In case of Nitrogen K-edge calculations for acetonitrile-water, sixteen electrons were distributed over thirteen orbitals. These orbitals have the same character as those considered in the active space for acetonitrile as shown in panel (b) of Fig. 1.

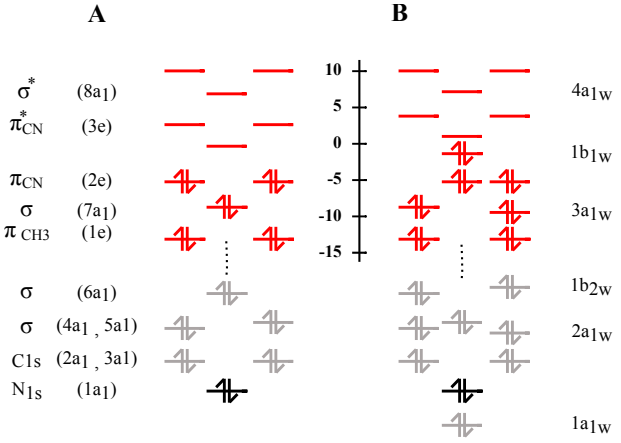

Fig. 1 Molecular orbitals (MOs) included in active space for **A.** ACN **B.** ACN-water complex. The active orbitals are shown in red.

3.2 Spectroscopy

The absorption cross-section for a transition from state $|g\rangle$ to $|n\rangle$ is calculated using Fermi's Golden Rule

$$\sigma(\omega) = (4\pi^2/c)\hbar\omega\sum_n |\langle n|T_2|g\rangle|^2 \times \frac{Gamma_n/2\pi}{\hbar\omega_n - \hbar\omega_g - \hbar\omega + \frac{\Gamma_n^2}{4}} \quad (1)$$

where $\hbar\omega$ is the incident photon energy, $\hbar\omega_g, \hbar\omega_n$ are energies of ground and intermediate states and Γ being the lifetime broadening and matrix elements of transition operator $\hat{T}$ between two states $|f\rangle$ and $|g\rangle$ descibing the strength of electric dipole transitions were calculated by using the RASSI approach[37,41] over RASSCF wave functions. Similarly, the RIXS intensities are calculated by the Kramers-Heisenberg relation without taking into

account system progration during the core-excited state[42,43]

$$F(\omega,\omega') = \sum_f \left| \sum_n \frac{\langle f|T_1|n\rangle\langle n|T_2|g\rangle}{\hbar\omega_g - \hbar\omega_n - \hbar\omega + i\frac{\Gamma_n}{2}} \right|^2 \times \frac{\frac{\Gamma_f}{2\pi}}{(\hbar\omega_g - \hbar\omega_f - \hbar\omega + \hbar\omega')^2 + \frac{\Gamma_f^2}{4}} \quad (2)$$

where $\hbar\omega$ and $\hbar\omega'$ are energies of incident and emitted photon; $\hbar\omega_{g,n,f}$ are energies of electronic configurations involved; T_1 and T_2 are transition dipole operators. The energies of all intermediate and final states are related to same reference state by defining $\hbar\omega - \hbar\omega'$ energy transfer. RIXS being second-order process can be described by coherently coupled absorption and emission processes. Due to this coupling, interference effects of intermediate states decaying to same final state are characteristic for this type of spectroscopy.[44,45].The spectra are broadened by Γ_n along incident energy and by Γ_f along energy transfer $(\hbar\omega - \hbar\omega')$, where Γ_n and Γ_f being the lifetime broadening of intermediate and final states respectively.

For a particular transition $(g \to n\ ;\ n \to f)$, the unpolarized intensity of transition summed over all directions is proportional to the square of expectation value of dipole operator which can be written in terms of transition operator at resonance energies as

$$I_o^{(g,n,f)} = \frac{8}{\pi} \cdot \frac{1}{\Gamma_n^2 \cdot \Gamma_f} \left| \sum_{\rho,\lambda} \langle f|T_{1\rho}|n\rangle\langle n|T_{2\lambda}|g\rangle \right|^2 \quad (3)$$

where the summation indices ρ,λ are taken to run over the three components x, y, z for the transition dipole operator. For linearly polarized absorbed and emitted photons at an angle θ, the polarization dependent intensity can be written as[46–48]

$$I(\theta) = I_o[1 - R(\frac{3}{2}\sin^2(\theta) - 1)] \quad (4)$$

where θ is the angle between the directions of absorbed and emitted photon, I_o is the total unpolarized intensity; R is anisotropy parameter of polarization. For well separated final states f, R takes the simple form;

$$R = R_f = \frac{1}{5}(3\cos^2(\phi_f) - 1) \quad (5)$$

where ϕ_f is an angle between the transition dipole moments of XA and XE. It is clear from section 3.2 and eqs. (3) and (4) that the knowledge of both the transition moment from electronic ground state to the core excited state in XAS and transition from the core excited state to valance excited state in XES is necessary for the calculations of angular anisotropy (R). The value of anisotropy parameter R is dependent upon the symmetry of emitting and initially excited orbital. The anisotropy R takes a value of $\frac{2}{5}$ when the emitting orbital has the same symmetry as that of the intially excited orbital. For emmision orginating from an orbital of different symmetry, R becomes -$\frac{1}{5}$ [46]. In our experiments, the geometry is such that the spectra are recorded at an angle $\theta = 0$. The emission intensity can be written as

$$I(0^\circ) = I_o(1 - R) \quad (6)$$

To allow for comparison, theoretical results of computed angular anisotropy for ACN and H-bonded were convoluted using a Voigt line shape. The Lorentzian line shape is used with half width at half maximum (HWHM) of 0.2 eV to account for lifetime broadening. These results are further convoluted with a Gaussian line shape with half width at half maximum of 0.2 eV in order to account for experimental spectrometer resolution. The parameters for Voigt profile and algorithm are taken from the literature[49,50].

4 Results and Discussions

4.1 RIXS maps

Experimental RIXS data were collected by scanning the incident photon energy ω by using a monochromator and emitted photon energy ω' by grating spectrograph. The two dimensional data for incident energy plotted against emitted photon energy gives the resultant intensity distributions (RIXS map). The experimental RIXS maps for acetonitrile and acetonitrile-water along with energy loss maps are reported in Fig. 2. The width of elastic peak as labelled by line 'A'is not in wide energy range; therefore elastic resonance can be considered as straight line. The slope of this line can be used for the calibration of incident photon energy. Incident energy calibrated according to slope of elastic peak gives the energy loss map as indicated in panel c and panel d of Fig. 2.

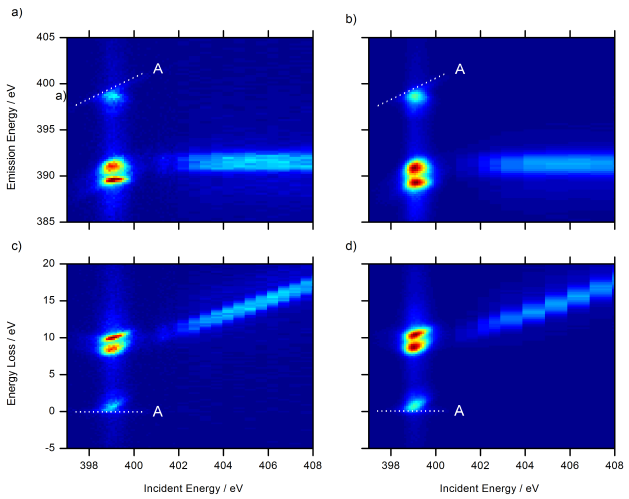

Fig. 2 Experimental results of RIXS map for **(a)**acetonitrile **(b)** acetonitrile-water complex. The corresponding energy loss maps for acetonitrile and acetonitrile-water complex are shown on panel **(c)** and panel **(d)** respectively.

Although theoretical results lack vibrational progressions, however these calculations are very useful to assign electronic character to every final state involved in RIXS at specific incident photon energy. These calculations can also reproduce the qualitative features of experimental data depending upon the selection of active and inactive orbitals in the active space. The detailed study of fluorescence core-hole decay helps to understand the valence ex-

citations.

4.2 X-Ray Absorption and Emission Spectra

In the following we compare the experimentally measured XAS spectra of the N 1s as total fluorescence yield (TFY) and partial fluorescence yield (PFY), with *ab initio* calculations. The *ab initio* calculations provide the information about the nature of MOs contributing in XAS spectra. Each spectrum of discrete transitions, based on absorption cross sections obtained by using eq. (1), is broadened by using a Voigt profile. The simulated

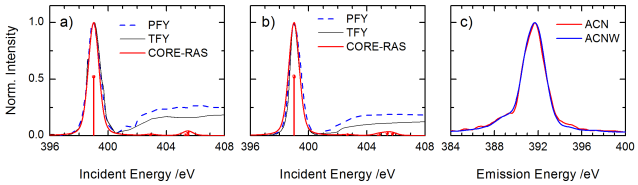

Fig. 3 Comparison of theoretical and experimental results for XAS of **(a)** ACN **(b)** ACN-water complex. Vertical bars represent the spectra without broadening. Experimental non-resonant XES for ACN and ACN-water is presented in panel **(c)**.

XA of the Nitrogen K-edge are presented in Fig. 3. Experimentally measured spectra in TFY and PFY mode are also plotted in the same figure for comparison.The comparison between theoretical and experimental results is in excellent agreement, with all qualitative features reproduced accurately. Panel **a)**, showing simulated and measured absorption spectra at the K-edge of nitrogen for acetonitrile, has one pronounced feature at 399 eV. On the basis of RASSCF calculations, it is assigned to the $N_{1s} \rightarrow 3e$ transitions. The low intensity peak near energy 405 eV is mainly due to the transitions $N_{1s} \rightarrow 8a1$. On Panel **b)**, absorption spectra at the K-edge of nitrogen for acetonitrile-water complex are presented. In case of acetonitrile-water, simulated absorption spectra were shifted to the red with respect to the experiment by about 2 eV for the purpose of comparison. This shift may correspond to the size of active space which is different in case of acetonitrile-water compared to acetonitrile. The XA spectra for acetonitrile-water complex have almost same feature as that of acetonitrile. The experimentally observed RIXS spectra for acetonitrile and acetonitrile-water complex provides no information for excitation energies above the π^* resonance, therefore low intensity peaks occurring at 405 eV have no further role in the current studies. The non-resonant XES observed experimentally is presented on panel **c** of Fig. 3. The XES spectra does not provide any additional structural information which can be useful for understanding the hydrogen bonding involved in acetonitrile-water complex. Therefore energy loss spectra are considered for better insight into the features observed experimentally.

4.3 Energy Loss Spectra

On the panel (a) of Fig. 4, the experimental energy loss spectrum for acetonitrile is presented. In order to get insight into the MOs involved in the transition peaks observed experimentally, simulated energy loss spectra is calculated and presented on Panel **c)** of Fig. 4. Overall, the theoretical spectra resembles that of the one obtained experimentally, except energy loss is slightly overestimated by simulated spectra. The orbitals involved in transitions corresponding to different peaks in spectra, help to assign anisotropy. The intensity of transitions involving orbitals of same symmetry as that of 3e should decrease and for transitions originating from orbitals of different symmetry ('a'), intensity should increase due to value of anisotropy parameter R. On the basis of theoretical assignment, the relaxation of degenerate 3e (antibonding π^*) orbital to fill core hole gives rise to peak A leaving system in ground state. The peak B observed at energy loss of about 8 eV is attributed to the relaxations of two MOs of symmetry 2e and energetically separated by about 0.38 eV. The intensity is weaker under horizontally polarized excitations because both MOs have the same symmetry as that of 3e. The next transition

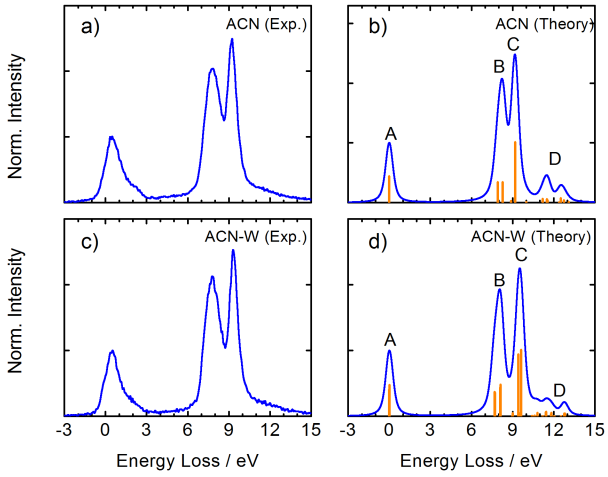

Fig. 4 Energy loss spectra for pure acetonitrile **(a)** Experimental spectrum **(b)** Theoretically calculated spectrum. Energy loss spectra for acetonitrile-water mixture **(c)** Experimental spectrum **(d)**Theoretical calculated spectrum. Vertical bars represent the spectra without broadening.

occurring at energy loss of 9.2 eV giving rise to peak C is due to $N_{1s} \leftarrow 7a_1$ transition. The stronger intensity is expected by the transition originating from the orbital $7a_1$. This is due to the fact that the orbital involved in this relaxation is of different symmetry from the excited $3e$ orbital and gives rise to stronger intensity in horizontally polarized excitations (cf. (eqs. (5) and (6))). There are some other transitions occurring at energy loss of about 12 eV due to orbitals mainly of $1e$ symmetry with very weak intensities.

To understand the effects of hydrogen bonding, energy loss spectra of acetonitrile-water are presented on panel **b**) and panel **d**) in Fig.4. According to these results, the spectra for acetonitrile-water is brodended at peak B and peak C as compared to pure acetonitrile and is shown in Fig. 4. The reason for broadening in peak C is relaxation of $7a_1$ orbital to fill core hole, generated by excitations to energetically different states. It is also notable that the peak C occurs at greater energy loss as compared to pure acetonitrile by an amount of 0.4 eV. This is due to the reason that orbital $7a_1$ becomes stabilized by hydrogen bonding through lowering of the energy gap with the core orbital. The majpor con-

tributions are due to dipole-dipole interactions and mixing of orbitals with the water orbitals[51]. On the basis of orbital occupancy, as π character of N changes due to addition of water, the energies of the orbitals are affected (due to hydrogen bonding) which manifest in the slight shift towards lower energy loss of peak B on panel **b**) and panel **d**) in Fig.4.The main features observed for acetonitrile are originating from the orbitals as reported[52].

All energies utilized in calculating the energy loss spectra are obtained by multi-state (MS) RASPT2. RASPT2 calculations have been performed using the default value for ionization potential electron affinity (IPEA) and an imaginary shift of 0.3 to avoid intruder states[53].

It is important to know the effects of hydrogen bonding, resulting from water molecule in acetonitrile-water complex, on the orbitals involved in active space shown in 1. It is reasonable to assign the orbital of lower energy from sp hybrid orbitals of nitrile group as lone pair of electron on N and remaining two degenerate hybrid orbitals as π bonds[54]. The *ab initio* calculations provide insight into the experimentally observed peaks and help in assignment of MOs that majoraly contribute to these peaks. From the *ab initio* calculations, the (π^* orbital involved in resonant transition and giving main observed features in absorption is shown on top of both panels of Fig. 5. The main features observed in energy loss spectra are due to the relaxations of valence orbitals of type σ and π. The π and one of σ orbitals involved in transitions are presented in Fig. 5. The isosurface of these orbitals shows the effect of hydrogen bonding on lone pair orbital of acetonitrile-water complex.

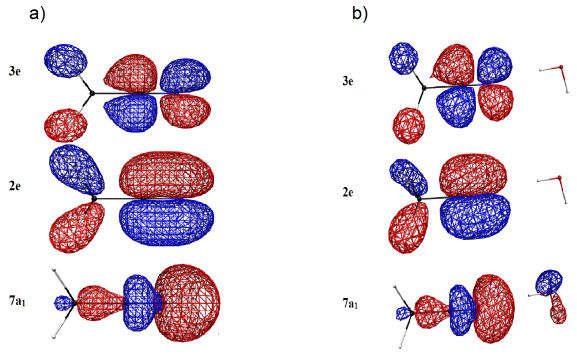

Fig. 5 Isosurface of orbitals from top to bottom in each panel, valence 3e orbital, 2 orbital and lone pair electron $7a_1$ orbital of **a) acetonitrile b) acetonitrile-water mixture.**

4.4 Structural Properties of the ACN-water complex

The experimental results for different geometrical parameters of the acetonitrile molecule in gas phase are well known[55]. The optimized structural parameters for acetonitrile in gas phase are reported in Table 1, where they have been compared with experimental data and theoretically predicted results[56].

Table 1 Selected parameters for acetonitrile and water bonded acetonitrile

	ACN		$ACN-H_2O$	
Description*	Computational	Experiment	Computational	Literature**
R_{C-C}	1.465	1.4584	1.464	1.467
$R_{C\equiv N}$	1.129	1.1571	1.126	1.134
R_{C-H}	1.080	1.1036	1.080	1.082
$R_{N\ldots H}$	–	–	2.254	2.249
$R_{N\ldots O}$	–	–	3.194	3.183
$\theta_{C-C\equiv N}$	179.973	–	179.9	179.9
θ_{C-C-H}	109.660	109.5	109.6	109.7
θ_{H-C-H}	109.279	109.5	109.4	109.3
$\theta_{N\ldots H-O}$	–	–	174.3	169.5
$\theta_{C\equiv N\ldots O}$	–	–	172.0	171.6

*Distances (R) in and angles (θ) in degrees.
**Ref.[20]

5 Conclusions

The influence of hydrogen bonding on the electronic structure of the nitrogen atoms in cyano-groups, acetonitrile and acetonitrile-water mixtures have been investigated using X-ray absorption spectroscopy and Resonant Inelastic X-ray Scattering (RIXS). We employed a *ab initio* RASSCF calculations in order to interpret experimental electronic structure probes via nitrogen core-level transitions. These calculations give explicit access to each electronic state with the extracted information allowing to assign the dominant transitions in the X-ray absorption spectrum, and unearthing the electronic character of every final valence excitation resulting from RIXS at a specific incident photon energy. The computed shift of the CN stretching mode to higher frequency is found which is in agreement with reported results.[57,58] This can be distinctly seen in the corresponding vibrational frequency, but also very clearly as a marked shift in the Raman UV line at 9.2 eV. These spectral shifts pinpoint the stabilization of the lone pair orbital on the nitrogen atom of the acetonitrile-water complex.

Our calculations helps to links UV excitations of the electronic system to the molecular structure which is important for understanding the interplay of electronic and nuclear degrees of freedom. This work also indicates that RIXS spectroscopy of cyano groups may detect even a very weak hydrogen bonding hydrogen bonding in solvated systems or small model peptides. Further investigations of different nitrogen-containing functional groups and more complex electrostatic environments will follow.

References

1 G. R. Desiraju and T. Steiner, *The weak hydrogen bond: in structural chemistry and biology*, Oxford University Press, Oxford, 1999.

2 S. J. Grabowski, *Journal of Physical Organic Chemistry*, 2003, **17**, 18–31.

3 G. R. Desiraju, *Angewandte Chemie International Edition*, 2010, **50**, 52–59.

4 S. Fulle and H. Gohlke, *Biophysical Journal*, 2008, **94**, 4202–4219.

5 L. Pauling, R. B. Corey and H. R. Branson, *Proceedings of the National Academy of Sciences*, 1951, **37**, 205–211.

6 C. C. F. Blake, D. F. Koenig, G. A. Mair, A. C. T. North, D. C. Phillips and V. R. Sarma, *Nature*, 1965, **206**, 757–761.

7 J. D. WATSON and F. H. C. CRICK, *Nature*, 1953, **171**, 737–738.

8 N. Huse, H. Wen, D. Nordlund, E. Szilagyi, D. Daranciang, T. A. Miller, A. Nilsson, R. W. Schoenlein and A. M. Lindenberg, *Physical Chemistry Chemical Physics*, 2009, **11**, 3951.

9 D. Rapaport, *Molecular Physics*, 1983, **50**, 1151–1162.

10 E. Guardia, I. Skarmoutsos and M. Masia, *The Journal of Physical Chemistry B*, 2015, **119**, 8926–8938.

11 Y. Tao, W. Zou, J. Jia, W. Li and D. Cremer, *Journal of Chemical Theory and Computation*, 2017, **13**, 55–76.

12 *Ultrafast Hydrogen Bonding Dynamics and Proton Transfer Prosesses in the Condensed Phase*, ed. T. Elsaesser and H. J. Bakker, Springer Netherlands, 2002.

13 H. Ishikita and K. Saito, *Journal of The Royal Society Interface*, 2013, **11**, 20130518–20130518.

14 E. T. J. Nibbering and T. Elsaesser, *Chemical Reviews*, 2004, **104**, 1887–1914.

15 K. Heyne, N. Huse, E. T. J. Nibbering and T. Elsaesser, *Journal of Physics: Condensed Matter*, 2002, **15**, S129–S136.

16 T. Takamuku, M. Tabata, A. Yamaguchi, J. Nishimoto, M. Kumamoto, H. Wakita and T. Yamaguchi, *The Journal of Physical Chemistry B*, 1998, **102**, 8880–8888.

17 G. Eaton, A. S. Pena-Nuñez, M. C. R. Symons, M. Ferrario and I. R. McDonald, *Faraday Discuss. Chem. Soc.*, 1988, **85**, 237–253.

18 G. Eaton, A. S. Pena-Nuñez and M. C. R. Symons, *Journal of the Chemical Society, Faraday Transactions 1: Physical Chemistry in Condensed Phases*, 1988, **84**, 2181.

19 D. Jamroz, J. Stangret and J. Lindgren, *Journal of the American Chemical Society*, 1993, **115**, 6165–6168.

20 J. E. Bertie and Z. Lan, *The Journal of Physical Chemistry B*, 1997, **101**, 4111–4119.

21 K. L. Rowlen and J. M. Harris, *Analytical Chemistry*, 1991, **63**, 964–969.

22 M. Stoev, A. Makarow and J. M. A. Robledo, *Spectroscopy Letters*, 1995, **28**, 1251–1258.

23 D. S. Venables and C. A. Schmuttenmaer, *The Journal of Chemical Physics*, 1998, **108**, 4935–4944.

24 C. Desfrancois, H. Abdoul-Carime, C. P. Schulz and J. P. Schermann, *Science*, 1995, **269**, 1707–1709.

25 R. Rivelino, V. Ludwig, E. Rissi and S. Canuto, *Journal of Molecular Structure*, 2002, **615**, 257–266.

26 E. Rissi, E. E. Fileti and S. Canuto, *Theoretical Chemistry Accounts: Theory, Computation, and Modeling (Theoretica Chimica Acta)*, 2003, **110**, 360–366.

27 H. Kovacs and A. Laaksonen, *Journal of the American Chemical Society*, 1991, **113**, 5596–5605.

28 E. Hawlicka, *Polish Journal of Chemistry*, 1996, **70**, 827.

29 D. S. Venables and C. A. Schmuttenmaer, *The Journal of Chemical Physics*, 2000, **113**, 11222–11236.

30 K. Kunnus, I. Rajkovic, S. Schreck, W. Quevedo, S. Eckert, M. Beye, E. Suljoti, C. Weniger, C. Kalus, S. GrÃijbel, M. Scholz, D. Nordlund, W. Zhang, R. W. Hartsock, K. J. Gaffney, W. F. Schlotter, J. J. Turner, B. Kennedy, F. Hennies, S. Techert, P. Wernet and A. FÃűhlisch, *Review of Scientific Instruments*, 2012, **83**, 123109.

31 K. Pierloot, B. Dumez, P.-O. Widmark and B. O. Roos, *Theoretica chimica acta*, **90**, 87–114.

32 K. Andersson, P. Å. Malmqvist and B. O. Roos, *The Journal of Chemical Physics*, 1992, **96**, 1218–1226.

33 K. Andersson, P. Å. Malmqvist, B. O. Roos, A. J. Sadlej and K. Wolinski, *The Journal of Physical Chemistry*, 1990, **94**, 5483–5488.

34 P. Å. Malmqvist, K. Pierloot, A. R. M. Shahi, C. J. Cramer and L. Gagliardi, *The Journal of Chemical Physics*, 2008, **128**, year.

35 F. Aquilante, L. De Vico, N. Ferré, G. Ghigo, P. Å. Malmqvist, P. Neogrády, T. B. Pedersen, M. Pitoňák, M. Reiher, B. O. Roos, L. Serrano-Andrés, M. Urban, V. Veryazov and R. Lindh, *J. Comput. Chem.*, 2010, **31**, 224–247.

36 M. J. Frisch, G. W. Trucks, H. B. Schlegel, G. E. Scuseria, M. A. Robb, J. R. Cheeseman, G. Scalmani, V. Barone, B. Mennucci, G. A. Petersson, H. Nakatsuji, M. Caricato, X. Li, H. P. Hratchian, A. F. Izmaylov, J. Bloino, G. Zheng, J. L. Sonnenberg, M. Hada, M. Ehara, K. Toyota, R. Fukuda, J. Hasegawa, M. Ishida, T. Nakajima, Y. Honda, O. Kitao, H. Nakai, T. Vreven, J. A. Montgomery, Jr., J. E. Peralta, F. Ogliaro, M. Bearpark, J. J. Heyd, E. Brothers, K. N. Kudin, V. N. Staroverov, R. Kobayashi, J. Normand, K. Raghavachari, A. Rendell, J. C. Burant, S. S. Iyengar, J. Tomasi, M. Cossi, N. Rega, J. M. Millam, M. Klene, J. E. Knox, J. B. Cross, V. Bakken, C. Adamo, J. Jaramillo, R. Gomperts, R. E. Stratmann, O. Yazyev, A. J. Austin, R. Cammi, C. Pomelli, J. W. Ochterski, R. L. Martin, K. Morokuma, V. G. Zakrzewski, G. A. Voth, P. Salvador, J. J. Dannenberg, S. Dapprich, A. D. Daniels, . Farkas, J. B. Foresman, J. V. Ortiz, J. Cioslowski and D. J. Fox, *GaussianâĹij09 Revision E.01*, Gaussian Inc. Wallingford CT 2009.

37 P. Å. Malmqvist, B. O. Roos and B. Schimmelpfennig, *Chemical Physics Letters*, 2002, **357**, 230 – 240.

38 W. L. Jorgensen and L. Salem, *The Organic Chemist's Book of Orbitals p.118.*, Academic Press, New York, 1973.

39 A. Minchinton, C. Brion, J. Cook and E. Weigold, *Chemical Physics*, 1983, **76**, 89 – 101.

40 F. Edard and M. Tronc, *Journal of Physics B: Atomic and Molecular Physics*, 1987, **20**, L265.

41 P. Å. Malmqvist and B. O. Roos, *Chemical Physics Letters*, 1989, **155**, 189 – 194.

42 M. Odelius, *The Journal of Physical Chemistry A*, 2009, **113**, 8176–8181.

43 P. Glatzel, J. Yano, U. Bergmann, H. Visser, J. H. Robblee, W. Gu, F. M. de Groot, S. P. Cramer and V. K. Yachandra, *Journal of Physics and Chemistry of Solids*, 2005, **66**, 2163 – 2167.

44 F. Gel'mukhanov and H. Ågren, *Phys. Rep.*, 1999, **312**, 87–330.

45 A. Kotani and S. Shin, *Rev. Mod. Phys.*, 2001, **73**, 203–246.

46 Y. Luo, H. Ågren and F. Gel'mukhanov, *Phys. Rev. A*, 1996, **53**, 1340–1348.

47 Y. Horikawa, T. Tokushima, A. Hiraya and S. Shin, *Phys. Chem. Chem. Phys.*, 2010, **12**, 9165–9168.

48 S. Kashtanov, A. Augustsson, Y. Luo, J.-H. Guo, C. Såthe, J.-E. Rubensson, H. Siegbahn, J. Nordgren and H. Ågren, *Phys. Rev. B*, 2004, **69**, 024201.

49 L. F. J. Piper, L. Colakerol, T. Learmonth, P.-A. Glans, K. E. Smith, F. Fuchs, J. Furthmüller, F. Bechstedt, T.-C. Chen, T. D. Moustakas and J.-H. Guo, *Phys. Rev. B*, 2007, **76**, 245204.

50 F. Schreier, *Journal of Quantitative Spectroscopy and Radiative Transfer*, 2011, **112**, 1010 – 1025.

51 L. Weinhardt, E. Ertan, M. Iannuzzi, M. Weigand, O. Fuchs, M. Bar, M. Blum, J. D. Denlinger, W. Yang, E. Umbach, M. Odelius and C. Heske, *Phys. Chem. Chem. Phys.*, 2015, **17**, 27145–27153.

52 B. Dierker, E. Suljoti, K. Atak, K. M. Lange, N. Engel, R. Golnak, M. Dantz, K. Hodeck, M. Khan, N. Kosugi and E. F. Aziz, *New Journal of Physics*, 2013, **15**, 093025.

53 N. Forsberg and P. Å. Malmqvist, *Chemical Physics Letters*, 1997, **274**, 196 – 204.

54 A. N. Rosli, M. A. A. Bakar, N. S. A. Manan, P. M. Woi, V. S. Lee, S. M. Zain, M. R. Ahmad and Y. Alias, *Sensors*, 2013, **13**, 13835.

55 C. C. Costain, *The Journal of Chemical Physics*, 1958, **29**, 864–874.

56 J. R. Damewood and R. A. Kumpf, *The Journal of Physical Chemistry*, 1987, **91**, 3449–3452.

57 F. Muniz-Miranda, M. Pagliai, G. Cardini and R. Righini, *The Journal of Chemical Physics*, 2012, **137**, year.

58 W. R. Fawcett, *Liquids, solutions, and interfaces: from classical macroscopic descriptions to modern microscopic details*, Oxford University Press, 2004.

Chapter 4

Understanding ultrafast reaction dynamics using X-ray absorption spectroscopy

It is of paramount importance to understand the chemical reactions on levels of atoms and electronic configurations in many fields of chemistry ranging from biochemistry to material sciences. Sulfur is an important element in many chemical compounds due to its abundance and existance in a variety of oxidation states. *Ab initio* calculations are employed to validate and understand the character of new transitions in time-resolved sulfur-1s spectroscopy. These calculations are helpful in modeling an electronically excited, light-induced chemical reaction pathways for sulfur model systems.

In **paper I**, a model system 4-methylthiophenol (4-MTP) was used to study the light-induced radical formation and thione isomerization by time-resolved sulfur-1s absorption spectroscopy. The differential absorptions spectrum was obtained following irradiation with 267 nm (4.64 eV) light at two different fluences: 25 mJ cm-2 (low) and 50 mJ cm-2 (high). At 100 ps time delay of pump-probe, two prominent signals were observed; a negative signal corresponding to the bleach of the ground state along with three induced absorption peaks emerging at energies of 2467.0, 2468.5, and 2470.3 eV, respectively. In order to understand origin of the induced absorption features, first principles multi-reference RASSCF method employing an active space comprisng of 14 electrons distributed over 13 orbitals was used with no symmetry imposed. Furthermore, a constant shift of -2.8 eV was applied to match the computed spectrum of different molecular species with the experimental one. The absorption spectra of relevant species namely, 4-methylthiophenoxy radical, the formally hydride-abstracted cation, and the thiolate anion along with three possible thione isomers as a possible photoproducts were computed to explain emergence of three induced absorption peaks. The spectral feature observed at 2467.0 eV underscores a photoinduced homolytic bond cleavage on comparison with computed spectra of 4-methylthiophenoxy radical. The induced absorption peak observed at 2468.5 eV matches very well to the computed spectra of two thione isomers namely, para-thione and ortho-thione with

small variation in intensity and energy of the dominant transition. The third induced absorption peak observed at 2470.3 eV is assigned to fluence-dependent anion formation as it appears only at high fluence (50 mJ/cm2). From this picture different reaction pathways emerged as anion generation, thione isomerization and radical formation.

It is important to understand the photophysics and photochemistry of disulfide due to their existence between cysteine residues in proteins. In **paper III**, the simplest disulfide containing molecule, dimethyl disulfide (DMDS) was used to investigate different photoproducts as a consequence of photolytic bond cleavage. The differential absorption spectrum was obtained following irradiation with 267 nm (4.64 eV) light. The transient spectrum at a time delay of 100 ps indicates a negative signal corresponding to the bleach of the ground state with two prominent peaks at energy values of 2471.5 and 2473.0 eV along with two distinct induced absorption peaks emerging at energies of 2466.5 and 2467.3 eV, respectively. In addition to these induced absorption peaks, a broad shoulder in the energy range of 2467.8 to 2469.7 eV is also a part of differential signal. In order to assign the spectral features in the differential absorption signal and thus to gain insight about the nature of the photoproducts, first principles multi-reference RASSCF calculations with no symmetry were carried out. The active space for the simulated spectrum of the ground state and perthiyl radical comprises of 14/13 electrons in 12 orbitals respectively, which is reduced to 11 electrons in 11 orbitals for simulation of thiyl radical spectrum. In addition, aug-cc- pvdz basis was used for all atomic centers. However, the results obtained by aug-cc- pvtz basis for all atomic centers do not converge for the thyil and perthiyl radicals due to intrude state problems. The absorption spectra of relevant species namely, dimethyl disulfide cation, thiyl radical, perthiyl radical, and different allotropes of sulfur were computed to explain the emergence of induced absorption features. The spectral feature observed at 2467.3 eV compares well with the computed spectrum of the perthiyl radical and thus underscores the photoinduced homolytic C-S bond cleavage. The induced absorption peak observed at 2466.5 eV matches very well to the computed spectra of thiyl radical formed by an S-S homolytic bond cleavage. Several photoionization products to interpret the shoulder in energy range of 2467.8 to 2469.7 eV have been considered. However, the absorption spectrum of DMDS cation fits in the region of the shoulder but according to reported literature the ionization energy (8.13 eV) of DMDS to its cation is not accessible in our experiment at 4.6 eV excitation energy. Consideration of two-photon absorption effects gives rise to energy of 9.2 eV at which photoionization of DMDS might be possible. Also, reported data for the cation formation had been extracted from the experiments in the gas phase. In short, photochemical dynamics of DMDS results in S-S and C-S bond cleavage as two dominant reaction pathways giving rise to the formation of thiyl and perthiyl radical, respectively.

JACS
JOURNAL OF THE AMERICAN CHEMICAL SOCIETY

Article

pubs.acs.org/JACS

Light-Induced Radical Formation and Isomerization of an Aromatic Thiol in Solution Followed by Time-Resolved X-ray Absorption Spectroscopy at the Sulfur K-Edge

Miguel Ochmann,[†,‡,■] Inga von Ahnen,[†,#,■] Amy A. Cordones,[§,▽] Abid Hussain,[†,‡] Jae Hyuk Lee,[§,○] Kiryong Hong,[§,∥,▼] Katrin Adamczyk,[†,‡] Oriol Vendrell,[⊥,◆] Tae Kyu Kim,[*,∥] Robert W. Schoenlein,[*,§,¶] and Nils Huse[*,†,‡]

[†]Department of Physics, University of Hamburg and Center for Free Electron Laser Science, 22761 Hamburg, Germany
[‡]Max Planck Institute for the Structure and Dynamics of Matter, 22761 Hamburg, Germany
[§]Ultrafast X-ray Science Lab, Chemical Sciences Division, Lawrence Berkeley National Laboratory, Berkeley, California 94720, United States
[∥]Department of Chemistry and Chemistry Institute of Functional Materials, Pusan National University, Busan 46241, South Korea
[⊥]Center for Free-Electron Laser Science, DESY and The Hamburg Centre for Ultrafast Imaging, 22607 Hamburg, Germany

Supporting Information

ABSTRACT: We applied time-resolved sulfur-1s absorption spectroscopy to a model aromatic thiol system as a promising method for tracking chemical reactions in solution. Sulfur-1s absorption spectroscopy allows tracking multiple sulfur species with a time resolution of ∼70 ps at synchrotron radiation facilities. Experimental transient spectra combined with high-level electronic structure theory allow identification of a radical and two thione isomers, which are generated upon illumination with 267 nm radiation. Moreover, the regioselectivity of the thione isomerization is explained by the resulting radical frontier orbitals. This work demonstrates the usefulness and potential of time-resolved sulfur-1s absorption spectroscopy for tracking multiple chemical reaction pathways and transient products of sulfur-containing molecules in solution.

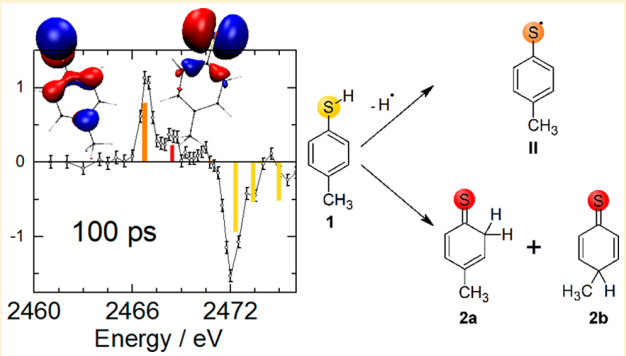

INTRODUCTION

Understanding chemical reactions on levels of atoms and electronic configurations is of major interest in most fields of chemistry, ranging from biochemistry to material sciences in order to mimic biological reactions, optimize existing chemical processes on a lab or industrial scale, or access new synthetic routes. Complex chemical reactions can be broken down into basic reaction steps, most of which involve a functional group containing one or more heteroatoms, e.g., oxygen, nitrogen, or sulfur at the reacting functional group. Sulfur is of high chemical importance as it is the tenth most abundant element in the universe and in particular, the earth's crust[1,2] and can be found in a variety of oxidation states, ranging from −2 to +6.[2,3] Its electronic versatility makes it an important element in many chemical compounds, ranging from polymers, nanoparticles, and electrode materials in batteries to molecular electronics devices. In the latter, sulfur is widely used as anchoring group for "molecular wires"[4] and in the form of thiophene-containing π-systems in organic field-effect transistors (OFETs), organic light-emitting diodes (OLEDs), and organic photovoltaics (OPVs).[5,6] Furthermore, sulfur plays an important role in biochemistry: In both peptide chains and reaction centers of proteins, sulfur is an important element, i.e., as one of the amino acids methionine (thioether) or cysteine (thiol) and as sulfide in metal−sulfur-complexes, respectively.[7]

The thiol group has a central function in many biologically important reactions such as the formation of disulfide bridges via several thiol−disulfide interchange reactions in proteins.[8−10] Thiols are also active in radical repair by donating an H atom to a radical thereby forming the more stable S-centered thiyl radical.[8,11] Thiols in general are known for their antioxidant and radical scavenging properties. The thiyl radical as the product of the repair reaction and the intermediate of thiol-including reactions in biochemistry can undergo many different secondary reactions of which some are potentially biologically harmful.[12−14] Increased protein folding and unfolding of disulfide-containing proteins by addition of substituted thiophenols in vitro has been observed as well.[10,15] Accordingly, the chemical behavior of aromatic thiols and corresponding

Received: December 22, 2016
Published: February 20, 2017

DOI: 10.1021/jacs.6b12992
J. Am. Chem. Soc. XXXX, XXX, XXX−XXX

thiyl radicals and thiolates are of major interest for biochemical and biological applications.

Aromatic thiols show a higher nucleophilicity and reactivity toward disulfides than aliphatic thiols.[8] Photoexcitation of thiophenol and its derivatives with ultraviolet light seems to primarily result in the formation of the S-centered thiyl radicals (thiophenoxy radicals) via homolytic bond cleavage of the S−H bond.[16−18] Riyad et al. investigated the reaction kinetics of the thiophenoxy radical after photodissociation of several substituted thiophenols including 4-methylthiophenol (4-MTP, **1**) with laser flash photolysis.[18] Theory predicts the photodissociation to result from population of the repulsive $\pi\sigma^*$-state (S_2). In solution, the formation of a conical intersection between the S_2 and the ground-state S_0 would allow for direct relaxation back to the ground state, but the dissociation pathway which leads to radical formation dominates.[19−22] Accordingly, the reported decay rates of the radical population are consistent with diffusion-limited recombination. In addition, a second product was ascribed to a hydrogen adduct (H-adduct) resulting from the reaction of a hydrogen atom with the aromatic ring of the parent thiophenol molecule. A third product appearing within ∼15 μs was hypothesized to be the disulfide dimer formed by the reaction of two thiophenoxy radicals.

More recently, femtosecond ultraviolet absorption spectroscopy revealed the formation of a secondary photoproduct after photodissociation of 4-MTP on a time scale of tens of picoseconds with the same spectral footprint as the H-adduct observed by Riyad et al.,[18] which suggested the appearance of this photoproduct to coincide with the initial decay of the thiophenoxy radical.[19−21] The structure of this species was suggested to be a thione isomer, where the H atom is bound at the *ortho*-, *meta*-, or *para*-position of the phenyl ring.[21,22] Since the *meta*-adduct is thermodynamically less stable than the other products, the Bradforth group concluded that this recombination pathway is strongly disfavored.[19] However, this interpretation is tentative as the dynamical UV and vibrational studies are based in part on theoretical predictions with only qualitative agreement with experiment. A clear spectral identification of the transient photoproducts is paramount for a reliable understanding of the reaction mechanism. Unfortunately, optical probes are generally very difficult to simulate quantitatively, even with high-level electronic structure calculations, due to strong electron−electron correlations and the broad and often nondescript nature of valence-to-valence transitions.

In this work we investigate the photochemistry of 4-MTP (**1**) with time-resolved X-ray absorption spectroscopy (TRXAS) at the sulfur K-edge, which is capable of following reaction dynamics of sulfur-containing systems with elemental specificity. The abundant body of literature on studies employing static sulfur K-edge XAS to molecular systems both experimentally and theoretically[23−40] underscores the usefulness and important information content of sulfur-1s spectroscopy. Pairing the high chemical specificity of spectroscopy in the soft,[41−44] tender,[45−48] and hard[49−55] X-ray range with time-resolved methods is becoming an established spectroscopic tool for structural dynamics by tracking the relevant atomic species during ultrafast chemical reactions. TRXAS exploits the inherent element specificity of core-level transitions, the initial state of which is highly localized and of well-defined symmetry and spin. Moreover, distinct spectral features of atomic species in different oxidation and spin states permit the precise assignment of photoproducts, thereby allowing TRXAS to follow dynamics of electronic and molecular structure more precisely than valence spectroscopy permits. The sensitivity of X-ray absorption spectra to bond order, symmetry, and valence charge distribution around the absorbing atomic species can be particularly useful in the identification of different reaction intermediates and products when multiple reaction pathways are present. In particular, sulfur-1s absorption spectroscopy is known to exhibit large spectral separations for different chemical environments of the sulfur atom.[56−61] It permits identifying the chemical state of sulfur-containing functional groups very precisely and with atomic resolution for spectrally distinct sulfur sites within a molecule or among different photoproducts. In the following, we present a time-resolved study at the sulfur K-edge with sulfur 1s → 3p transitions as a probe of molecular dynamics of 4-MTP in cyclohexane solution.

METHODS

Experimental Setup. All experiments were conducted at beamline 6.0.1. of the Advanced Light Source in Berkeley, California, and the experimental setup has been described previously.[62,63] The experimental setup is shown in Figure 1. The filling pattern of the storage

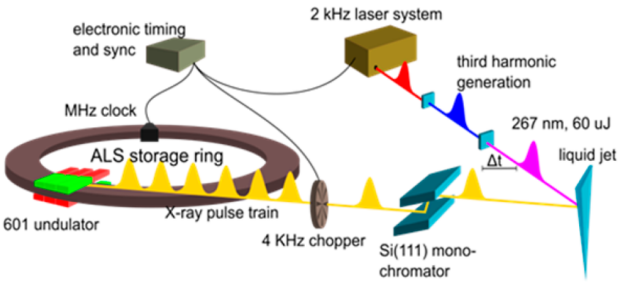

Figure 1. Schematic drawing of the experimental setup at beamline 6.0.1 of the Advanced Light Source.

ring consists of 276 electron bunches, one of which is placed in a 100 ns gap for isolated detection. A 4-kHz heat-load chopper transmits 10-μs long X-ray bunch trains. The X-ray beam is monochromatized with a cryogenically cooled Si(111) double-crystal monochromator ($\Delta E/E$ = 1/7000). The X-ray pulses are focused to 170 μm × 250 μm at the sample position.

Pump pulses at 267 nm from a third harmonic generator (THG) of the Ti:sapphire 800 nm pulses are focused with a CaF_2 lens to 270 μm × 300 μm with 60 μJ at the sample position, impinging on the liquid jet at an angle of 15° with respect to the X-ray pulses. The laser oscillator is locked to the subharmonic of the 500 MHz radio frequency (RF) clock of the synchrotron storage ring while the Pockels cells of the laser amplifier are triggered by the X-ray chopper. Timing between X-rays and laser pulses is controlled by a phase shifter between the laser oscillator and the RF clock.

Static absorption spectra were collected in total fluorescence yield (TFY) using an integrating photodiode and a current amplifier. Transient differential absorption spectra are recorded in transmission at 4 kHz while the sample is intermittently excited at 2 kHz. The X-ray probe pulses impinged on an avalanche photodiode (APD) which is shielded from laser radiation with 200 nm of aluminum foil. The APD signal is amplified and sent to a boxcar integrator. The sample is delivered through a 100-μm wide sapphire nozzle by a gear pump at flow rates of >0.5 mL/s. Prior to data collection, the sample chamber was evacuated and filled with helium to 1 atm.

Chemicals and Materials. 4-MTP and cyclohexane were purchased from Sigma-Aldrich, and used without further purification. Cyclohexane solutions of 4-MTP (200 mM) were prepared by

DOI: 10.1021/jacs.6b12992
J. Am. Chem. Soc. XXXX, XXX, XXX−XXX

dissolving 12.4 g of 4-MTP in 500 mL of cyclohexane. Samples were always replaced after 8 h of use.

Theoretical Calculations. The equilibrium geometries of all molecular species were obtained by second order Møller−Plesset perturbation theory[64] (MP2) with the Dunning correlation consistent basis set aug-cc-pvtz[65] using the Gaussian 09 program package.[66] In order to simulate the X-ray absorption spectra, the first-principles multireference restricted active space self-consistent field (RASSCF) method was used with no symmetry imposed. The active space for simulated XAS comprised 14 electrons distributed over 13 orbitals. The aug-cc-pvtz basis is used for sulfur and the three adjacent carbon atoms, while aug-cc-pvdz was used on all other atomic centers. The energies of the computed states were further improved by applying second order perturbation theory (RASPT2)[67−69] to RASSCF wave functions to account for dynamic correlation effects. In the RASSCF calculations of core-excited states, the core orbital was kept in the RAS3-subspace, thus restricting the possible configurations to those with at least one electron missing from the core orbital and preventing a variational collapse during the wave function optimization that would refill the core-hole with a valence electron (this sorting of electrons into active spaces is known as the core-RAS method).[70] RASSCF/RASSI calculations were performed with the Molcas 7.8 program suite.[71] All transition energies were rescaled by a constant factor (equating to an energy shift of about −2.8 eV) such that the computed 4-MTP spectrum matches the experimental one.

RESULTS AND DISCUSSION

Figure 2A shows the static X-ray absorption spectrum of 4-MTP in cyclohexane at the sulfur K-edge. Two prominent transitions are observed at 2472.5 and 2473.6 eV, along with additional less resolved transitions above 2475 eV which merge into the actual continuum edge. The resulting differential absorption spectrum upon ultraviolet excitation at 267 nm (4.64 eV) at a pump−probe time delay of 100 ps is shown in Figure 2B. The negative bleaching signal at 2472.5 eV signals a loss of absorption and coincides with the two main absorption peaks of the ground state. Three induced absorption features emerge at energies of 2467.0, 2468.5, and 2470.3 eV, respectively. The apparent area ratio of the energetically lowest two peaks is about 1:3 while the small induced absorption is hard to quantify and only appears at high excitation fluence (see discussion below). Pump−probe transients at photon energies of the strongest absorption changes fully emerge within the time resolution of our experiment (~70 ps) and stay constant over the observed time frame of about 500 ps, as does the ground-state bleaching signal. For details on the experimental time traces and their modeling see the Supporting Information.

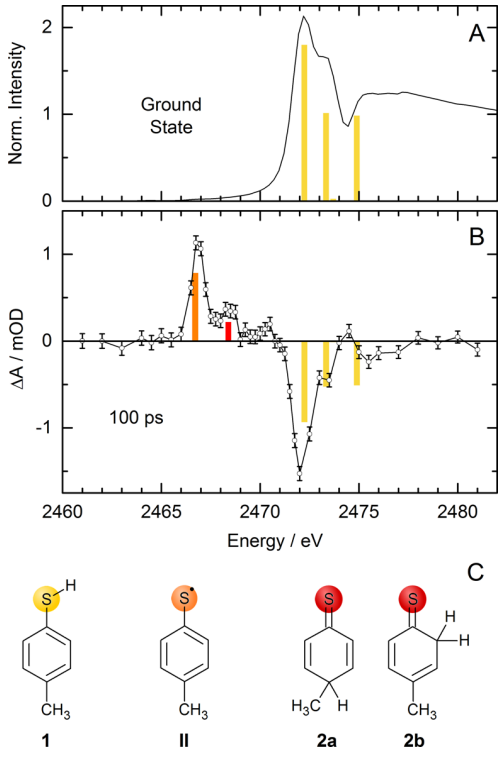

Figure 2. (A) Static sulfur-1s absorption spectrum of 4-MTP in cyclohexane solution and calculated lowest S-1s transitions (yellow). (B) Differential absorption spectrum at 100 ps after 267 nm excitation (50 mJ/cm^2), and calculated S-1s transitions for ground-state bleach and observed photoproducts: 4-MTP (yellow), radical (orange), and thione isomers (red). (C) Structures of 4-MTP (**1**), 4-methylthiophenoxy radical (**II**), and *ortho*- (**2a**) and *para*- (**2b**) thiones.

In order to identify the spectra in Figure 2, we employed RASSCF calculations to predict the sulfur-1s transitions of the ground state of 4-MTP (**1**) and possible photoproducts in order to recreate the experimental differential spectrum at 100 ps. Figure 2A shows three distinct transitions that match the experimentally observed ground-state transitions around 2472 eV very well. We have not convolved the transition lines with a Voigt profile for clarity. However, a monochromator resolution of σ = 0.35 eV and a Lorentzian lifetime broadening of 0.8 eV reproduce the main absorption features in Figure 2A (for convolved data see Figure S2). We note that our high-level electronic structure calculations neither describe the Rydberg series nor the atomic continuum absorption edge. Other theoretical approaches would be more appropriate for describing multiple scattering and the EXAFS region. However, RASSCF provides a very accurate approach to describing electronic correlations, and the bound−bound transitions relevant to this experimental study.

The initial chemical reaction step in 4-MTP upon excitation with 267 nm pulses is the cleavage of the S−H bond. Oliver et al. reasoned for homolytic bond dissociation with production of a hydrogen atom, a 4-methylthiophenoxy radical, and an additional adduct.[19] The 4-methylthiophenoxy radical (**II**) as shown in Figure 2C exhibits a theoretical S-1s spectrum that matches the experimentally observed induced absorption peak at 2467 eV, underscoring that indeed photoinduced homolytic bond cleavage occurs. However, the methylthiophenoxy radical alone does not reproduce our experimentally observed differential absorption spectrum at 100 ps. Another induced absorption peak at 2468.5 eV is clearly discernible.

In order to identify this feature, we have computed spectra for two 4-methylthiophenoxy ions, as these are most closely related to the 4-methylthiophenoxy radical (**II**): the formally hydride-abstracted cation (**Ia**) and the thiolate anion (**III**), both of which could be produced through heterolytic S−H bond dissociation. However, the computed sulfur-1s transitions of the cations (**Ia** and **Ib**) and the thiolate anion (**III**) deviate notably from the experimentally observed spectral feature at 2468.5 eV (see Figure S3). Moreover, the ejection of a hydride anion seems very unlikely since sulfur is the more electronegative atom in the S−H bond, polarizing the bond toward the sulfur atom. Two-photon ionization of 4-MTP toward the cation (**Ib**) at 9.3 eV seems possible[72] albeit the first ionization energy of elementary sulfur is at 10.36 eV.[73]

DOI: 10.1021/jacs.6b12992
J. Am. Chem. Soc. XXXX, XXX, XXX−XXX

Instead, we consider the three possible thione isomers to explain the observed emergence of this new spectral feature. These species can emerge when the photolytically cleaved hydrogen atom attaches to the aromatic ring of the parent 4-MTP radical residue, either in the *ortho-* (**2a**), *para-* (**2b**), or *meta-* (**2c**) position (see also Scheme S1), thereby disrupting the π-conjugation of the ring. The corresponding calculated lowest sulfur-1s transitions for **2a** and **2b**, namely, 4-methylcyclohexa-2,4-diene-1-thione (**2a**) and 4-methylcyclohexa-2,5-diene-1-thione (**2b**), henceforth denoted as *ortho-* (**2a**) and *para-* (**2b**) thione, respectively, both match the second observed induced absorption peak at 2468.5 eV very well. The dominant transition of the *ortho*-thione is predicted 0.15 eV lower in spectral position and with 20% higher amplitude than the *para*-thione. A distinction between the two isomers with sulfur-1s absorption spectroscopy is difficult due to the inherent lifetime broadening of ~0.8 eV. The *ortho*-thione assignment matches slightly better with the experimental data.

The nearly identical transition energies of both thione isomers point to the fact that the S-1s transitions are strongly influenced by the bonding order and oxidation state of the sulfur atom. For both thione isomers, the dominating feature is the C═S double bond. The position of the newly formed sp^3-hybridized carbon does not influence the electronic structure of the sulfur atom substantially because the sulfur atom and the newly formed CH_2 (**2a**) or $CHCH_3$ (**2b**) group are separated by either two (**2a**) or four (**2b**) chemical bonds, respectively. The *meta*-adduct **2c** cannot be described as a stable thione product in the conventional Lewis formalism but has to be conceived as a delocalized biradical which manifests itself as an energetically highly disfavored species[19] with sulfur-1s transitions appearing at much higher energy than the induced absorption peak at 2468.5 eV in Figure 2B (see also Scheme S1). Recently, Reva et al. found clear evidence for the formation of the thione isomers **2a** and **2b** upon photoexcitation. Steady-state infrared spectroscopy was used in cryogenic argon matrices in which these isomers form extremely long-lived metastable states.[74] Moreover, no evidence for the formation of the *meta*-adduct **2c** was found while photoexcitation with 267 nm light resulted in the formation of **2a** and **2b**. These results are in excellent agreement with our findings. However, our method observes the photochemistry of 4-MTP under ambient conditions in real time, i.e., in the liquid phase at room temperature, with a site-specific electronic- and structural-probe.

Our theoretical calculations provide detailed information on the electronic structure of the different sulfur species. In the following, we discuss the character of the spectral lines in terms of highest occupied and lowest unoccupied molecular orbitals (HOMOs and LUMOs, respectively), as well as the singly occupied molecular orbital (SOMO) for the 4-MTP radical. In the ground state of 4-MTP, we observe three major transitions as observed in Figure 2A. The lowest sulfur-1s transition is predominantly (>90%) described by the population of the LUMO + 2 orbital as shown in Figure 3. The two higher-lying transitions in Figure 2A are well-described by linear combinations of LUMO + 3 ± LUMO + 5 with less than 10% from other states. For the 4-MTP radical (**II**) and the thione isomers **2a** and **2b**, only one major transition in each species is found. These transitions are dominated by a single configuration, populating the LUMO (thione) and the SOMO (radical), respectively (Figure 3). Additional transitions are

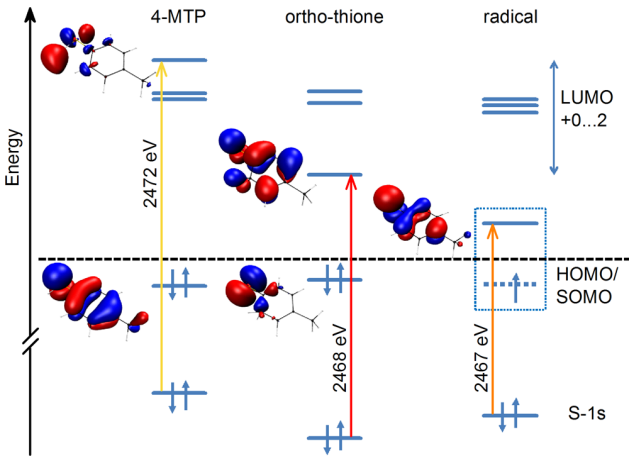

Figure 3. Molecular orbitals and corresponding isosurfaces relevant to the lowest sulfur-1s transitions in the three main species (4-MTP (**1**), *ortho*-thione (**2a**), 4-MTP radical (**II**)).

smaller by at least 2 orders of magnitude compared to the respective major transitions depicted in Figure 2. From the orbital scheme in Figure 3, the relative shift of the lowest absorptive sulfur-1s transitions in Figure 2B can be inferred qualitatively for each species: The HOMO−LUMO gap follows a clear trend that reflects the relative energetic stability of the three sulfur species. The relative energy difference between the sulfur-1s orbital and the dominating orbital of the sulfur-1s excitations decreases in the same order from 4-MTP (1s → LUMO + 2) via the thione (1s → LUMO + 0) to the radical (1s → β-SOMO). In the radical, the energy level scheme exhibits additional complexity because the unpaired electron divides the transitions into α- and β-densities, owing to the fact that transition energies of spin-up and spin-down excitations interact differently with the unpaired electron of the SOMO. The calculations are also able to explain the regioselectivity of the observed thione isomerization: In the 4-MTP radical (**II**), the HOMO is a SOMO, which governs the radical's chemistry. As can be seen from the isosurface for the SOMO in Figure 3, even though the radical is mainly sulfur-centered, there is also electron density at the *ortho-* and *para*-carbon atoms and none at the *meta*-carbon atoms. This is a manifestation of the regioselectivity of the observed thione isomerization reaction which strongly disfavors the *meta*-form.

It is also instructive to consider the trend of the sulfur-1s orbital energies for **1**, **II**, and **2a**: Recent publications provide evidence that the 1s-orbital energies in transition-metal complexes are strongly correlated with the amount of effective valence charge on a bound nitrogen atom.[44,75,76] The N-1s spectra were found to be similarly correlated because they depended mainly on the N-1s orbital energy in these compounds. We performed a natural population analysis to check for a similar correlation between valence charge and S-1s orbital energy. The results are given in Table 1 along with the calculated sulfur−carbon bond distance. There is a significant

Table 1. Bond Distance and Natural Populations

	4-MTP	thione	radical
d(C−S)/Å	1.77	1.64	1.73
nat pop	0.042	−0.043	0.056[a]

[a]Natural populations of α and β spin densities were added.

DOI: 10.1021/jacs.6b12992
J. Am. Chem. Soc. XXXX, XXX, XXX−XXX

Scheme 1. Reaction Pathways of 4-MTP upon 267 nm Excitation

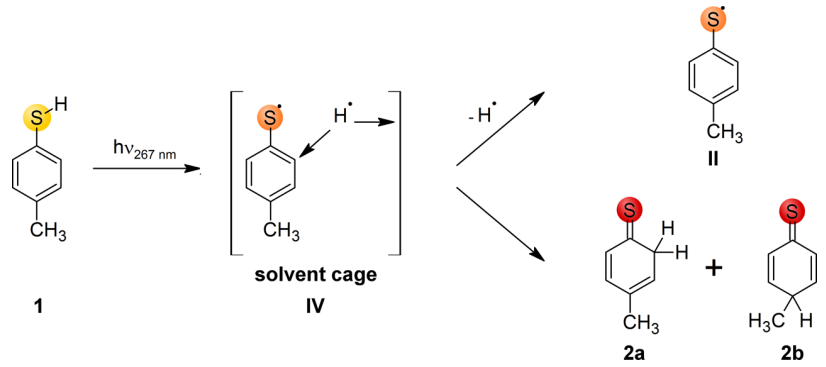

bond contraction (>10 pm) between the sulfur and carbon atom upon transition from the ground-state 4-MTP molecule to the thione isomers **2a** or **2b** as expected for a double bond formation. This change is accompanied by a significant reduction in the natural population of the sulfur atom, leading to a lower S-1s orbital energy and signaling a reduced valence charge density on the sulfur atom. The sulfur radical does not reveal significant differences from the 4-MTP parent compound. We interpret this finding as a manifestation of the relative inertness and stability of sulfur radicals compared to the very reactive oxygen radicals. X-ray photoemission spectroscopy is sensitive to these binding energies while transition energies of X-ray absorption spectra depend not only on the binding energy of the core-level electrons but also on the dipole selection rules dictated by the symmetries of the respective LUMO states. This fact can lead to a seeming lack of systematic ordering of transitions while the basic concept of core−electron screening by an atom's valence charge density still holds.

The differential spectrum in Figure 2B exhibits a third induced absorption peak at 2470.3 eV which appears only at high pump fluence of 50 mJ/cm^2 while it is absent at half the fluence (Figure S4). We have considered several possible species (Scheme S1) for this induced absorption peak of which the calculated 4-MTP anion (**III**) absorption best matches the observed spectral position (Figure S3). We cannot exclude that the anion species could emerge from highly excited states upon multiphoton absorption. However, it is known that cyclic aliphatic hydrocarbons undergo multiphoton absorption in strong femtosecond laser fields, producing fast decaying hydrocarbocations and free solvated electrons.[77] Such electrons constitute a highly reactive species and could react via a single electron transfer (SET) process with a 4-MTP radical (**II**) to yield the 4-MTP anion (**III**) within our time resolution. A second species with nearby sulfur-1s transitions is the 4-MTP dimer, the generation of which can result from two 4-MTP radicals (**II**). This diffusion-limited process cannot occur in the measured time frame (<1 ns) although Riyad et al. observed a product formation on microsecond time scales which they interpreted as dimerization. Only the formation of prearranged dimers, trimers, and tetramers of aromatic thiols would allow for dimerization to occur rapidly enough. Oligomers of aromatic thiols have been reported in solution, where the thiol group of one molecule coordinates to the π-system of another molecule. It is possible that such dimer formation occurs under our experimental conditions of 200 mM 4-MTP concentration. However, the 4-MTP dimer has its lowest absorption peak above 2471 eV. We therefore exclude dimerization and attribute the fluence-dependent induced absorption to anion formation.

We end the discussion with a few considerations of the temporal evolution of the 4-MTP photochemistry. The observed initial photofragmentation of 4-MTP into 4-MTP radicals (**II**) and hydrogen atoms occurs on an ultrafast time scale which eludes our time resolution of ∼70 ps, and for the initial reaction dynamics, we refer to Zhang et al.[20] Upon UV excitation the 4-MTP molecule is photodissociated to generate a radical pair **IV** in Scheme 1. The excess excitation energy is converted to kinetic energy and carried largely by the hydrogen atom, which is ejected into the solvent shell with an average ejection length of 9 Å or about two to three solvent spheres.[20] Suppression of fast geminate S−H recombination at such large ejection lengths is characteristic of weak solute−solvent interaction as found in cyclohexane solution. The initial radical concentration was observed to partially decay to a constant value within less than 50 ps.[20] The H-adduct, which we identify as the thione isomers **2a** and **2b**, emerges at the same rate.[20] No change in the relative populations occurs in the observed subnanosecond time frame, in agreement with the time evolution of the signal (Figure S1).

The reaction pathways are depicted in Scheme 1: Upon photoexcitation, 4-MTP (**1**) is promoted to a dissociative state, and the hydrogen atom is ejected into the surrounding solvent cage (**IV** in Scheme 1). The H atom will either escape the solvation shell, producing the long-lived 4-methylthiophenoxy radical (**II**), or attach to the aromatic ring of the parent 4-MTP molecule yielding the thione isomers **2a** and **2b**. If the 4-MTP radical (**II**) survives, it will only be consumed upon diffusion-limited recombination with a hydrogen atom or another 4-MTP radical (**II**). Solvent hydrogen abstraction seems less likely given the long radical lifetime extracted from flash-photolysis studies.[18] Matrix isolation studies[74] have demonstrated optical switching between the thione isomers **2a** and **2b**, but it is unclear whether these two isomers will form both or interconvert at room temperature in solution. Time-resolved vibrational exchange spectroscopy could provide an answer because the isomers have discernible infrared spectral fingerprints.[74] Lastly, we note that in the same matrix isolation studies UV excitation of thione adducts has resulted in reformation of the 4-MTP ground state. This observation explains the low quantum yield of radical formation in nanosecond flash-photolysis studies: Thione formation occurs within a few picoseconds, and a nanosecond UV excitation pulse will therefore partly consume the thione isomers and generate the 4-MTP parent species again.

DOI: 10.1021/jacs.6b12992
J. Am. Chem. Soc. XXXX, XXX, XXX−XXX

CONCLUSIONS AND OUTLOOK

We have successfully followed a chemical reaction in the liquid phase using sulfur-1s absorption spectroscopy to reveal the different reaction pathways of an aromatic thiol model system (4-MTP) following irradiation with 267 nm light, namely radical generation, thione isomerization, and anion formation. High-level theoretical calculations permit assigning the two prominent spectral signatures to the 4-MTP radical and the thione isomers. The regioselectivity of the isomerization reaction is governed by the radical SOMO which only has high electron density on the sulfur and the *ortho*- and *para*-carbon atoms, favoring S−H recombination or isomerization to the observed *ortho*- and *para*-thiones.

Time-resolved sulfur-1s spectroscopy provides new insight beyond the corresponding optical spectroscopy techniques: It is element specific and well-described by theory. The high spectral sensitivity to different oxidation states and chemical surroundings of the sulfur atom renders this technique a valuable tool to study chemical reactions involving sulfur functional groups. Sulfur-1s spectroscopy can be applied to various systems, both in solution and in solids, and could be especially useful in the field of battery research and X-ray radiation damage of proteins (in operando, in crystallo). In combination with free-electron lasers or laser-plasma sources, sulfur-1s spectroscopy can follow chemical reactions of sulfur functional groups on atomic and possibly electronic time scales due to ultrashort and bright femtosecond X-ray pulses. This would allow for the observation of initial reaction steps and help disentangle the emergence of different photoproducts and their potential conversion of one initially formed photoproduct into another. In summary, our study underscores the potentially broad applicability of time-resolved sulfur-1s spectroscopy to follow the evolution of sulfur atoms in a variety of different bonding situations and oxidation states making it a valuable tool to study chemical reactions of sulfur-containing functional groups and materials.

ASSOCIATED CONTENT

Supporting Information

The Supporting Information is available free of charge on the ACS Publications website at DOI: 10.1021/jacs.6b12992.

Overview over all described species, and calculated sulfur 1s-spectra of all described species (PDF)

AUTHOR INFORMATION

Corresponding Authors

*tkkim@pusan.ac.kr
*rwschoen@slac.stanford.edu
*nils.huse@uni-hamburg.de

ORCID

Oriol Vendrell: 0000-0003-4629-414X
Tae Kyu Kim: 0000-0002-9578-5722
Nils Huse: 0000-0002-3281-7600

Present Addresses

[#]I.v.A.: Division of Solid State Physics, NanoLund, Lund University, Lund 221 00, Sweden.
[▽]A.A.C.: PULSE Institute, SLAC National Accelerator Laboratory, Menlo Park, CA 94025, United States.
[○]J.H.L.: Pohang Accelerator Laboratory, San-31 Hyoja-dong Pohang, Kyungbuk 790-784, South Korea.
[▼]K.H.: Center for Gas Analysis, Division of Metrology for Quality of Life, Korea Research Institute of Standards and Science, Daejeon 34113, Republic of Korea.
[◆]O.V.: Department of Physics and Astronomy, Aarhus University, 8000 Aarhus, Denmark.
[¶]R.W.S.: Linac Coherent Light Source, SLAC National Accelerator Laboratory, Menlo Park, CA 94025, United States.

Author Contributions

[■]M.O. and I.v.A. contributed equally.

Notes

The authors declare no competing financial interest.

ACKNOWLEDGMENTS

This work was supported by the Director, Office of Science, Office of Basic Energy Sciences, the Chemical Sciences, Geosciences, and Biosciences Division under the Department of Energy, Contract No. DE-AC02-05CH11231 (A.A.C., K.H., J.H.L., and R.W.S.). This research was supported by Basic Science Research Program (2013S1A2A2035406, 2014R1A4A1001690 and 2016R1E1A1A01941978) and in part by the Max Planck POSTECH/KOREA Research Initiative Program (2016K1A4A4A01922028) through the National Research Foundation of Korea (NRF) funded by Ministry of Science, ICT & Future Planning (T.K.K. and K.H.). M.O., I.v.A., K.A., and N.H. acknowledge funding from the Max Planck Society and the City of Hamburg. M.O. and N.H. gratefully acknowledge financial support of this work through the Deutsche Forschungsgemeinschaft within the Sonderforschungsbereich 925 “Light induced dynamics and control of correlated quantum systems”. This research used resources of the Advanced Light Source (LBNL), which is a DOE Office of Science User Facility. The authors would like to thank Bruce Rude for his continuous support of the experimental hardware.

REFERENCES

(1) Alpher, R. A.; Herman, R. C. *Rev. Mod. Phys.* **1950**, *22*, 153.
(2) 15—Sulfur. In *Chemistry of the Elements*, 2nd ed.; Greenwood, N.N., Earnshaw, A., Eds., Butterworth-Heinemann: Oxford, 1997; pp 645 − 746.
(3) Vairavamurthy, A. *Spectrochim. Acta, Part A* **1998**, *54* (12), 2009−2017.
(4) Reed, M. A.; Zhou, C.; Muller, C. J.; Burgin, T. P.; Tour, J. M. *Science* **1997**, *278* (5336), 252−254.
(5) Meng, L.; Fujikawa, T.; Kuwayama, M.; Segawa, Y.; Itami, K. *J. Am. Chem. Soc.* **2016**, *138* (32), 10351−10355.
(6) Johnson, A. S.; Miseikis, L.; Wood, D. A.; Austin, D. R.; Brahms, C.; Jarosch, S.; Strüber, C. S.; Ye, P.; Marangos, J. P. *Struct. Dyn.* **2016**, *3*, 062603.
(7) Dey, A.; Chow, M.; Taniguchi, K.; Lugo-Mas, P.; Davin, S.; Maeda, M.; Kovacs, J. A.; Odaka, M.; Hodgson, K. O.; Hedman, B.; Solomon, E. I. *J. Am. Chem. Soc.* **2006**, *128*, 533−541.
(8) Schoeneich, C. *Methods Enzymol.* **1995**, *251*, 45.
(9) Mamathambika, B. S.; Bardwell, J. C. *Annu. Rev. Cell Dev. Biol.* **2008**, *24* (1), 211−235.
(10) DeCollo, T. V.; Lees, W. J. *J. Org. Chem.* **2001**, *66* (12), 4244−4249.
(11) von Sonntag, C.; Schuchmann, H.-P. *Methods Enzymol.* **1994**, *233*, 47.
(12) Schoeneich, C.; Dillinger, U.; von Bruchhausen, F.; Asmus, K.-D. *Arch. Biochem. Biophys.* **1992**, *292* (2), 456−467.
(13) Deneke, S. M *Curr. Top. Cell. Regul.* **2001**, *36*, 151−180.
(14) Asmus, K.-D. *Methods Enzymol.* **1990**, *186*, 168−180.
(15) Gough, J. D.; Gargano, J. M.; Donofrio, A. E.; Lees, W. J. *Biochemistry* **2003**, *42* (40), 11787−11797.
(16) Thyrion, F. C. *J. Phys. Chem.* **1973**, *77* (12), 1478−1482.

DOI: 10.1021/jacs.6b12992
J. Am. Chem. Soc. XXXX, XXX, XXX−XXX

(17) Nakamura, M.; Ito, O.; Matsuda, M. *J. Am. Chem. Soc.* **1980**, *102* (2), 698−701.
(18) Riyad, Y. M.; Naumov, S.; Hermann, R.; Brede, O. *Phys. Chem. Chem. Phys.* **2006**, *8* (14), 1697.
(19) Oliver, T. A. A.; Zhang, Y.; Ashfold, M. N. R.; Bradforth, S. E. *Faraday Discuss.* **2011**, *150*, 439−458.
(20) Zhang, Y. Y.; Oliver, T. A. A.; Ashfold, M. N. R.; Bradforth, S. E. *Faraday Discuss.* **2012**, *157*, 141−163.
(21) Zhang, Y.; Oliver, T. A. A.; Das, S.; Roy, A.; Ashfold, M. N. R.; Bradforth, S. E. *J. Phys. Chem. A* **2013**, *117* (46), 12125−12137.
(22) Murdock, D.; Harris, S. J.; Karsili, T. N. V.; Greetham, G. M.; Clark, I. P.; Towrie, M.; Orr-Ewing, A. J.; Ashfold, M. N. R. *J. Phys. Chem. Lett.* **2012**, *3* (24), 3715−3720.
(23) Smith, T. A.; Dewitt, J. G.; Hedman, B.; Hodgson, K. O. *J. Am. Chem. Soc.* **1994**, *116* (9), 3836−3847.
(24) Evans, J.; Corker, J. M.; Hayter, C. E.; Oldman, R. J.; Williams, B. P. *Chem. Commun.* **1996**, *12*, 1431−1432.
(25) Glaser, T.; Hedman, B.; Hodgson, K. O.; Solomon, E. I. *Acc. Chem. Res.* **2000**, *33* (12), 859−868.
(26) Szilagyi, R. K.; Bryngelson, P. A.; Maroney, M. J.; Hedman, B.; Hodgson, K. O.; Solomon, E. I. *J. Am. Chem. Soc.* **2004**, *126* (10), 3018−3019.
(27) Dey, A.; Glaser, T.; Moura, J. J. G.; Holm, R. H.; Hedman, B.; Hodgson, K. O.; Solomon, E. I. *J. Am. Chem. Soc.* **2004**, *126* (51), 16868−16878.
(28) Dey, A.; Okamura, T.; Ueyama, N.; Hedman, B.; Hodgson, K. O.; Solomon, E. I. *J. Am. Chem. Soc.* **2005**, *127* (34), 12046−12053.
(29) Dey, A.; Chow, M.; Taniguchi, K.; Lugo-Mas, P.; Davin, S.; Maeda, M.; Kovacs, J. A.; Odaka, M.; Hodgson, K. O.; Hedman, B.; Solomon, E. I. *J. Am. Chem. Soc.* **2006**, *128* (2), 533−541.
(30) Dey, A., Jr.; Jenney, F. E.; Francis, E.; Adams, M. W. W.; Johnson, M. K.; Hodgson, K. O.; Hedman, B.; Solomon, E. I. *J. Am. Chem. Soc.* **2007**, *129* (41), 12418−12431.
(31) Dey, A.; Jiang, Y.; Ortiz de Montellano, P.; Hodgson, K. O.; Hedman, B.; Solomon, E. I. *J. Am. Chem. Soc.* **2009**, *131* (22), 7869−7878.
(32) Sarangi, R.; Frank, P.; Benfatto, M.; Morante, S.; Minicozzi, V.; Hedman, B.; Hodgson, K. O. *J. Chem. Phys.* **2012**, *137* (20), 205103.
(33) Hackett, M. J.; Smith, S. E.; Paterson, P. G.; Nichol, H.; Pickering, I. J.; George, G. N. *ACS Chem. Neurosci.* **2012**, *3* (3), 178−185.
(34) Pin, S.; Huthwelker, T.; Brown, M. A.; Vogel, F. *J. Phys. Chem. A* **2013**, *117* (35), 8368−8376.
(35) Koenig, C. F. J.; Schuh, P.; Huthwelker, T.; Smolentsev, G.; Schildhauer, T. J.; Nachtegaal, M. *Catal. Today* **2014**, *229*, 56−63.
(36) Donahue, C. M.; Lezama Pacheco, J. S.; Keith, J. M.; Daly, S. R. *Dalton Trans.* **2014**, *43* (24), 9189−9201.
(37) Ha, Y.; Tenderholt, A. L.; Holm, R. H.; Hedman, B.; Hodgson, K. O.; Solomon, E. I. *J. Am. Chem. Soc.* **2014**, *136* (25), 9094−9105.
(38) Pascal, T. A.; Pemmaraju, C. D.; Prendergast, D. *Phys. Chem. Chem. Phys.* **2015**, *17* (12), 7743−7753.
(39) Wujcik, K. H.; Pascal, T. A.; Pemmaraju, C. D.; Devaux, D.; Stolte, W. C.; Balsara, N. P.; Prendergast, D. *Adv. Energy Mater.* **2015**, *5* (16), 1500285.
(40) Martin-Diaconescu, V.; Kennepohl, P. *J. Am. Chem. Soc.* **2007**, *129* (11), 3034−3035.
(41) Wen, H.; Huse, N.; Schoenlein, R. W.; Lindenberg, A. M. *J. Chem. Phys.* **2009**, *131*, 234505.
(42) Wernet, Ph.; Kunnus, K.; Josefsson, I.; Rajkovic, I.; Quevedo, W.; Beye, M.; Schreck, S.; Grübel, S.; Scholz, M.; Nordlund, D.; Zhang, W.; Hartsock, R. W.; Schlotter, W. F.; Turner, J. J.; Kennedy, B.; Hennies, F.; de Groot, F. M. F.; Gaffney, K. J.; Techert, S.; Odelius, M.; Föhlisch, A. *Nature* **2015**, *520*, 78−81.
(43) Hong, K.; Cho, H.; Schoenlein, R. W.; Kim, T. K.; Huse, N. *Acc. Chem. Res.* **2015**, *48* (11), 2957−2966.
(44) Van Kuiken, B. E.; Cho, H.; Hong, K.; Khalil, M.; Schoenlein, R. W.; Kim, T. K.; Huse, N. *J. Phys. Chem. Lett.* **2016**, *7* (3), 465−470.
(45) Gawelda, W.; Johnson, M.; de Groot, F. M. F.; Abela, R.; Bressler, C.; Chergui, M. *J. Am. Chem. Soc.* **2006**, *128* (15), 5001−5009.
(46) Van Kuiken, B. E.; Huse, N.; Cho, H.; Strader, M. L.; Lynch, M. S.; Schoenlein, R. W.; Khalil, M. *J. Phys. Chem. Lett.* **2012**, *3*, 1695.
(47) Van Kuiken, B. E; Valiev, M.; Daifuku, S. L; Bannan, C.; Strader, M. L; Cho, H.; Huse, N.; Schoenlein, R. W; Govind, N.; Khalil, M. *J. Phys. Chem. A* **2013**, *117*, 4444.
(48) Ross, M.; Van Kuiken, B. E.; Strader, M. L.; Cordones-Hahn, A.; Cho, H.; Schoenlein, R. W.; Kim, T. K.; Khalil, M. *Springer Proc. Phys.* **2015**, *162*, 403−406.
(49) Rittmann-Frank, M. H.; Milne, C. J.; Rittmann, J.; Reinhard, M.; Penfold, T. J.; Chergui, M. *Angew. Chem.* **2014**, *126*, 5968−5972.
(50) Canton, S. E.; Kjær, K. S.; Vankó, G.; van Driel, T. B.; Adachi, S.-i.; Bordage, A.; Bressler, C.; Chabera, P.; Christensen, M.; Dohn, A. O.; Galler, A.; Gawelda, W.; Gosztola, D.; Haldrup, K.; Harlang, T.; Liu, Y.; Møller, K. B.; Németh, Z.; Nozawa, S.; Pápai, M.; Sato, T.; Sato, T.; Suarez-Alcantara, K.; Togashi, T.; Tono, K.; Uhlig, J.; Vithanage, D. A.; Wärnmark, K.; Yabashi, M.; Zhang, J.; Sundström, V.; Nielsen, M. M. *Nat. Commun.* **2015**, *6*, 6359.
(51) Gawelda, W.; Szlachetko, J.; Milne, C. J. *X-Ray Spectroscopy at Free Electron Lasers*; John Wiley & Sons, Ltd., 2016; pp 637−669.
(52) Chergui, M. *Struct. Dyn.* **2016**, *3* (3), 031001.
(53) Shelby, M. L.; Lestrange, P. J.; Jackson, N. E.; Haldrup, K.; Mara, M. W.; Stickrath, A. B.; Zhu, D.; Lemke, H. T.; Chollet, M.; Hoffman, B. M.; Li, X.; Chen, L. X. *J. Am. Chem. Soc.* **2016**, *138* (28), 8752−8764.
(54) Biasin, E.; van Driel, T. B.; Kjær, K. S.; Dohn, A. O.; Christensen, M.; Harlang, T.; Chabera, P.; Liu, Y.; Uhlig, J.; Pápai, M.; Németh, Z.; Hartsock, R.; Liang, W.; Zhang, J.; Alonso-Mori, R.; Chollet, M.; Glownia, J. M.; Nelson, S.; Sokaras, D.; Assefa, T. A.; Britz, A.; Galler, A.; Gawelda, W.; Bressler, C.; Gaffney, K. J.; Lemke, H. T.; Møller, K. B.; Nielsen, M. M.; Sundström, V.; Vankó, G.; Wärnmark, K.; Canton, S. E.; Haldrup, K. *Phys. Rev. Lett.* **2016**, *117*, 013002.
(55) Zhang, W.; Kjaer, K. S.; Alonso-Mori, R.; Bergmann, U.; Chollet, M.; Fredin, L. A.; Hadt, R. G.; Hartsock, R. W.; Harlang, T.; Kroll, T.; Kubicek, K.; Lemke, H. T.; Liang, H. W.; Liu, Y.; Nielsen, M. M.; Persson, P.; Robinson, J. S.; Solomon, E. I.; Sun, Z.; Sokaras, D.; van Driel, T. B.; Weng, T.-C.; Zhu, D.; Warnmark, K.; Sundstrom, V.; Gaffney, K. J. *Chem. Sci.* **2017**, *8*, 515−523.
(56) Haase, J. *J. Phys.: Condens. Matter* **1997**, *9* (18), 3647−3670.
(57) Myneni, S. C. B. *Rev. Mineral. Geochem.* **2000**, *40*, 113−172.
(58) Solomon, E. I.; Hedman, B.; Hodgson, K. O.; Dey, A.; Szilagyi, R. K. *Coord. Chem. Rev.* **2005**, *249* (1−2), 97−129.
(59) Mori, R. A.; Paris, E.; Giuli, G.; Eeckhout, S. G.; Kavcic, M.; Zitnik, M.; Bucar, K.; Pettersson, L. G. M.; Glatzel, P. *Anal. Chem.* **2009**, *81* (15), 6516−6525.
(60) Sproules, S.; Wieghardt, K. *Coord. Chem. Rev.* **2011**, *255* (7−8), 837−860.
(61) Queen, M. S.; Towey, B. D.; Murray, K. A.; Veldkamp, B. S.; Byker, H. J.; Szilagyi, R. K. *Coord. Chem. Rev.* **2013**, *257* (2), 564−578.
(62) Cho, H.; Hong, K.; Strader, M. L.; Lee, J. H.; Schoenlein, R. W.; Huse, N.; Kim, T. K. *Inorg. Chem.* **2016**, *55* (12), 5895−5903.
(63) Khalil, M.; Marcus, M. A.; Smeigh, A. L.; McCusker, J. K.; Chong, H. H. W.; Schoenlein, R. W. *J. Phys. Chem. A* **2006**, *110* (1), 38−44.
(64) Head-Gordon, M.; Pople, J. A.; Frisch, M. J. *Chem. Phys. Lett.* **1988**, *153* (6), 503−506.
(65) Dunning, T. H. *J. Chem. Phys.* **1989**, *90* (2), 1007−1023.
(66) Frisch, M. J.; Trucks, G. W.; Schlegel, H. B.; Scuseria, G. E.; Robb, M. A.; Cheeseman, J. R.; Scalmani, G.; Barone, V.; Mennucci, B.; Petersson, G. A.; Nakatsuji, H.; Caricato, M.; Li, X.; Hratchian, H. P.; Izmaylov, A. F.; Bloino, J.; Zheng, G.; Sonnenberg, J. L.; Hada, M.; Ehara, M.; Toyota, K.; Fukuda, R.; Hasegawa, J.; Ishida, M.; Nakajima, T.; Honda, Y.; Kitao, O.; Nakai, H.; Vreven, T.; Montgomery, J. A., Jr.; Peralta, J. E.; Ogliaro, F.; Bearpark, M.; Heyd, J. J.; Brothers, E.; Kudin, K. N.; Staroverov, V. N.; Kobayashi, R.; Normand, J.; Raghavachari, K.; Rendell, A.; Burant, J. C.; Iyengar, S. S.; Tomasi, J.; Cossi, M.; Rega,

DOI: 10.1021/jacs.6b12992
J. Am. Chem. Soc. XXXX, XXX, XXX−XXX

N.; Millam, J. M.; Klene, M.; Knox, J. E.; Cross, J. B.; Bakken, V.; Adamo, C.; Jaramillo, J.; Gomperts, R.; Stratmann, R. E.; Yazyev, O.; Austin, A. J.; Cammi, R.; Pomelli, C.; Ochterski, J. W.; Martin, R. L.; Morokuma, K.; Zakrzewski, V. G.; Voth, G. A.; Salvador, P.; Dannenberg, J. J.; Dapprich, S.; Daniels, A. D.; Farkas, Ö.; Foresman, J. B.; Ortiz, J. V.; Cioslowski, J.; Fox, D. J., *Gaussian 09 Revision E.01*; Gaussian Inc.: Wallingford CT, 2009.
(67) Andersson, K.; Malmqvist, P. A.; Roos, B. O.; Sadlej, A. J.; Wolinski, K. *J. Phys. Chem.* **1990**, *94* (14), 5483−5488.
(68) Andersson, K.; Malmqvist, P. A.; Roos, B. O. *J. Chem. Phys.* **1992**, *96* (2), 1218−1226.
(69) Malmqvist, P. A.; Pierloot, K.; Shahi, A. R. M.; Cramer, C. J.; Gagliardi, L. *J. Chem. Phys.* **2008**, *128* (20), 204109.
(70) Pinjari, R. V.; Delcey, M. G.; Guo, M.; Odelius, M.; Lundberg, M. *J. Chem. Phys.* **2014**, *141* (12), 124116.
(71) Aquilante, F.; De Vico, L.; Ferre, N.; Ghigo, G.; Malmqvist, P. A.; Neograd y, P.; Pedersen, T. B.; Pitonak, M.; Reiher, M.; Roos, B. O.; Serrano-Andres, L.; Urban, M.; Veryazov, V.; Lindh, R. *J. Comput. Chem.* **2010**, *31* (1), 224−247.
(72) Dewar, P.; Ernstbrunner, E.; Gilmore, J.; Godfrey, M.; Mellor, J. *Tetrahedron* **1974**, *30*, 2455−2459.
(73) Martin, W. C.; Zalubas, R.; Musgrove, A. *J. Phys. Chem. Ref. Data* **1990**, *19* (4), 821−880.
(74) Reva, I.; Nowak, M. J.; Lapinski, L.; Fausto, R. *Phys. Chem. Chem. Phys.* **2015**, *17* (7), 4888−4898.
(75) García-Lastra, J. M.; Cook, P. L.; Himpsel, F. J.; Rubio, A. *J. Chem. Phys.* **2010**, *133*, 151103.
(76) Johnson, P. S.; Cook, P. L.; Zegkinoglou, I.; García-Lastra, J. M.; Rubio, A.; Ruther, R. E.; Hamers, R. J.; Himpsel, F. J. *J. Chem. Phys.* **2013**, *138* (4), 044709.
(77) Castillejo, M.; Couris, S.; Koudoumas, E.; Martín, M. *Chem. Phys. Lett.* **1998**, *289* (3−4), 303−310.

DOI: 10.1021/jacs.6b12992
J. Am. Chem. Soc. XXXX, XXX, XXX−XXX

UV-induced photochemistry of dimethyl disulfide: Evidence of thione and disulfide formation by time-resolved X-ray absorption spectroscopy at the sulfur K-Edge

Miguel Ochmann[a,‡], Abid Hussain[a,‡], Amy A. Cordones-Hahn[b], Inga von Ahnen[a], Jae Hyuk Lee[b], Kiryong Hong[c], Katrin Adamczyk[a], Rory Ma[c], Tae Kyu Kim[c], Robert W. Schoenlein[b], Oriol Vendrell[d] and Nils Huse[a,*]

[a]*Department of Physics and Max Planck Research Group at the University of Hamburg, Center for Free Electron Laser Science, Hamburg, Germany*

[b]*Ultrafast X-ray Science Lab, Chemical Sciences Division, Lawrence Berkeley National Laboratory, Berkeley, California, USA*

[c]*Department of Chemistry and Chemistry Institute of Functional Materials, Pusan National University, Busan, South Korea*

[d]*Center for Free-Electron Laser Science, DESY and The Hamburg Centre for Ultrafast Imaging, Hamburg, Germany*

[‡]The authors contributed equally to this work

We have investigated dimethyl disulfide as the simplest disulfide system with picosecond time-resolved X-ray absorption spectroscopy at the sulfur K-edge to study the photochemistry initiated by 267-nm femtosecond pulses. We observe a broad but distinct induced absorption spectrum which decays on at least two time scales in the nanosecond range. We employed RASSCF electronic structure calculations to simulate the sulfur-1s transitions of multiple possible chemical species and identified unambiguously the methylthiyl and methylperthiyl radicals as the primary reaction products. In addition, we identify disulfur and the CH_2S thione as the secondary reaction products of the perthiyl radical that are most likely to explain the observed spectral and kinetic signatures of our experiment. Our study underscores the importance of elemental specificity and the potential of time-resolved X-ray spectroscopy to identify short-lived reaction products, providing a complex reaction scheme that underlies the rich photochemistry of disulfide systems.

Introduction

Sulfur is an important element in biochemistry and is found in many proteins and enzymes either as metal-sulfur active sites[1] or as one of two amino acids, L-methionine or L-cysteine incorporated into the protein backbone.[2] The latter is very important in structure determination of a protein's tertiary structure as the side chains of two L-Cysteine amino acids can be covalently linked via the oxidative formation of a disulfide bond. Since disulfide bonds strongly influence the tertiary structure of many proteins, they play an important role in the protein folding process and for structure retention.

The stability of a protein's structure is pivotal in maintaining its biological function. However, the structure and thus their function is dependent on many environmental factors such as temperature [3], pH [4], oxidizing environment[5], solvent[6] and hard and soft radiation exposure from cosmic radiation[7] and hard X-rays[8,9] to near ultraviolet and visible radiation.[10] It is well-known that the disulfide bond is most prone to cleavage when exposed to UV radiation. Investigation of the early timescale kinetics of the UV induced disulfide bond breakage is therefore crucial in order to understand the photostability and photodamage repair mechanisms in proteins.

Dimethyl disulfide (DMDS)—the simplest organic disulfide—can serve as a model system for the photochemistry of disulfide bonds. DMDS is one of the major volatile organic sulfur compounds (VOSCs) and considered very toxic for all organisms.[11] Naturally, DMDS occurs as a decomposition product in the microbial degradation pathway of sulfur-containing amino acids[12] and is also a luring agent dead-horse arum (Helicodiceros muscivorus).[13] This plant uses the odor of DMDS along with the VOSCs

dimethyl sulfide and dimethyl trisulfide as fly-attracting luring agents to help with pollination. DMDS also plays an important role in the atmospheric sulfur cycle as a sulfur reserve and is primarily found emanating in swamps and salt marshes.[14] Accordingly, the photochemistry of DMDS is important in order to understand its atmospheric UV-induced photochemistry. More importantly, simple organic disulfides such as DMDS is a very suitable initial model system for the investigation of the disulfide bond motif of proteins and has already been studied with both static and time-resolved optical methods both in the gas phase[15,16] and in solution. [17]

Early on, organic disulfides were found to form free radicals upon irradiation with suitable light, undergoing various subsequent chemical transformations rather than reforming the S-S bond.[18] It was also established that the two major initial chemical reaction steps are breakage of the S-S and the C-S bond, which yield thiyl and perthiyl radicals as reactive species, respectively.[17] Furthermore, early time-resolved studies of the S–S bond breakage in 4-aminophenyl disulfide showed that the initial bond cleavage is ultrafast and takes places on a sub-picosecond timescale.[19]

The first time-resolved optical studies of pure DMDS in the gas phase on microsecond timescales reported two dominant reaction pathways upon excitation with either mid-infrared multiphoton absorption or with UV light. Accordingly, DMDS would either decay via a molecular four-centered transition state producing S_2 and C_2H_6 or to dissociate homolytically to yield $CH_3S\cdot$ thiyl radicals.[20] Further studies on the UV-photodissociation of aliphatic disulfides in the gas phase using time-of-flight mass spectrometry revealed two major photoproducts: (i) S-S bond cleavage, producing thiyl radicals or (ii) C-S bond cleavage, yielding perthiyl radicals.[21] At wavelengths shorter than 250 nm, S-S bond cleavage was reported to dominate and only at longer wavelengths, C-S bond cleavage becomes competitive. From these findings, Bookwalter *et al.* concluded that the dissociation has to occur from an excited state and not the ground state because the bond enthalpy of the C-S bond (235 kJ/mol, 2.4 eV) is lower than that of the S-S bond (280 kJ/mol, 2.9 eV). Resonance Raman spectroscopy with 267 nm excitation and semi-empirical calculations by Rinker et al.[14] indicated that excitation into the lowest singlet excited states favors a C-S bond cleavage along the C-S stretching vibration and features a barrier for S-S dissociation, while the opposite is the case for next higher excited state. Rinker et al. concluded that 267 nm excitation accesses the lower excited state, while excitation as shorter wavelengths also promotes the system into the second excited state. More recently, theoretical studies with high-level SA-CASSCF and MS-CASPT2 approaches were applied by Luo *et al.* to investigate both the vertical excitation energies and the photodissociation mechanism of DMDS.[22] These calculations indicate that both, the S_1 and S_2 state, strongly favor S-S bond fission due to a barrier for C-S bond cleavage. C-S bond fission at 267-nm excitation should occur from the ground state. Clearly, the reaction pathways are neither fully understood nor all products unambiguously identified for a given excitation wavelength.

More recent time-resolved mass spectrometry (TRMS) studies of model disulfide compounds indicate that structural restriction render disulfide bonds in proteins more stable because the produced radicals remain in the vicinity of each other to geminately recombine. [23,24] The restoration of the disulfide bond in the model system 1,2 dithiane was found to take place within 2.75 ± 0.23 ps. For comparison, this time-scale is much slower than observed excited state quenching in DNA.[25,26] However, the radical recombination is still faster than the intramolecular vibrational energy redistribution (IVR). The latter would allow the carbon backbone of the protein to move the two radicals away from each other resulting in partial loss of the tertiary structure. Comparison of these findings for the cyclic disulfide 1,2-dithiane with the linear diethyl disulfide (DEDS) further points toward the photostability of the disulfide bonds in proteins to be a structural property

that confines the sulfur radical spatially.[24] The disulfide bond may therefore also act as radiation shield in proteins, protecting the integrity of the proteins tertiary structure by absorption of harmful radiation and energy dissipation through fast radical reformation and subsequent (not preceding) vibrational energy redistribution.

Recently, time-resolved spectroscopy at the sulfur K-edge has been employed as a valuable new tool for understanding photochemical reactions of sulfur-containing compounds.[27,28] . Sulfur is very sensitive for its electronic and chemical environment. This sensitivity reflects in sulfur-1s transitions in the X-ray spectral range shifting substantially depending on the respective sulfur atoms binding state. Combining this spectral fingerprint of sulfur chemistry with time-resolved measurements and electronic structure calculations (RASSCF, DFT) yields a powerful method to follow sulfur chemistry with elemental specificity. For instance, we investigated the photochemistry of an aromatic thiol upon 267-nm illumination which features two dominant reaction pathways: The first is the expected homolytic bond cleavage of the S-H bond, which yields hydrogen atoms and thiyl radicals. The second pathway is the isomerization of the aromatic molecule to a thione isomer. The latter pathway is somewhat surprising, as aromatic systems usually exhibit a high stability and do not undergo isomerization by revoking their conjugated aromatic system. These experiments provided insight into the UV photochemistry of the thiol group, which also plays a very important role in protein chemistry.

In previous studies by the Kennepohl group static X-ray absorption spectroscopy has already been used to investigate radiation damage and photochemistry in biomolecules and biologically relevant molecules.[29,30] Herein, we report the first time-resolved study of the photochemistry of the simple disulfide model system, DMDS, in a solvent environment by employing TRXAS at the sulfur K-edge. We establish the basic photochemical behavior of disulfide containing linear molecules upon UV irradiation at 267 nm and provide insights and implications for the radiation stability of disulfide bonds in proteins on sub-nanosecond to sub-microsecond timescales.

Methods

Experimental Setup

All measurements were conducted at beamline 6.0.1 of the Advanced Light Source in Berkeley, California. Details of the experimental setup have been reported previously.[27,31] The sample was excited by 267-nm laser pulses of 100 fs duration obtained by third harmonic generation (THG) of the 800-nm fundamental wavelength of a Ti:Sa regenerative amplifier. A fluence of 50 mJ/cm² was used for all measurements. Long delay scans at specific energies were corrected for electronic background variation by subtracting these electronic artefacts with no X-rays on the sample. Static spectra were recorded with an integrating photodiode in total fluorescence yield (TFY) mode. Time-resolved spectra were recorded with an avalanche photodiode which was shielded with a 100-nm thick aluminum foil. The sample was delivered through a sapphire-nozzle liquid jet driven by a gear pump with flow rates of ≥450 mL/min.

Chemicals and Materials

Dimethyl disulfide and cyclohexane were purchased from Sigma Aldrich and were used as received without further purification. DMDS solutions (100 mM) were prepared by filling up 1.8 mL DMDS with cyclohexane to 200 mL. Samples were run in a continuous loop for up to 6 hours before being replaced by a fresh sample.

Theoretical Calculations

The equilibrium geometries of all studied molecular species were obtained at the second order of Møller-Plesset perturbation theory[32] (MP2) with the Dunning correlation consistent basis set aug-cc- pvtz[33]. The vibrational frequency calculations confirm that the computed structures are true energy minimum structures. Geometry optimizations were obtained using very tight convergence criteria in the Gaussian09[34] suite of programs.

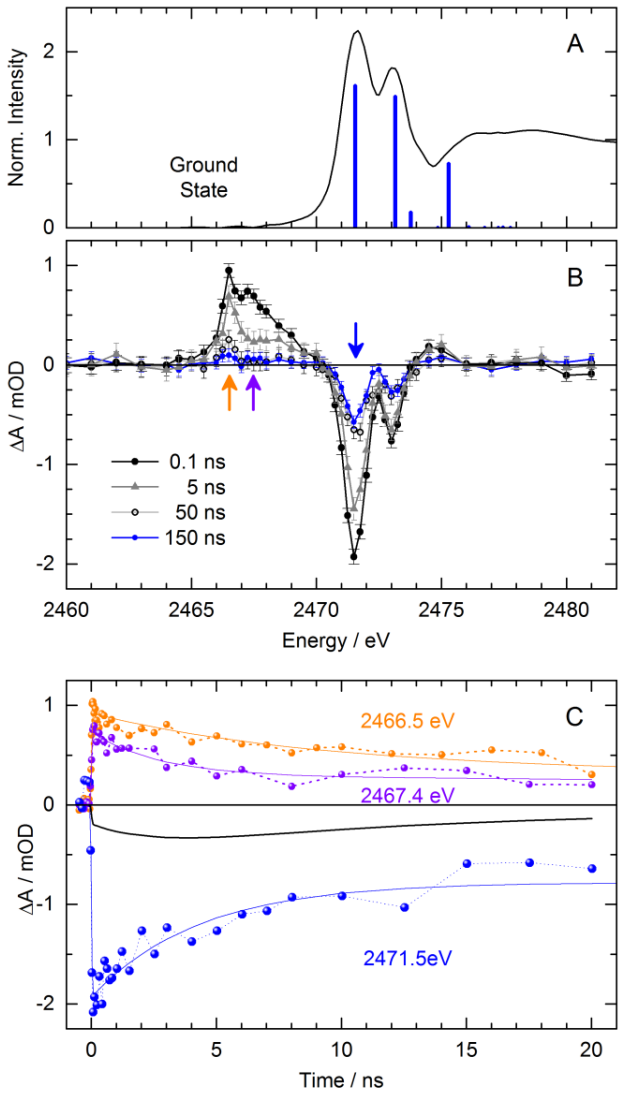

Figure 1. The static sulfur K-edge spectrum is shown in panel **A** along with the computed energetically lowest sulfur-1s transitions. Beneath, differential absorption spectra at time delays of 0.1, 5, 50, and 150 ns after excitation with 267-nm pulses are shown in panel **B**. The corresponding time evolution at three distinct photon energies, indicated by color-coded arrows in panel B, show the temporal evolution of the absorbance changes (spheres and doted lines) along with exponential decay models (solid lines) fit to the experimental data in panel **C**. The black trace in panel C is the difference of the modeled time traces at 2466.0 eV and 2467.4 eV

The X-ray absorption transitions were simulated using the first principles multi reference restricted active space self-consistent field (RASSCF) method with no symmetry imposed. The active space for the simulated sulfur-1s transitions for dimethyl disulfide and the perthiyl radical comprised 14 electrons distributed over 12 orbitals. The active space for thiyl radical was reduced to 11 electrons in 11 orbitals. The aug-cc- pvdz basis was used for all other atomic centers. The active space in the RASSCF calculations is divided into two subspaces, namely RAS2 containing all orbitals without occupational constraints and RAS3, comprising the two sulfur 1-s core electrons of which at most one electron is allowed to be excited (thus suppressing configurations with a doubly-filled sulfur-1s core orbital). The wave function during the RASSCF calculations and the presence of irrelevant low-energy configurations during the calculation of core excitations are avoided by grouping the excitations in this way. The energies of the core excitation obtained by RASSCF calculations were further improved by applying multi-state second order perturbation theory (MS-RASPT2)[35] while for the ground state energy single-state CASPT2[36,37] was used with 0.25 Hartree for the ionization potential electron affinity (IPEA) shift and an imaginary shift of 0.3 Hartree to avoid intruder states. The RASSI module is used for the calculations of the transition dipole moments on the wave functions obtained from the RASSCF calculations. RASSCF/RASSI calculations were performed with the Molcas 7.8 program suite[38].

Results and Discussion

Figure 1A shows the static X-ray absorption spectrum of DMDS in cyclohexane solution at the sulfur K-edge. Two major transitions are observed at 2471.6 and 2473.1 eV along with additional less pronounced transitions above 2475.0 eV, which merge into the continuum edge. Below, panel B shows the differential absorption spectrum 100 ps after 267-nm (4.64 eV) excitation. The negative absorbance change at 2471.5 and 2473.0 eV coincides with the main absorption peaks of the DMDS spectrum, signaling loss of ground-state absorption. Two distinct induced absorption peaks are observed at 2466.5 eV and 2467.4 eV are accompanied by a broader shoulder between 2468 eV and 2470 eV. The observed pump-probe signals fully emerge within the time resolution of our experiment (~70 ps) and decay in a bimodal

fashion on timescales of nanoseconds and tens of nanoseconds. Notably, even after 50 ns, signals still persist. In fact, the bleach signal persists at least up to 150 ns while the induced absorption decays to very small levels. The reasons for this behavior will be discussed below.

The recorded time traces at the three probe energies of 2466.5 eV, 2467.4 eV, and 2471.5 eV along with biexponential decay models are shown in Figure 1C. The difference of the two decay models for the evolution of the induced absorption is also plotted as a black solid line, indicating a maximum difference of induced absorption at 2466.5 eV and 2467.4 eV at 4 ns delay. The convolution of the instrumental response function (given by the 70-ps X-ay pulses) with the response of the DMDS has been modelled with:

$$\Delta A(E;t) = \{1+\mathrm{erf}[(t-t_0)/(\sqrt{2}\cdot\sigma)]\}/2 \cdot \ldots$$

$$\{A_1\cdot\exp[(t-t_0)/\tau_1] + A_2\cdot\exp[(t-t_0)/\tau_2]\}.$$

This approximation is adequate because the X-ray pulse duration is much shorter than the observed time-evolution of the molecular system (for details see the supporting information of reference [27]. We have modeled the persistent bleach signal with an additional component of the form $A_3\cdot\{1-\exp[(t-t_0)/\tau_2]\}$ to account for a long-lived signal beyond the maximum measured time delay of 150 ns.

The long time-constant τ_2 shows similar values for all three time traces and we have chosen to use a global fit routine with t_0 and τ_2 as common fit parameters. The X-ray pulse duration was set to σ = 30 ps, amounting to 70 ps FWHM. The long decay constant assumed a fit value of τ_2 = 160 ps while τ_1-values of (9±3) ps, (3±1) ps, and (4±1) ps yielded an optimal fit for the data at 2466.5 eV, 2467.4 eV, and 2471.5 eV, respectively. We note that time traces are generally harder to measure with similar signal-to noise ratio but despite the larger error bars the data in panels B and C of Figure 1 are fully consistent and show that the spectral region of induced absorption above 2476 eV initially decays more rapidly than the induced absorption peak at 2466.5 eV. We will relate

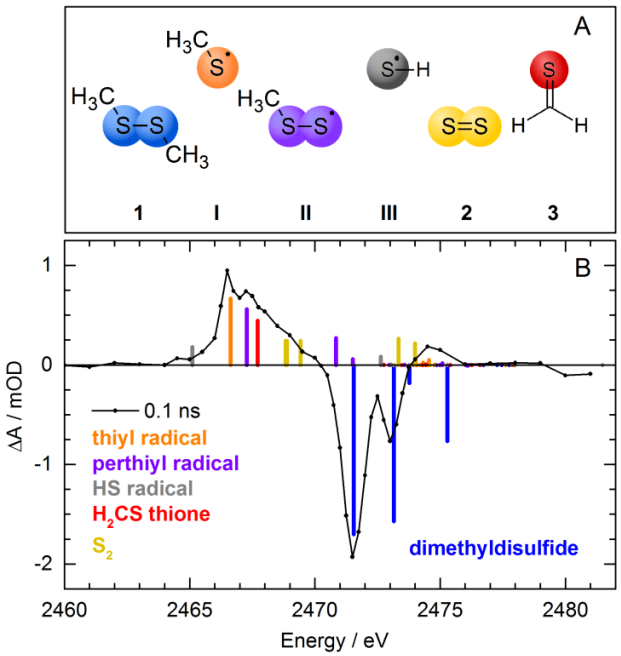

Figure 2. Possible sulfur species are displayed in a color-coded fashion in panel **A** with roman numerals assigned to transient species (i.e. radicals). The computed energetically lowest sulfur-1s transitions for all species are overlaid with the differential absorption spectrum at a time delay of 100 ps after excitation with 267-nm pulses in panel **B**. Scaling is arbitrary but the dominating species are the thiyl and perthiyl radicals (orange and purple transitions, respectively).

the implication of this result to the spectral interpretation in the next discussion section.

We have employed RASSCF calculations to predict the sulfur-1s transitions of the ground state of DMDS and possible photoproducts to interpret our experimentally obtained spectrum at 100 ps. Figure 1A shows three distinct sulfur 1s transitions that match our experimental ground state spectrum very well. For clarity, we have not convolved the transition lines with a Voigt profile. However, a lineshape function with a Gaussian broadening due to the finite monochromator resolution with σ=0.35 eV and a Lorentzian lifetime broadening of 0.8 eV reproduces the main absorption features in Figure 1A well. Solely the strength of the first transitions relative to the second one falls about 10% short. We note that our high-level electronic structure calculations provide a very accurate approach to describe electronic correlations and the bound-bound transitions

relevant to this study. However, these calculations can neither describe the Rydberg series nor the atomic absorption edge and other theoretical approaches provided by programs such as FEFF[39] would be more suitable to describe the EXAFS region.

Two major initial reaction pathways in the UV induced photochemistry of DMDS have previously been proposed: S-S and C-S bond cleavage, yielding methylthiyl and methylperthiyl radicals, henceforth abbreviated as thiyl (**I**) and perthiyl (**II**) radical, respectively. Figure 2 shows the species that have been discussed in the literature along with the calculated sulfur-1s transitions overlaid with the differential absorption spectrum at 100ps delay. The thiyl radical (**I**) exhibits a theoretical sulfur 1s spectrum that fits our experimentally observed induced absorption feature at 2466.5 eV similar to our previous findings[27]. The theoretical sulfur-1s spectrum of the perthiyl radical **II,** however, behaves slightly different. Two dominant transitions are predicted of which the energetically lower one matches our second observed induced absorption feature at 2467.4 eV. The second appreciable transition overlaps with the lowest DMDS transition and would therefore be masked by the bleach signal.

Our theoretical predictions show very good agreement with the two accepted photoproducts and we can already conclude that the thiyl and perthiyl radical species are produced with similar yields, thereby settling the question for 267-nm excitation. The transients in Fig. 1C provide interesting additional information: the perthiyl radical initially decays more rapidly, a conclusion that may have added to the confusion of product yields when investigating disulfide systems with poorer time-resolution or more ambiguous probes. Perthiyl radicals are generally less stable than thiyl radicals and our measurements underscore this difference between the two radical species.

Our differential absorption spectrum shows a pronounced should that cannot be explain by either, thiyl or perthiyl radical sulfur-1s transitions. Microsecond time-resolved studies by Kumar *et al.* suggested that one possible reaction pathway could lead to the production of S_2.[20] We therefore calculated S_2 as a possible by-product of the photo reaction. Four theoretical transitions of disulfur (**2**) emerge of which two are found at 2468.8 eV and 2469.3 eV while the higher-lying transitions are again masked by the bleach signal of the missing DMDS absorption. The energetically lowest transitions could explain the observed shoulder between 2468.5 eV and 2470 eV (considering a lineshape function of slightly less than 1 eV). We cannot fully exclude the formation of DMDS cations by two-photon absorption during the excitation process because the short pump pulse duration and relatively high fluence would provide 9.2 eV for such an ionization process and Borkar *et al.* have reported an adiabatic ionization energy for DMDS of 8.13 eV.[44] However, our spectral interpretation of disulfur formation from perthiyl radicals is consistent with the fact that a relative increase of absorption between 2468.5 eV and 2470.0 eV compared to the absorption between 2467.4 eV and 2468.5 eV has occurred at 5 ns delay. Cation formation would require a different decay channel of the perthiyl radical that does not absorb in the latter spectral region. To our knowledge, literature does not provide such an explanation.

Indeed, there are several studies of other groups that suggest that **2** is a decay product of the perthiyl radical **II**.[40-42] While early studies promote the idea of disulfur (**2**) being generated by spontaneous decay of hot **II**,[43] later studies foster the idea that ground state **II** could be photo-triggered by UV light to dissociate into methyl radicals and disulfur (**2**).[41] Our experimental results point to the conclusions from earlier studies since our initial UV excitation pulses are of 100-fs duration—too short for perthiyl generation and subsequent photo-excitation within one single pump pulse. Since the bond enthalpy of a C-S bond is about 2.4 eV but the exciting photons carry 4.6-eV light quanta, it is certainly valid to assume that the nascent radical species are vibrationally hot enough for a perthiyl radical to decay into disulfur and a methyl radical.

Scheme 1. Reaction Pathways of dimethyl disulfide upon 267-nm Excitation.

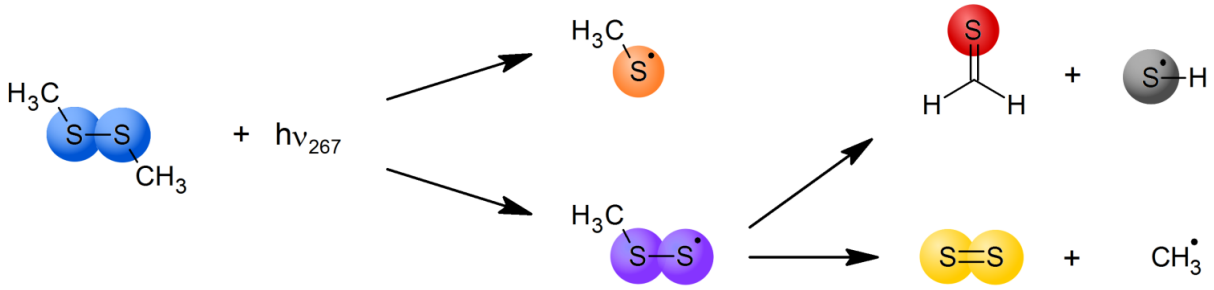

We end our discussion on the decay of the perthiyl radical **II** with a suggestion by Cole-Filipiak *et al.* which considers another reaction channel that would lead to the formation of an SH radical (**III**) and the thione CH_2S (**3**). Our calculated sulfur-1s absorption spectrum for **III** shows one major transition at 2465.1 eV and another one with roughly half the intensity at 2472.6 eV. The latter one would again be masked by the ground state bleach signal of DMDS but the first transition at 2465.1 eV overlaps with a small signal at the rising edge of the induced absorption of the thiyl radical (**I**). This signal is barely significant but the simultaneous thione generation would have a predicted transition at 2467.8 eV. Such a formation process would explain the broad induced absorption between the predicted perthiyl and disulfur transitions.

Scheme 1 summarizes our findings on the 100-picosecond to sub-microsecond timescales of the photochemistry of DMDS observed with sulfur K-edge TRXAS. Upon illumination with 267 nm light, two dominant reaction pathways are accessible: S-S and C-S bond cleavage to yield methylthiyl (**I**) and methylperthiyl (**II**) in similar branching ratios. Both **I** and **II** have distinct lowest-energy sulfur-1s transitions as shown in Fig. 2B. Disulfur (**2**) is one of the most likely decay products of **II** as is the formation pairwise formation of a hydrogen sulfide radical (**III**) and the CH_2S thione (**3**). The relatively complex reaction scheme highlights the need for advanced spectroscopies. It would certainly be interesting to extend this study to other disulfide systems that to relate important research fields such as aerosol chemistry or radical migration in proteins. Furthermore, femtosecond X-ray sources in the 2-3 keV photon energy range are currently coming online and be able to access the very early dynamics of the reactions allowing to also understand the mechanisms by which product formation occurs.

Conclusions

We have unambiguously identified the thiyl and perthiyl radicals as the primary reaction products of a model disulfide system (dimethyl disulfide) in solution and under ambient conditions excited with 267-nm femtosecond pulses. Additional spectral absorption features and their temporal evolution provide clear evidence for disulfur and CH_2S thione formation. This study underscores the usefulness and potential of time-resolved X-ray spectroscopy by virtue of its elemental specificity and sensitivity to electronic structure changes and altered chemical bonding. With an increasing number of X-ray free – electron lasers providing new instrumentation, it will be possible to carry studies as the one presented into the femtosecond regime to observe the early time evolution of complex photoinduced reactions which in turn will help unravel the underlying causes that lead to the rich photochemistry of sulfur-containing systems.

Author Information

Corresponding Author:
nils.huse@uni-hamburg.de

Present Addresses:
I.v.A.: Division of Solid State Physics, NanoLund, Lund University, Lund 221 00, Sweden.

A.A.C.: PULSE Institute, SLAC National Accelerator Laboratory, Menlo Park, CA 94025, United States.
J.H.L.: Pohang Accelerator Laboratory, San-31 Hyoja-dong Pohang, Kyungbuk 790-784, South Korea.
K.H.: Center for Gas Analysis, Division of Metrology for Quality of Life, Korea Research Institute of Standards and Science, Daejeon 34113, Republic of Korea.
O.V.: Department of Physics and Astronomy, Aarhus University, 8000 Aarhus, Denmark.
R.W.S.: Linac Coherent Light Source, SLAC National Accelerator Laboratory, Menlo Park, CA 94025, United States.

Acknowledgements

This work was supported by the Director, Office of Science, Office of Basic Energy Sciences, the Chemical Sciences, Geo-sciences, and Biosciences Division under the Department of Energy, Contract No. DE-AC02-05CH11231 (A.C., K.H., J.L., and R.W.S.). This research has been supported by National Research Foundation of Korea grants (2007-0056095, 2013S1A2A2035406, 2013R1A1A2009575, 2014R1A4A1001690), in part by the Global Research Laboratory Program (grant 2009-00439), and by the Max Planck POSTECH/KOREA Research Initiative Program (grant 2011-0031558) through the National Research Foundation of Korea (NRF) funded by Ministry of Science, ICT & Future Planning (T.K.K. and K.H.). M.O., I.v.A., K.A., and N.H. acknowledge funding from the Max Planck Society and the City of Hamburg. M.O. and N.H. gratefully acknowledge financial support by the Deutsche Forschungsgemeinschaft within the Sonderforschungsbereich 925 (project A4). This research used resources of the Advanced Light Source (LBNL), which is a DOE Office of Science User Facility. The authors would like to thank Bruce Rude for his continuous support of the experimental hardware.

Bibliography

(1) Jamie L. Bingaman, Casey L. Kohnhorst, Glenn A. Van Meter, Brent A. McElroy, Elizabeth A. Rakowski, Benjamin W. Caplins, Tiffany A. Gutowski, Christopher J. Stromberg, Charles Edwin Webster, and Edwin J. Heilweil, "Time-resolved vibrational spectroscopy of [fefe]-hydrogenase model compounds", *J. Phys. Chem. A* **116**, pp. 7261–7271 (2012).
(2) Thomas E. Creighton, "Disulphide bonds and protein stability", *Bioessays* **8**, pp. 57–63 (1988).
(3) Yoshinori Matsuura, Michiyo Takehira, Yasumasa Joti, Kyoko Ogasahara, Tomoyuki Tanaka, Naoko Ono, Naoki Kunishima, and Katsuhide Yutani, "Thermodynamics of protein denaturation at temperatures over 100?°c: Cuta1 mutant proteins substituted with hydrophobic and charged residues", *Sci. Rep.* **5**, pp. 15545 (2015).
(4) Gero Miesenbock, Dino A. De Angelis, and James E. Rothman, "Visualizing secretion and synaptic transmission with ph-sensitive green fluorescent proteins", *Nature* **394**, pp. 192–195 (1998).
(5) Michael J. Davies, "Protein oxidation and peroxidation", *Biochem. J.* **473**, pp. 805–825 (2016).
(6) Satoshi Yasuda, Hiraku Oshima, and Masahiro Kinoshita, "Structural stability of proteins in aqueous and nonpolar environments", *J. Chem. Phys.* **137**, pp. 135103 (2012).
(7) Vipan K. Parihar, Barrett D. Allen, Chongshan Caressi, Stephanie Kwok, Esther Chu, Katherine K. Tran, Nicole N. Chmielewski, Erich Giedzinski, Munjal M. Acharya, Richard A. Britten, Janet E. Baulch, and Charles L. Limoli, "Cosmic radiation exposure and persistent cognitive dysfunction", *Sci. Rep.* **6**, pp. 34774 (2016).
(8) Lisa M. Utschig, Sergey D. Chemerisov, David M. Tiede, and Oleg G. Poluektov, "Electron paramagnetic resonance study of radiation damage in photosynthetic reaction center crystals", *Biochemistry* **47**, pp. 9251–9257 (2008).
(9) Martin Weik, Raimond B. G. Ravelli, Gitay Kryger, Sean McSweeney, Maria L. Raves, Michal Harel, Piet Gros, Israel Silman, Jan Kroon, and Joel L. Sussman, "Specific chemical and structural damage to proteins produced by synchrotron radiation", *Proc. Natl. Acad. Sci. U. S. A.* **97**, pp. 623–628 (1999).
(10) Richard H. G. Baxter, Brandon-Luke Seagle, Nina Ponomarenko, and James R. Norris, "Specific radiation damage illustrates light-induced structural changes in the photosynthetic reaction center", *J. Am. Chem. Soc.* **126**, pp. 16728–16729 (2004).
(11) Takashi Ito, Tatsuro Miyaji, Tomoyuki Nakagawa, and Noboru Tomizuka, "Degradation of dimethyl disulfide by pseudomonas fluorescens strain 76", *Biosci. Biotechnol. Biochem.* **71**, pp. 366–370 (2007).
(12) Pietro Buzzini, Chiara Gasparetti, Benedetta Turchetti, Maria Rita Cramarossa, Ann Vaughan-Martini, Alessandro Martini, Ugo Maria Pagnoni, and Luca Forti, "Production of volatile organic compounds (vocs) by yeasts isolated from the ascocarps of black (tuber melanosporum vitt.) and white (tuber magnatum pico) truffles", *Arch. Microbiol.* **184**, pp. 187–193 (2005).
(13) Marcus C. Stensmyr, Isabella Urru, Ignazio Collu, Malin Celander, Bill S. Hansson, and Anna-Maria Angioy, "Pollination: Rotting smell of dead-horse arum florets", *Nature* **420**, pp. 625–626 (2002).
(14) Adam Rinker, Christopher D. Halleman, and Michael R. Wedlock, "Photodissociation dynamics of dimethyl disulfide", *Chem. Phys. Lett.* **414**, pp. 505–508 (2005).
(15) A. Yokozeki and S. H. Bauer, "Structures of dimethyl disulfide and methyl ethyl disulfide, determined by gas-phase electron diffraction. a vibrational analysis for mean square amplitudes", *J. Phys. Chem.* **80**, pp. 618–625 (1976).
(16) Joseph J. Grabowski and Lijian Zhang, "Dimethyl disulfide: anion-molecule reactions in the gas phase at 300 k", *J. Am. Chem. Soc.* **111**, pp. 1193–1203 (1989), -.
(17) Gerald H. Morine and Robert R. Kuntz, "Observations of c-s and s-s bond cleavage in the photolysis of disulfides in solution", *Photochem. Photobiol.* **33**, pp. 1–5 (1981).
(18) W. E. Lyons, "Photolysis of organic disulphides", *Nature* **162**, pp. 1004 (1948).
(19) Niko P. Ernsting, "Solvation of photolytically generated p-aminophenylthiyl radicals studied by sub-picosecond transient absorption", *Chem. Phys. Lett.* **166**, pp. 221–226 (1990).
(20) Awadhesh Kumar, P.K. Chowdhury, K.V.S. Rama Rao, and J.P. Mittal, "Four-centered concerted ethane elimination in the ir and uv laser photolysis of dimethyldisulfide. real-time observation of s2 and ch3s radicals", *Chem. Phys. Lett.* **198**, pp. 406–412 (1992).
(21) C. W. Bookwalter, D. L. Zoller, P. L. Ross, and M. V. Johnston, "Bond-selective photodissociation of aliphatic disulfides", *J. Am. Soc. Mass Spectrom.* **6**, pp. 872–876 (1995).
(22) Cheng Luo, Wei-Na Du, Xue-Mei Duan, Jing-Yao Liu, and Ze-Sheng Li, "Theoretical study on the excited states and

photodissociation mechanism of dimethyldisulfide", *Chem. Phys. Lett.* **469**, pp. 242–246 (2009).
(23) Anne B. Stephansen, Rasmus Y. Brogaard, Thomas S. Kuhlman, Liv B. Klein, Jørn B. Christensen, and Theis I. Sølling, "Surprising intrinsic photostability of the disulfide bridge common in proteins", *J. Am. Chem. Soc.* **134**, pp. 20279–20281 (2012).
(24) Anne B. Stephansen, Martin A.B. Larsen, Liv. B. Klein, and Theis I. Sølling, "On the photostability of the disulfide bond: An electronic or a structural property?", *Chem. Phys.* **442**, pp. 77—80 (2014).
(25) CE Crespo-Hernandez, B Cohen, and B Kohler, "Base stacking controls excited-state dynamics in A-T DNA", *Nature* **436**, pp. 1141–1144 (2005).
(26) CE Crespo-Hernandez, B Cohen, and B Kohler, "Molecular spectroscopy: Complexity of excited-state dynamics in DNA - Reply", *Nature* **441**, pp. E8 (2006).
(27) Miguel Ochmann, Inga von Ahnen, Amy A. Cordones, Abid Hussain, Jae Hyuk Lee, Kiryong Hong, Katrin Adamczyk, Oriol Vendrell, Tae Kyu Kim, Robert William Schoenlein, and Nils Huse, "Light-induced radical formation and isomerization of an aromatic thiol in solution followed by time-resolved x-ray absorption spectroscopy at the sulfur k-edge", *J. Am. Chem. Soc.* **139**, pp. 4789–4796 (2017).
(28) Benjamin E. Van Kuiken, Matthew R. Ross, Matthew L. Strader, Amy A. Cordones, Hana Cho, Jae Hyuk Lee, Robert W. Schoenlein, and Munira Khalil, "Picosecond sulfur k-edge x-ray absorption spectroscopy with applications to excited state proton transfer", *Struct. Dynamics* **4**, pp. 044021 (2017).
(29) Vlad Martin-Diaconescu and Pierre Kennepohl, "Sulfur k-edge xas as a probe of sulfur-centered radical intermediates", *J. Am. Chem. Soc.* **129**, pp. 3034–3035 (2007).
(30) Anusha Karunakaran-Datt and Pierre Kennepohl, "Redox photochemistry of methionine by sulfur k-edge x-ray absorption spectroscopy: Potential implications for cataract formation", *J. Am. Chem. Soc.* **131**, pp. 3577–3582 (2009).
(31) Benjamin E. Van Kuiken, Nils Huse, Hana Cho, Matthew L. Strader, Michael S. Lynch, Robert W. Schoenlein, and Munira Khalil, "Probing the electronic structure of a photoexcited solar cell dye with transient x-ray absorption spectroscopy", *J. Phys. Chem. Lett.* **3**, pp. 1695 (2012).
(32) Chr. Møller and M. S. Plesset, "Note on an approximation treatment for many-electron systems", *Phys. Rev.* **46**, pp. 618–622 (1934).
(33) Thom H. Dunning, "Gaussian basis sets for use in correlated molecular calculations. I. The atoms boron through neon and hydrogen", *J. Chem. Phys.* **90**, pp. 1007–1023 (1989).
(34) M. J. Frisch, G. W. Trucks, H. B. Schlegel, G. E. Scuseria, M. A. Robb, J. R. Cheeseman, G. Scalmani, V. Barone, B. Mennucci, G. A. Petersson, H. Nakatsuji, M. Caricato, X. Li, H. P. Hratchian, A. F. Izmaylov, J. Bloino, G. Zheng, J. L. Sonnenberg, M. Hada, M. Ehara, K. Toyota, R. Fukuda, J. Hasegawa, M. Ishida, T. Nakajima, Y. Honda, O. Kitao, H. Nakai, T. Vreven, J. A. Montgomery, Jr., J. E. Peralta, F. Ogliaro, M. Bearpark, J. J. Heyd, E. Brothers, K. N. Kudin, V. N. Staroverov, R. Kobayashi, J. Normand, K. Raghavachari, A. Rendell, J. C. Burant, S. S. Iyengar, J. Tomasi, M. Cossi, N. Rega, J. M. Millam, M. Klene, J. E. Knox, J. B. Cross, V. Bakken, C. Adamo, J. Jaramillo, R. Gomperts, R. E. Stratmann, O. Yazyev, A. J. Austin, R. Cammi, C. Pomelli, J. W. Ochterski, R. L. Martin, K. Morokuma, V. G. Zakrzewski, G. A. Voth, P. Salvador, J. J. Dannenberg, S. Dapprich, A. D. Daniels, Ö. Farkas, J. B. Foresman, J. V. Ortiz, J. Cioslowski, and D. J. Fox, "Gaussian 09, Revision E.01" (2009), Gaussian Inc., Wallingford, CT.
(35) James Finley, Per-Åke Malmqvist, Björn O. Roos, and Luis Serrano-Andrés, "The multi-state CASPT2 method", *Chem. Phys. Lett.* **288**, pp. 299–306 (1998).
(36) Kerstin. Andersson, Per Åke Malmqvist, Bjoern O. Roos, Andrzej J. Sadlej, and Krzysztof. Wolinski, "Second-order perturbation theory with a CASSCF reference function", *J. Phys. Chem.* **94**, pp. 5483–5488 (1990).
(37) Kerstin Andersson, Per-Åke Malmqvist, and Björn O. Roos Roos, "Second-order perturbation theory with a complete active space self-consistent field reference function", *J. Chem. Phys.* **96**, pp. 1218–1226 (1992).
(38) Francesco Aquilante, Luca De Vico, Nicolas Ferré, Giovanni Ghigo, Per Åke Malmqvist, Pavel Neogrády, Thomas Bondo Pedersen, Michal Pitonák, Markus Reiher, Björn O. Roos, Luis Serrano-Andrés, Miroslav Urban, Valera Veryazov, and Roland Lindh, "MOLCAS 7: The next generation", *J. Comput. Chem.* **31**, pp. 224–247 (2010).
(39) John J. Rehr, Joshua J. Kas, Fernando D. Vila, Micah P. Prange, and Kevin Jorissen, "Parameter-free calculations of x-ray spectra with feff9", *Phys. Chem. Chem. Phys.* **12**, pp. 5503–5513 (2010).
(40) S. Nourbakhsh, C.?L. Liao, and C. Y. Ng, "A 193 nm laser photofragmentation time?of?flight mass spectrometric study of ch3ssch3, ssch3, and sch3", *J. Chem. Phys.* **92**, pp. 6587–6593 (1990).
(41) Neil C. Cole-Filipiak, Bogdan Negru, Gabriel M. P. Just, Dayoung Park, and Daniel M. Neumark, "Photodissociation dynamics of the methyl perthiyl radical at 248 nm via photofragment translational spectroscopy", *J. Chem. Phys.* **138**, pp. 054301 (2013).
(42) Aaron W. Harrison, Mikhail Ryazanov, Erin N. Sullivan, and Daniel M. Neumark, "Photodissociation dynamics of the methyl perthiyl radical at 248 and 193 nm using fast-beam photofragment translational spectroscopy", *J. Chem. Phys.* **145**, pp. 024305 (2016).
(43) B. Martinez-Haya, M. J. Bass, M. Brouard, C. Vallance, I. Torres, and J. Barr, "Photodissociation and multiphoton dissociative ionization processes in ch3s2ch3 at 193 nm studied using velocity-map imaging", *J. Chem. Phys.* **120**, pp. 11042–11052 (2004).
(44) Sampada Borkar, Bálint Sztáray, and Andras Bodi, "Energetics and dissociation pathways of dimethyl disulfide and dimethyl diselenide using photoelectron photoion coincidence spectroscopy", *J. Electron Spectrosc. Relat. Phenom.* **196**, pp. 165–172 (2014).
(45) James J. Butler, Tomas Baer, and Slayton A. Evans, "Energetics and structures of organosulfur ions: Ch3ssch3+, ch3ss+, c2h5s+, and ch2sh+", *J. Am. Chem. Soc.* **105**, pp. 3451–3455 (1983).
(46) Wai?Kee Li, See?Wing Chiu, Z.?X. Ma, C.?L. Liao, and C. Y. Ng, "Adiabatic ionization energy of ch3ssch3", *J. Chem. Phys.* **99**, pp. 8440–8444 (1993).
(47) Debashree Ghosh, Olexandr Isayev, Lyudmila V. Slipchenko, and Anna I. Krylov, "Effect of solvation on the vertical ionization energy of thymine: From microhydration to bulk", *J. Phys. Chem. A* **115**, pp. 6028–6038 (2011).

Chapter 5

Conclusions and Outlook

In this PhD work, RASSCF calculations were employed for the accurate modelling of multiple light-induced transient products of sulfur-containing molecules in solution. In addition, *ab initio* quantum chemistry calculations have been performed to probe the influence of hydrogen bonding and electric dipoles on the electronic structure of nitrile containing molecules.

The chemical reaction of 4-MTP and dimethyl disulfide (DMDS) in the liquid phase were successfully followed using sulfur-1s absorption spectroscopy to reveal the different reaction pathways. Upon ultraviolet excitation in solution phase, the different reaction pathways of 4-MTP namely radical generation, thione isomerization, and anion formation were revealed using sulfur-1s absorption spectroscopy. Explicitly, I have performed quantum chemical calculations to interpret the experimental data obtained for a model aromatic thiol system. RASSCF calculations were used to assign the sulfur-1s transitions of the ground state of 4-MTP and the induced absorption peaks providing insight to the nature of the photoproducts. In a joint experimental and theoretical study, light-induced radical formation and Isomerization was explained with the help of high level electronic structure calculations. Furthermore, the regioselectivity of the thione isomerization was explained by the resulting radical frontier orbitals.

The basic photochemical behaviour of disulfide containing linear molecules of DMDS have been investigated using sulfur-1s absorption spectroscopy. The energy of the excitation photon is sufficient (4.6 eV) to break a C-S bond (2.4 eV), as well as an S-S bond (2.9 eV). In order to understand the observed spectral features, quantum chemical RASSCF calculations were performed for the ground state and other possible photoproducts for correct assignment of experimental peaks. In these simulations, an explicit access to each electronic state with the extracted information allows to assign the dominant transitions. Therefore, simulations were paramount in providing detailed information on the electronic structure of the different sulfur species. For clear spectral identification of the transient photoproducts and a reliable understanding of the reaction mechanism, several photoionization products were simulated. Radical formation by C-S and S-S bond cleavage was confirmed with computed spectra in accordance with the reported UV induced photochemistry of DMDS.

The RIXS process corresponds to a photon-in photon-out mechanism, which is a highly useful tool for studying the electronic structure and chemistry of gaseous and condensed matter systems. RIXS spectroscopy is suitable tool providing relevant information on chemical bonding and can also serve as a probe for weak hydrogen bonding between molecules. A RIXS event can be considered as a consecutive process of X-ray absorption and emission. In addition, the RIXS technique provides a local probe of both the unoccupied and the occupied electronic orbitals in a single experiment, and in an element and site-selective manner. For the specific molecular system HCN, it is shown that the axial dipole charge distribution lowers the energy of the σ orbital and leads to a strengthening of the CN bond. Further insight in this respect is provided by the anomalous frequency shift as well as very clearly marked shift in the Raman UV line originating from the σ orbital. The analysis based on dominant transitions is used to understand altered charge distributions caused by electrostatic dipole field. The simulations show that *ab initio* quantum chemistry calculations allowed to combine electronic and structural probes to comprehensively understand a nitrile model system subjected to hydrogen bonding and electric dipoles. Furthermore, these simulations address and gauge the anomalous frequency shift of the nitrile stretching vibration and link it to the changes in electronic structure. Experimental evidence for the predicted behaviour of HCN requires a less toxic and more practical system. The effects of (weak) hydrogen bonding on the electronic structure of acetonitrile have been investigated using XAS, RIXS, and electronic structure calculations. The spectral differences could largely be attributed to hydrogen bonding, highlighting the sensitivity of RIXS even for weak interactions.

Outlook

The work presented in this thesis has facilitated a number of research projects that should be explored in the future. The work based on tracking the light-induced reaction dynamics in solution has opened up the prospect to conduct pump-probe experiments at femtosecond timescales to reveal the different reaction pathways. This method would be a viable tool to probe proton transfer and other charge transfer processes in sulfur containing molecular, biological, and material systems. In addition, combined experimental and theoretical studies on different sulfur and nitrogen containing molecules have been planned. The purpose of this work would be to follow different photo-excited dynamic processes like proton transfer and selective chemical bond deformation. Moreover, one step beyond the RASSCF calculations will be to model reaction pathways using non-MEP (non-minimum energy path) involving reaction path bifurcations, roaming and non-statistical dynamic effects. This methodology has been explained and implemented by J. Rehbein and B. Wulff [200] to accumulate detailed information on dynamics of various reactions.

The stage is also set to perform systematic investigations on the response of other nitrogen-containing functional groups such as diazo group. Diazo groups have a more tunable and a broader range of reactivity which is responsible for their chemoselectivity in chemical biology [201]. Diazo compounds have served as chemical probes and evoked novel modifications of proteins and nucleic acids. Moreover, their diverse reactivity is exemplified by their ability to alkylate oxygen, nitrogen, sulfur, and even carbon [202]. Therefore, the simplest molecule diazomethane would be a good starting point for theory in order to establish basic principles of interaction of the diazo group with its environment. A detailed *ab initio* initio study would be performed to probe the influence of hydrogen bonding and electric dipoles for comprehensive understanding of electronic and structural changes.

In this thesis, nitrogen and sulfur containing small molecules have been investigated with high-level *ab* initio methods. The rapid growth of computational cost for these methods limits their applicability to treat the effects of systems embedded in a larger environment, for instance solvent molecules. Mixed quantum mechanics/molecular mechanics (QM/MM) simulations have the potential to describe chemical reactions and other chemical processes, such as charge transfer or electronic excitation in systems influenced by an interacting larger environment. QM/MM method leads to a better understanding of chemical reactions, and the mechanisms by which in particular protein environments control these reactions. These simulations not only predict the chemical properties accurately but have become an almost routine tool for modeling of biomolecular systems and for the investigation of inorganic/organometallic and solid-state systems [203–205]. In QM/MM methods, the region of the system in which the chemical process takes place is modelled at the *ab* initio quantum chemical level, whereas the remainder is described by a molecular mechanics force field. Thus I would envision to plan simulations of nitrogen and sulfur containing systems (e.g., enzymes) to investigate electrostatic interactions and hydrogen bonding with their environment using Raman spectroscopy and QM/MM calculations.

References

[1] S. Jones, *Nucleic Acids Research* **29**, 943 (2001).

[2] K. Nadassy, S. J. Wodak, J. Janin, *Biochemistry* **38**, 1999 (1999).

[3] A.-C. Clairaut, *Théorie de la figure de la terre; tirée des principes de l'hydrostatique* (Paris Courcier, 1808).

[4] P. S. Laplace, Traité de mécanique céleste, tome quatrième (1805).

[5] C. Gauß, *Principia generalia theoriae figurae fluidorum in statu aequilibrii* (Dieterichianis, 1830).

[6] W. Sutherland, *Philosophical Magazine Series 5* **36**, 507 (1893).

[7] R. Clausius, *Annalen der Physik und Chemie* **176**, 353 (1857).

[8] W. Keesom, *Physikalische Zeitschrift* **22**, 129 (1921).

[9] P. Debye, *Journal of the Society of Chemical Industry* **48**, 1036 (1929).

[10] F. London, *Zeitschrift für Physik* **63**, 245 (1930).

[11] H.-J. Schneider, A. K. Yatsimirsky, *Chem. Soc. Rev.* **37**, 263 (2008).

[12] R. Saalfrank, H. Maid, A. Scheurer, *Angewandte Chemie International Edition* **47**, 8794 (2008).

[13] G. Oshovsky, D. Reinhoudt, W. Verboom, *Angewandte Chemie International Edition* **46**, 2366 (2007).

[14] M. Kruppa, B. König, *Chemical Reviews* **106**, 3520 (2006).

[15] J. Taraszewska, M. Koźbiał, *Journal of inclusion phenomena and macrocyclic chemistry* **53**, 155 (2005).

[16] R. Paulini, K. Müller, F. Diederich, *Angewandte Chemie International Edition* **44**, 1788 (2005).

[17] C. A. Hunter, *Angewandte Chemie International Edition* **43**, 5310 (2004).

[18] E. A. Meyer, R. K. Castellano, F. Diederich, *Angew. Chem. Int. Ed.* **42**, 1210 (2003).

[19] L. R. Nassimbeni, *Accounts of Chemical Research* **36**, 631 (2003).

[20] H. Gohlke, G. Klebe, *Angewandte Chemie International Edition* **41**, 2644 (2002).

[21] H.-J. Schneider, *Chemical Society Reviews* **23**, 227 (1994).

[22] H.-J. Schneider, *Angewandte Chemie International Edition* **48**, 3924 (2009).

[23] K. Müller-Dethlefs, P. Hobza, *Chemical Reviews* **100**, 143 (2000).

[24] S. Burley, G. Petsko, *Science* **229**, 23 (1985).

[25] S. Li, V. R. Cooper, T. Thonhauser, B. I. Lundqvist, D. C. Langreth, *The Journal of Physical Chemistry B* **113**, 11166 (2009).

[26] D. Y. Kim, N. J. Singh, J. W. Lee, K. S. Kim, *Journal of Chemical Theory and Computation* **4**, 1162 (2008).

[27] J. T. Stivers, Y. L. Jiang, *Chemical Reviews* **103**, 2729 (2003).

[28] H. Rydberg, *et al.*, *Physical Review Letters* **91** (2003).

[29] L. Henrard, E. Hernández, P. Bernier, A. Rubio, *Physical Review B* **60**, R8521 (1999).

[30] N. Kurita, H. Inoue, H. Sekino, *Chemical Physics Letters* **370**, 161 (2003).

[31] F. London, *Transactions of the Faraday Society* **33**, 8b (1937).

[32] K. H. Sippel, F. A. Quiocho, *Protein Science* **24**, 1040 (2015).

[33] G. R. Desiraju, *Crystal Growth & Design* **11**, 896 (2011).

[34] C. B. Aakeröy, K. R. Seddon, *Chem. Soc. Rev.* **22**, 397 (1993).

[35] M. M.-N. (Mautner), *Chemical Reviews* **105**, 213 (2005).

[36] G. R. Desiraju, *Molecular Crystals and Liquid Crystals Science and Technology. Section A. Molecular Crystals and Liquid Crystals* **211**, 63 (1992).

[37] A. Werner, *Justus Liebigs Annalen der Chemie* **322**, 261 (1902).

[38] T. S. Moore, T. F. Winmill, *J. Chem. Soc., Trans.* **101**, 1635 (1912).

[39] W. M. Latimer, W. H. Rodebush, *Journal of the American Chemical Society* **42**, 1419 (1920).

[40] L. Pauling, *Proceedings of the National Academy of Sciences* **14**, 359 (1928).

[41] P. Pfeiffer, P. Fischer, J. Kuntner, P. Monti, Z. Pros, *Justus Liebigs Annalen der Chemie* **398**, 137 (1913).

[42] L. Pauling, R. B. Corey, H. R. Branson, *Proceedings of the National Academy of Sciences* **37**, 205 (1951).

[43] C. C. F. Blake, *et al.*, *Nature* **206**, 757 (1965).

[44] J. D. Watson, F. H. C. Crick, *Nature* **171**, 737 (1953).

[45] K. Chen, *et al.* **405**, 814.

[46] H. Langhals, *Angewandte Chemie International Edition* **43**, 5291 (2004).

[47] T. Elsaesser, H. J. Bakker, eds., *Ultrafast Hydrogen Bonding Dynamics and Proton Transfer Prosesses in the Condensed Phase*, vol. 23 (Kluwer Academic Publishers, 2002).

[48] S. Myneni, *et al.*, *J. Phys.: Condens. Matter* **14**, L213 (2002).

[49] J.-H. Guo, *et al.*, *Phys. Rev. Lett.* **89**, 137402 (2002).

[50] N. Huse, K. Heyne, J. Dreyer, E. T. J. Nibbering, T. Elsaesser, *Phys. Rev. Lett.* **91**, 197401 (2003).

[51] P. Wernet, *et al.*, *Science* **304**, 995 (2004).

[52] L. Weinhardt, *et al.*, *Phys. Chem. Chem. Phys.* **17**, 27145 (2015).

[53] G. M. Chaban, *J. Phys. Chem. A* **108**, 4551 (2004).

[54] Z. Getahun, *et al.*, *J. Am. Chem. Soc.* **125**, 405 (2003).

[55] M. M. Gromiha, K. Saraboji, S. Ahmad, M. Ponnuswamy, M. Suwa, *Biophys. Chem.* **107**, 263 (2004).

[56] P. Deb, *et al.*, *J. Phys. Chem. B* **120**, 4034 (2016).

[57] S. Bagchi, S. G. Boxer, M. D. Fayer, *J. Phys. Chem. B* **116**, 4034 (2012).

[58] G. A. Jeffrey, W. Saenger, *Hydrogen bonding in biological structures* (Springer Science & Business Media, 2012).

[59] E. G. Robertson, J. P. Simons, *Phys. Chem. Chem. Phys.* **3**, 1 (2001).

[60] M. S. de Vries, P. Hobza, *Annu. Rev. Phys. Chem.* **58**, 585 (2007).

[61] E. Garand, *et al.*, *Science* **335**, 694 (2012).

[62] P. Cabello, *Microbiology* **150**, 3527 (2004).

[63] T. Yamamoto, *et al.*, *Journal of the American Chemical Society* **118**, 10389 (1996).

[64] H. van Mullekom, *Materials Science and Engineering: R: Reports* **32**, 1 (2001).

[65] J. Reedijk, *Comprehensive Coordination Chemistry*, J. A. G.Wilkinson, R. D.Gillard, ed. (Pergamon Press, Oxford, 1987), vol. 2, p. p.73.

[66] A. T. Balaban, D. C. Oniciu, A. R. Katritzky, *Chemical Reviews* **104**, 2777 (2004).

[67] V. Froidevaux, C. Negrell, S. Caillol, J.-P. Pascault, B. Boutevin, *Chemical Reviews* **116**, 14181 (2016). PMID: 27809503.

[68] A. R. Padgett, E. F. Degering, *Industrial & Engineering Chemistry* **32**, 486 (1940).

[69] M. Negwer, *Organic-Chemical Drugs and Their Synonyms: An International Survey* (Berlin, Akademie Verlag, 1987).

[70] G. Rücker, *Pharmazie in Unserer Zeit* **24**, 169 (1995).

[71] E. Valeur, M. Bradley, *Chem. Soc. Rev.* **38**, 606 (2009).

[72] H. Schiff, *Annalen der Chemie und Pharmacie* **131**, 118 (1864).

[73] C. Gyanakumari, K. Mounika, A. Pragathi, *Journal of Scientific Research* **2** (2010).

[74] W. Radecka-Paryzek, I. Pospieszna-Markiewicz, M. Kubicki, *Inorganica Chimica Acta* **360**, 488 (2007).

[75] S. Li, *et al.*, *Corrosion Science* **41**, 1273 (1999).

[76] M. W. Sabaa, R. R. Mohamed, E. H. Oraby, *European Polymer Journal* **45**, 3072 (2009).

[77] Q.-C. Zhu, R. O. Hutchins, M. K. Hutchins, *Organic Preparations and Procedures International* **26**, 193 (1994).

[78] Y. Yang, *et al.*, *Synthetic Communications* **42**, 2540 (2012).

[79] C. Astbury, *et al.*, *Dyes and Pigments* **97**, 100 (2013).

[80] A. J. Fatiadi, *Triple-Bonded Functional Groups: Vol. 2 (1983)* (John Wiley & Sons, Ltd.), pp. 1057–1303.

[81] F. F. Fleming, L. Yao, P. C. Ravikumar, L. Funk, B. C. Shook, *Journal of Medicinal Chemistry* **53**, 7902 (2010).

[82] D. T. Mowry, *Chemical Reviews* **42**, 189 (1948).

[83] J. Evans, G.-S. Lo, *Spectrochimica Acta* **21**, 1033 (1965).

[84] B. Dierker, *et al.*, *New Journal of Physics* **15**, 093025 (2013).

[85] W. R. Fawcett, G. Liu, T. E. Kessler, *J. Phys. Chem.* **97**, 9293 (1993).

[86] D. Jamroz, J. Stangret, J. Lindgren, *J. Am. Chem. Soc.* **115**, 6165 (1993).

[87] F. Muniz-Miranda, M. Pagliai, G. Cardini, R. Righini, *J. Chem. Phys.* **137**, 244501 (2012).

[88] J. Niskanen, *et al.*, *Phys. Chem. Chem. Phys.* **18**, 26026 (2016).

[89] G. Eaton, A. S. Pena-Nunez, M. C. R. Symons, *J. Chem. Soc., Faraday Trans. 1* **84**, 2181 (1988).

[90] R. A. Nyquist, *Appl. Spectrosc.* **44**, 1405 (1990).

[91] J. E. Bertie, Z. Lan, *J. Phys. Chem. B* **101**, 4111 (1997).

[92] J. R. Reimers, L. E. Hall, *J. Am. Chem. Soc.* **121**, 3730 (1999).

[93] E. S. Kryachko, M. T. Nguyen, *J. Phys. Chem. A* **106**, 4267 (2002).

[94] S. H. Brewer, S. Franzen, *J. Chem. Phys.* **119**, 851 (2003).

[95] K. A. S. Sergio D. Dalosto, Jane M. Vanderkooi, *J. Phys. Chem. B* **108**, 6450 (2004).

[96] A. Warshel, *et al.*, *Chem. Rev.* **106**, 3210 (2006).

[97] M. G. Maienschein-Cline, C. H. Londergan, *J. Phys. Chem. A* **111**, 10020 (2007).

[98] C. T. Liu, *et al.*, *J. Am. Chem. Soc.* **136**, 10349 (2014).

[99] K. W. Mlynarski, U.s. geological survey, *Tech. rep.* (2000).

[100] A. E. N.N. Greenwood, *Sulfur. In Chemistry of the Elements* (Butterworth-Heinemann Oxford, 1997), second edition edn.

[101] A. Vairavamurthy, *Spectrochimica Acta Part A: Molecular and Biomolecular Spectroscopy* **54**, 2009 (1998).

[102] J. Toohey, A. Cooper, *Molecules* **19**, 12789 (2014).

[103] J. J. Griebel, R. S. Glass, K. Char, J. Pyun, *Progress in Polymer Science* **58**, 90 (2016).

[104] H. Chen, *et al.*, *Nano Letters* **15**, 798 (2015).

[105] L. Meng, T. Fujikawa, M. Kuwayama, Y. Segawa, K. Itami, *Journal of the American Chemical Society* **138**, 10351 (2016).

[106] M. E. B. John T. Brosnan, *The Journal of Nutrition* **136**, 1636S (2006).

[107] G. W. Luther, D. T. Rickard, *Journal of Nanoparticle Research* **7**, 389 (2005).

[108] M. L. Buchner J, *Oxidative folding of peptides and proteins*, no. pp 274–380 (RSC Biomolecular Sciences, Cambridge, 2009).

[109] W. J. Wedemeyer, E. Welker, M. Narayan, H. A. Scheraga, *Biochemistry* **39**, 4207 (2000).

[110] I. Annis, B. Hargittai, G. Barany, *Solid-Phase Peptide Synthesis* (Elsevier, 1997), pp. 198–221.

[111] J. Thornton, *Journal of Molecular Biology* **151**, 261 (1981).

[112] T. E. Creighton, *BioEssays* **8**, 57 (1988).

[113] C. Schöneich, *Methods in Enzymology* (Elsevier BV, 1995), pp. 45–55.

[114] C. von Sonntag, H.-P. Schuchmann, *Methods in Enzymology* (Elsevier BV, 1994), pp. 47–56.

[115] M. A. Reed, *Science* **278**, 252 (1997).

[116] L. Sun, *et al.*, *Chem. Soc. Rev.* **43**, 7378 (2014).

[117] L. Moroder, H.-J. Musiol, M. Götz, C. Renner, *Biopolymers* **80**, 85 (2004).

[118] E. Marshall, L. M. Costa, J. Gutierrez-Marcos, *Journal of Experimental Botany* **62**, 1677 (2011).

[119] S. W. Englander, L. Mayne, *Proceedings of the National Academy of Sciences* **111**, 15873 (2014).

[120] P. J. Hogg, *Trends in Biochemical Sciences* **28**, 210 (2003).

[121] A. A. Dombkowski, K. Z. Sultana, D. B. Craig, *FEBS Letters* **588**, 206 (2013).

[122] J. T. Flaherty, M. L. Weisfeldt, *Free Radical Biology and Medicine* **5**, 409 (1988).

[123] V. Lobo, A. Patil, A. Phatak, N. Chandra, *Pharmacognosy Reviews* **4**, 118 (2010).

[124] H. J. H. Fenton, *J. Chem. Soc., Trans.* **65**, 899 (1894).

[125] M. Gomberg, *Berichte der deutschen chemischen Gesellschaft* **33**, 3150 (1900).

[126] W. Schlenk, T. Weickel, A. Herzenstein, *Justus Liebig's Annalen der Chemie* **372**, 1 (1910).

[127] F. Paneth, W. Hofeditz, *Berichte der deutschen chemischen Gesellschaft (A and B Series)* **62**, 1335 (1929).

[128] H. Wieland, *Justus Liebig's Annalen der Chemie* **381**, 200 (1911).

[129] H. Wieland, H. Lecher, *Berichte der deutschen chemischen Gesellschaft* **45**, 2600 (1912).

[130] D. Harman, *Journal of Gerontology* **11**, 298 (1956).

[131] C. K. Mittal, F. Murad, *Proceedings of the National Academy of Sciences* **74**, 4360 (1977).

[132] K. Griesbaum, *Angewandte Chemie International Edition in English* **9**, 273 (1970).

[133] D. Crich, *Helvetica Chimica Acta* **89**, 2167 (2006).

[134] L. R. P. Hanns Fischer Prof., *Angewandte Chemie International Edition* (2001).

[135] B. Giese, *Radicals in organic synthesis: formation of carbon–carbon bonds* (Pergamon Press, Oxford, 1986).

[136] M. Z. Hoffman, E. Hayon, *Journal of the American Chemical Society* **94**, 7950 (1972).

[137] J. W. Purdie, H. A. Gillis, N. V. Klassen, *Canadian Journal of Chemistry* **51**, 3132 (1973).

[138] G. H. Morine, R. R. Kuntz, *Photochemistry and Photobiology* **33**, 1 (1981).

[139] D. W. Grant, J. H. Stewart, *Photochemistry and Photobiology* **40**, 285 (1984).

[140] C. von Sonntag, *The chemical basis of radiation biology* (Taylor & Francis in London, New York, NY, 1987).

[141] F. Dénès, M. Pichowicz, G. Povie, P. Renaud, *Chemical Reviews* **114**, 2587 (2014).

[142] A. H. Zewail, *Science* **242**, 1645 (1988).

[143] E. T. Nibbering, H. Fidder, E. Pines, *Annual Review of Physical Chemistry* **56**, 337 (2005).

[144] R. J. Levis, *Science* **292**, 709 (2001).

[145] S. M. Hurley, *Science* **292**, 648 (2001).

[146] R. W. Schoenlein, *Science* **287**, 2237 (2000).

[147] V. Šrajer, *et al.*, *Journal of Synchrotron Radiation* **7**, 236 (2000).

[148] H. Okamoto, *et al.*, *Physical Review B* **70** (2004).

[149] L. X. Chen, *Science* **292**, 262 (2001).

[150] R. van Grondelle, J. P. Dekker, T. Gillbro, V. Sundstrom, *Biochimica et Biophysica Acta (BBA) - Bioenergetics* **1187**, 1 (1994).

[151] A. Douhal, S. K. Kim, A. H. Zewail, *Nature* **378**, 260 (1995).

[152] N. Huse, *et al.*, *The Journal of Physical Chemistry Letters* **2**, 880 (2011).

[153] A. Plech, *et al.*, *Physical Review Letters* **92** (2004).

[154] M. Ochmann, *et al.*, *Journal of the American Chemical Society* (2017).

[155] J. Kim, *et al.*, *Chem. Commun.* **52**, 3734 (2016).

[156] A. Szabo, N. S. Ostlund, *Modern Quantum Chemistry : Introduction to Advanced Electronic Structure Theory* (New York; London: Free ; Collier Macmillan, 1982. Print., 1982).

[157] C. J. Cramer, *Essentials of Computational Chemistry: Theories and Models (2nd Edition)* (John Wiley & Sons, West Sussex, England, 2004).

[158] F. Jensen, *Introduction to Computational Chemistry* (John Wiley & Sons, 2006).

[159] M. Born, R. Oppenheimer, *Annalen der Physik* **389**, 457 (1927).

[160] D. R. Hartree, *Mathematical Proceedings of the Cambridge Philosophical Society* **24**, 89 (1928).

[161] V. Fock, *Zeitschrift für Physik* **61**, 126 (1930).

[162] J. C. Slater, *Physical Review* **34**, 1293 (1929).

[163] C. C. J. Roothaan, *Rev. Mod. Phys.* **23**, 69 (1951).

[164] G. G. Hall, *Proceedings of the Royal Society A: Mathematical, Physical and Engineering Sciences* **205**, 541 (1951).

[165] C. Møller, M. S. Plesset, *Physical Review* **46**, 618 (1934).

[166] M. L. Leininger, W. D. Allen, H. F. Schaefer, C. D. Sherrill, *The Journal of Chemical Physics* **112**, 9213 (2000).

[167] P. Hohenberg, W. Kohn, *Physical Review* **136**, B864 (1964).

[168] W. Kohn, L. J. Sham, *Physical Review* **140**, A1133 (1965).

[169] A. D. Becke, *The Journal of Chemical Physics* **98**, 1372 (1993).

[170] H. Iikura, T. Tsuneda, T. Yanai, K. Hirao, *The Journal of Chemical Physics* **115**, 3540 (2001).

[171] S. Grimme, *The Journal of Chemical Physics* **124**, 034108 (2006).

[172] B. O. Roos, P. R. Taylor, P. E. Siegbahn, *Chemical Physics* **48**, 157 (1980).

[173] V. Veryazov, P. Å. Malmqvist, B. O. Roos, *International Journal of Quantum Chemistry* **111**, 3329 (2011).

[174] H.-J. Werner, W. Meyer, *The Journal of Chemical Physics* **74**, 5794 (1981).

[175] P.-Å. Malmqvist, A. Rendell, B. O. Roos, *J. Phys. Chem.* **94**, 5477 (1990).

[176] R. V. Pinjari, M. G. Delcey, M. Guo, M. Odelius, M. Lundberg, *The Journal of Chemical Physics* **141**, 124116 (2014).

[177] P. E. M. Siegbahn, *The Journal of Chemical Physics* **72**, 1647 (1980).

[178] B. O. Roos, *Chemical Physics Letters* **15**, 153 (1972).

[179] L. Serrano-Andrés, M. Merchán, I. Nebot-Gil, R. Lindh, B. O. Roos, *The Journal of Chemical Physics* **98**, 3151 (1993).

[180] J.-P. Malrieu, J.-L. Heully, A. Zaitsevskii, *Theoretica Chimica Acta* **90**, 167 (1995).

[181] K. Andersson, P. Å. Malmqvist, B. O. Roos, A. J. Sadlej, K. Wolinski, *J. Phys. Chem.* **94**, 5483 (1990).

[182] K. Andersson, P.-Å. Malmqvist, B. O. R. Roos, *The Journal of Chemical Physics* **96**, 1218 (1992).

[183] J. Finley, P.-Å. Malmqvist, B. O. Roos, L. Serrano-Andrés, *Chemical Physics Letters* **288**, 299 (1998).

[184] R. O. Jones, O. Gunnarsson, *Reviews of Modern Physics* **61**, 689 (1989).

[185] E. Runge, E. K. U. Gross, *Physical Review Letters* **52**, 997 (1984).

[186] B. G. Levine, C. Ko, J. Quenneville, T. J. MartÍnez, *Molecular Physics* **104**, 1039 (2006).

[187] P. Elliott, S. Goldson, C. Canahui, N. T. Maitra, *Chemical Physics* **391**, 110 (2011).

[188] A. Bianconi, S. Doniach, D. Lublin, *Chemical Physics Letters* **59**, 121 (1978).

[189] A. Bianconi, R. Bauer, *Surface Science* **99**, 76 (1980).

[190] M. Belli, *et al.*, *Solid State Communications* **35**, 355 (1980).

[191] D. Koningsberger, R. Prins, *X-ray absorption: principles, applications, techniques of EXAFS, SEXAFS, and XANES* (John Wiley and Sons,New York, NY, 1988).

[192] S. Eisebitt, T. Böske, J.-E. Rubensson, W. Eberhardt, *Physical Review B* **47**, 14103 (1993).

[193] F. Meyer, J. Vrakking, *Surface Science* **33**, 271 (1972).

[194] T. X. Carroll, *et al.*, *Physical Review A* **61** (2000).

[195] R. Berera, R. van Grondelle, J. T. M. Kennis, *Photosynthesis Research* **101**, 105 (2009).

[196] A. Kotani, S. Shin, *Reviews of Modern Physics* **73**, 203 (2001).

[197] L. J. P. Ament, M. van Veenendaal, T. P. Devereaux, J. P. Hill, J. van den Brink, *Reviews of Modern Physics* **83**, 705 (2011).

[198] H. A. Kramers, W. Heisenberg, *Zeitschrift für Physik* **31**, 681 (1925).

[199] F. Gel'mukhanov, H. Ågren, *Phys. Rep.* **312**, 87 (1999).

[200] J. Rehbein, B. Wulff, *Tetrahedron Letters* **56**, 6931 (2015).

[201] K. A. Mix, M. R. Aronoff, R. T. Raines, *ACS Chemical Biology* **11**, 3233 (2016).

[202] A. Padwa, M. D. Weingarten, *Chemical Reviews* **96**, 223 (1996).

[203] B. Rode, C. Schwenk, T. Hofer, B. Randolf, *Coordination Chemistry Reviews* **249**, 2993 (2005).

[204] U. Eichler, C. M. Kölmel, J. Sauer, *Journal of Computational Chemistry* **18**, 463 (1997).

[205] H. M. Senn, W. Thiel, *Angewandte Chemie International Edition* **48**, 1198 (2009).

Acknowledgments

FIRST and foremost I offer my sincerest gratitude to my supervisor, Prof. Nils Huse for accepting the risk to take me as a PhD student for theoretical project and to the Prof. Oriol Vendrell for co-supervising me during this period. I am gratefully indebted to them for their very valuable suggestions and comments guided me to a successful completion of my dissertation. I acknowledge their considerable investments in my scientific training, including the participation at several conferences and that I consider immensely valuable.

This work is a result of many lengthy discussions with Dr. Michał A. Kochman, Dr. Zheng Li and Mickaël G. Delcey. They helped me a lot starting from basics of MOLCAS, Gaussian09 and motivating me at each and every step. I would also like to thank Dr. Stephan Niebling, Migual Ochmann, Dr. Katrin Adamczyk, Dr. Khalid Siddique and Dr. Fabian Westermeier for the proofreading different parts of my dissertation.

I am indebted to many CFEL colleagues for providing a stimulating and fun filled environment. My thanks go in particular to Ibrahym Dourki, Migual Ochmann, Amul Shinde, Christoph Testud, Stephan Niebling, Matthias Ruppert, Inga von Ahnen, Zheng Li, Khalid Siddique, Dr. Sang-Kil Son, and Peter Kroetz. Without their constant patience to answer my questions and to help me on difficult problems in physics, I could not have acquired enough knowledge to accomplish my Ph.D. thesis. It is hard to imagine that I could be smoothly approaching my Ph.D. degree without the help of IMPRS coordinators, past and present, Dr. Sonia Utermann and Dr. Julia Quante deserve to be highlighted with their excellent support in all non-scientific obstacles in a PhD students life.

I would also like to thank my some very close friends Taimoor Riaz, Dr. Zeeshan Shareef, Tayyab Qadeer, Sohaib Ehsan, Amir Rahat, M. Arif Shakir, Mohsin Nawaz and his family. Their encouragement, love, friendship and brotherhood means a lot to me. Also, I would like to thank all my teachers because of whose teaching at different stages of education has made it possible for me to reach this milestone. Because of their wonderful contribution I feel, was able to reach a stage where I could write this thesis.

On the personal side, I must express my very profound gratitude to my parents. I thank them for inculcating in me the pursuit of learning and scholarship. Most of all, I am eternally grateful to them for their loving affection and prayers. I would also like to thank my brothers and sisters for their love, encouragement, and concern for me.

Finally, I owe my deepest gratitude towards my wife, Anila for her eternal support and understanding of my goals and aspirations. Her infallible love and support has always been my strength. She has been extremely supportive of me throughout this entire process and has made countless sacrifices to help me get to this point. Without her help, I would not have been able to complete much of what I have done and become who I am. It would be ungrateful on my part if I thank Anila in these few words.

Eidesstattliche Versicherung
Declaration on Oath

Hermit erkläre ich an Eides statt, dass ich die vorliegende Dissertationsschrift selbst verfasst und keine anderen als die angegebenen Quellen und Hilfsmittel benutzt habe.

I hereby declare, on oath, that I have written the present dissertation by my own and have not used other than the acknowledged resources.

Hamburg, den Unterschrift